BRNO UNIVERSITY OF TECHNOLOGY
VYSOKÉ UČENÍ TECHNICKÉ V BRNĚ

FACULTY OF MECHANICAL ENGINEERING
FAKULTA STROJNÍHO INŽENÝRSTVÍ

INSTITUTE OF SOLID MECHANICS, MECHATRONICS AND BIOMECHANICS
ÚSTAV MECHANIKY TĚLES, MECHATRONIKY A BIOMECHANIKY

CONSTITUTIVE MODELLING OF COMPOSITES WITH ELASTOMER MATRIX AND FIBRES WITH SIGNIFICANT BENDING STIFFNESS
KONSTITUTIVNÍ MODELOVÁNÍ KOMPOZITŮ S ELASTOMEROVOU MATRICÍ A VLÁKNY S VÝZNAMNOU OHYBOVOU TUHOSTÍ

DOCTORAL THESIS
DIZERTAČNÍ PRÁCE

AUTHOR   Ing. Svitlana Fedorova
AUTOR PRÁCE

SUPERVISOR   prof. Ing. Jiří Burša, Ph.D.
ŠKOLITEL

CO-SUPERVISOR   Ing. Pavel Skácel, PhD
ŠKOLITEL SPECIALISTA

BRNO 2018

Abstract

Constitutive modelling of fibre reinforced solids is the focus of this work. To account for the resulting anisotropy of material, the corresponding strain energy function contains additional terms. Thus, tensile stiffness in the fibre direction is characterised by additional strain invariant and respective material constant. In this way deformation in the fibre direction is penalised.

Following this logic, the model investigated in this work includes the term that penalises change in curvature in the fibre direction. The model is based on the large strain anisotropic formulation involving couple stresses, also referred to as "polar elasticity for fibre reinforced solids". The need of such formulation arises when the size effect becomes significant.

Mechanical tests are carried out to confirm the limits of applicability of the classical elasticity for constitutive description of composites with thick fibres. Classical unimaterial models fail to take into account the size affect of fibres and their bending stiffness contribution.

The specific simplified model is chosen, which involves new kinematic quantities related to fibre curvature and the corresponding material stiffness parameters. In particular, additional constant k_3 (associated with the fibre bending stiffness) is considered. Within the small strains framework, k_3 is analytically linked to the geometric and material properties of the composite and can serve as a parameter augmenting the integral stiffness of the whole plate. The numerical tests using the updated finite element code for couple stress theory confirm the relevance of this approach.

An analytical study is also carried out, extending the existing solution by Farhat and Soldatos for the fibre-reinforced plate, by including additional extra moduli into constitutive description.

Solution for a pure bending problem is extended analytically for couple stress theory. Size effect of fibres is observed analytically.

Verification of the new constitutive model and the updated code is carried out using new exact solution for the anisotropic couple stress continuum with the incompressibility constraint. Perfect agreement is achieved for small strain case. Large strain problem is considered by finite element method only qualitatively.

Three cases of kinematic constraints on transversely isotropic material are considered in the last section: incompressibility, inextensibility and the double constraint case. They are compared with a general material formulation in which the independent elastic constants are manipulated in order to converge the solution to the "constraint" formulation solution. The problem of a thick plate under sinusoidal load is used as a test problem. The inclusion of couple stresses and additional bending stiffness constant is considered as well. The scheme of determination of the

additional constant d_{31} is suggested by using mechanical tests combined with the analytical procedure.

Key words: fibre-reinforced materials, fibre bending stiffness, hyperelasticity, constitutive modelling, polar elasticity

Acknowledgments

List of Figures

List of Tables

Nomenclature

A, A_I	fibre direction vector in the undeformed configuration
a, a_i	fibre direction vector in the deformed configurations
b, b_i	no name vector defined by eq. (5.4)
C, C_I	right Cauchy-Green deformation tensor
d	compressibility constant
d_{31}	material constant related to fibre bending stiffness
EVE	representative volume element of the equivalent homogeneous material
EIF	extensible incompressible formulation
D_{het}	bending stiffness of the heterogeneous model of the beam
D_{hom}	bending stiffness of the homogeneous model of the beam
D_{hom}^{full}	bending stiffness of the amended homogeneous model of the beam
E_{hom}	Young's modulus of homogenised beam in fibre direction
E_f	Young's modulus of fibre
E_m	Young's modulus of matrix
E_l	effective longitudinal Young's modulus
E_i	RVE effective Young's modulus in the x_i direction
F, F_{IJ}	deformation gradient tensor
G, G_{IJ}	deformed fibre gradient tensor
G	shear modulus for isotropic solid
G^f	fibre share modulus
G^m	matrix share modulus
G_{12}	effective in-plane shear modulus
GF	"general" (extensible and compressible) material formulation
ICF	inextensible compressible formulation

IIF	inextensible, incompressible formulation
I_1-I_{33}	invariants of the deformation gradient tensor and the "curvature-strain" tensor
$\bar{I}_1$	modified first invariant of the right Cauchy-Green deformation tensor
$\bar{I}_4$	modified deformation gradient tensor invariant related to tensile strain in fibre direction
$\bar{I}_6$	modified Λ tensor invariant related to the change in fibre curvature
J	Jacobian of the deformation gradient
J_f	second moment of the fibre cross-section
$\boldsymbol{k}$, k_{ij}	"curvature-strain" tensor
k_f	curvature of the initially straight fibre
k^{pure}	curvature of the beam in pure bending
M_2^{full}	bending moment in the amended homogeneous model of the beam
M_2	bending moment in the homogeneous model of the beam
M_{13}^{RVE}	cumulative bending moment acting on RVE
M^f	bending moment acting on fibre cross-section
$\boldsymbol{m}$, m_{ij}	couple stress
$\boldsymbol{m}^f$, m_{ij}^f	couple stress contributed by fibre in RVE
$\overline{\boldsymbol{m}}$, $\overline{m}_{ij}$	deviatoric part of (true) couple stress
p	hydrostatic pressure
RVE	composite representative volume element
S	cross-section area
S_f	fibre cross-section area
S_m	matrix cross-section area
$\boldsymbol{u}$, u_i	displacement vector
V	volume
W	strain energy density

W_a	anisotropic part of the strain energy density
W_{iso}	isotropic part of the strain energy density
α, β	elastic modulus for transversely isotropic solid
$\hat{\gamma}, \hat{\gamma}_{ij}$	average linear shear strain
$\hat{\varepsilon}, \hat{\varepsilon}_i$	RVE average linear longitudinal normal strain in the x_i direction
θ, θ_{ij}	rotation vector
Λ, Λ_{IJ}	tensor of kinematic quantity, related to the curvature of the deformed fibre
λ	Lame parameter
$\lambda_1, \lambda_2, \lambda_3$	principal stretches
$\tilde{\lambda}, \tilde{\lambda}_1, \tilde{\lambda}_2$	non-dimensional parameters related to intrinsic material length scales
μ	shear modulus (equal to G) for isotropic solid
μ_1, μ_T	shear moduli for transversely isotropic solid
$\bar{\mu}, \bar{\mu}_{ij}$	deviatoric part of Kirchhoff couple stress
$\boldsymbol{v}, v_i$	displacement rate vector
v	Poisson's ratio for isotropic material
v_{ji}	Poisson's ratio in the major convention (with j being the load direction)
v_{IT}	Poisson's ratio for the axis x_I and the isotropic plane
v_T	Poisson's ratio for the isotropic plane
$\boldsymbol{\sigma}, \sigma_{ij}$	Cauchy stress tensor component
$\boldsymbol{\sigma}_{()}, \sigma_{(ij)}$	symmetric part of Cauchy stress component
$\boldsymbol{\sigma}_{[]}, \sigma_{[ij]}$	antisymmetric part of Cauchy stress component
$\hat{\sigma}, \hat{\sigma}_i$	RVE average normal stress in the x_i direction
$\boldsymbol{\sigma}^f, \sigma_{ij}^{\ f}$	normal stress contributed by fibre in RVE
$\tilde{\sigma}, \tilde{\sigma}_{11}$	normal stress distribution as function of x_2 in RVE
$\boldsymbol{\tau}, \tau_{(ij)}$	symmetric part of Kirchhoff stress
$\hat{\boldsymbol{\tau}}, \hat{\tau}_{ij}$	average shear stress

$\tilde{\boldsymbol{\tau}}$, $\tilde{\tau}_{12}$	shear stress distribution as function of x_2
$\boldsymbol{\tau}^f$, $\tau_{ij}{}^f$	shear stress contributed by fibre in RVE
ψ^f	fibre volume fraction
$\boldsymbol{\omega},\ \omega_i$	spin vector
$\boldsymbol{X},\ X_i$	position vector in reference configuration
$\boldsymbol{x},\ x_i$	position vector in deformed configuration

Contents

1. Introduction

Fibre reinforced composite materials are widely used especially in automotive and aerospace industries. In particular, fibre-reinforced rubber is being used in pneumatic tyres, air springs, tubing and belt structures. In contrast to composites used for components of car or aircraft bodies, the main load bearing component of a tyre (i.e. body of a tyre) consists of layers of fibres embedded in rubber called plies. A radial-ply tyre contains belts of relatively inextensible fibres running in the circumferential direction under the tread of the tyre [1]. This construction reinforces the tyre and prevents rubber from excessive stretching. Metal, polymer or textile cords are being used in tyre plies. In particular, commercial vehicle tyres typically contain layers of steel fibres. Naturally, the orientation of the plies and fibre directions affect the performance of the tire.

Effective properties of a composite are generally influenced by the properties of constituents, volume fraction and directions of fibres, and quality of adhesion between rubber and fibres. Strength and stiffness in the preferred direction of the composite relate to properties of fibres, while properties of matrix determine material strength under shear, compression, tension perpendicularly to the fibres, and resistance of the composite to fatigue.

From the mechanical point of view, a tyre belt is made of a heterogeneous, anisotropic, nearly incompressible hyperelastic material consisting of a compliant matrix reinforced by fibres being several orders stiffer. While for textile fibres their bending stiffness is negligible, for steel fibres, especially if the fibre consists of one wire only with its diameter comparable with the thickness of the layer, the bending stiffness of individual fibres contributes significantly to the overall bending stiffness of the composite. This fact represents an additional challenge in terms of evaluation of effective properties and response of the heterogeneous structure. It is therefore of both practical and theoretical interests to develop a relevant anisotropic homogeneous model which takes both tensile and bending stiffness of fibres into consideration and is suitable large strain applications.

In the present work, fibres in the composite are regarded as slender beams embedded in the nonlinear or linear elastic matrix. Employing the kinematics and general constitutive formulation presented in [2] and some newer findings [3], [4], [5], [6], [1], [8], [9] the author investigates a homogeneous model taking both tensile and bending stiffness contributed by fibres into account. The effect of individual fibres is "smeared – out" so that the bending stiffness of the homogeneous model simulates bending behaviour of the real heterogeneous structure.

1.1. Goals of the thesis

The broad objective of the thesis is to extend the existing research concerning constitutive modelling of the fibre-reinforced materials with elastomer matrix with the use of couple stress theory. In this objective the following issues are included:

- realization of mechanical tests to illustrate the limits of applicability of the classical large strain elasticity for constitutive description of composites with thick fibres;
- choice of the strain energy density model on the basis of polar elasticity theory;
- new analytical solutions for polar elasticity or the extension of existing ones;
- modification of FEM formulation;
- verification of FE solutions for some analytically solvable problems;
- theoretical study of the additional elastic constants and their influence.

In the following chapter the works done on these issues are specified in greater detail.

1.2. Structure and order of the thesis

a) literature review about existing approaches to modelling of composite materials under large strains, in particular fibre-reinforced elastomers.

b) mechanical tests with the steel fibre-reinforced rubber specimens; their discrepancies with the simulation results and assessment of the causes.

c) recapitulation of the simplified approach to the effective constants derivation for composites; extension of this approach to include fibre size effect.

d) formulation of the polar constitutive model on the basis of [2] that includes specifically fibre bending mode deformation, disregarding splay mode and torsion; modification of the finite element code by Lasota [3] to incorporate additional invariant; examination of influence of the additional material parameter; proposal of a scheme to define its value for linear elastic case; test the solution to bending problem of the composite plate with inclined fibres.

e) precise verification of the aforementioned code by simulating the analytically solvable anisotropic polar elasticity problem for small strains; qualitative test of the code for large strains case.

f) literature search for analytic solutions for the linearised polar theory for fibre reinforced solids; additional complementary calculations;

g) plane strain linear problems that illustrate influence of fibre presence in bending

h) incompressibility and fibre inextensibility constraints; addition of the intrinsic anisotropic bending stiffness into the model; mathematical convergence of the models by manipulating certain parameters.

2. State of the art

In general, the fibre composite described above can be modelled in two ways. The first way implies explicit geometrical modelling of (linear elastic) fibres embedded in the (hyperelastic or even non-elastic) matrix. In accordance with Lasota [7], such models will be referred to as "bimaterial models" in this proposal. Even for relatively simple composite materials such as steel wire reinforced rubber, this approach is prohibitively expensive in computer time due to large number of fibres and consequently a large number of finite elements required for their real geometric models. Alternatively, a so called "unimaterial" model can be employed − it is based on geometry of the whole composite body only (without distinguishing its structural details) and includes phenomenological anisotropic constitutive model. The effect of tensile stiffness contributed by fibres is included mathematically into constitutive equations. Such model is computationally advantageous, but its application is limited, as will be explained further. In both models, constitutive parameters of rubber are based on various types of uniaxial and biaxial tests [9].

The use of phenomenological anisotropic models started with Spencer [11]. Anisotropic hyperelastic models typically include strain-energy density as a function of strain invariants with some of the invariants depending on the unit vector (vectors) of the reference fibre direction [11] [13], [12], [15]. In this way an intrinsic assumption of infinitesimally thin, densely and uniformly distributed fibres is implied, leading to their zero bending stiffness. The closer the composite structure is to these assumptions, the better agreement can be provided by the model. Such unimaterial finite strain models have been successfully employed for modelling of rubber reinforced by thin textile or carbon fibres [16], [17], [18], [19], [20], [5], [14]. However, these models fail if fibres are made (e.g.) of steel, and their bending stiffness may become relevant, especially in the case of steel wires; when multifibre ropes are used instead, their bending stiffness is lower but unfortunately hardly quantifiable. In general, these models are not applicable if the characteristic length scale of non-homogeneity is comparable with dimensions of the specimen [22] and so called size effects arise. It is often the case when microscale problems [23], [24], [25],[26], [27], [28], [29] or composite materials [22], [30], [31], [33] are considered. The applied classical Cauchy continuum theory is not able to account for the influence of the characteristic size of substructure on material behaviour.

In order to deal with the presence of size effects, non-classical continuum mechanics theories are typically employed. There are two classes of generalized continuum theories: higher-grade and higher-order theories [34]. In brief, higher-grade theories employ higher order gradients of the displacements, while higher-order continuum theories include additional

kinematic variables attached to the material point. In particular, Cosserat theory [35], [36] (also known as micropolar) adds independent rotational degrees of freedom to the classical continuum; a detailed review and bibliography of this theory can be found e.g. in Altenbach [33].

Phenomenological generalised continuum theories present an alternative to the explicit geometrical modelling of microstructure. The most general case of higher-order continuum is the so called micromorphic theory [37], in which material point possesses 9 additional degrees of freedom (three micro-rotations and six components of micro-strain tensor). Cosserat continuum [35] represents a simpler approach endowing each material point with the independent rotational degrees of freedom (without the micro-strain tensor). In this case the stress tensor is non-symmetric and, in addition, the couple stresses are present in the equilibrium equations. The models within this approach were developed, among others, by Eringen and Suhubi [39], [40], [41], and are known as micropolar elasticity models. The couple stress theory [42], [43], [44], [45] can be considered as a special case of the micropolar theory. In the CST rotations of the material point are not independent kinematic variables, but derived from the displacement field in a conventional way.

In this work the focus is on the fibre reinforced materials with one family of fibres – transversely isotropic material, generally hyperelastic. For such solids with the size effects related to the bending stiffness, a new constitutive framework using CST was developed by Spencer and Soldatos in 2007 [2]. The authors intended the model to represent the behaviour of the fibre reinforced elastomers when the fibre thickness is comparable with the lowest lateral dimension of the specimen. Constitutive formulation is mathematically based on the notion of deformed fibre curvature, in addition to invariants of the deformation gradient. The introduced theoretical framework allows taking into account the contribution of the individual fibres to the bending stiffness of composite by employing the continuum capable of bearing couple stresses. A subsequent progress in that area was made by Soldatos [46], [46], [48]. This is the framework adopted in the present work.

The latest contribution by Farhat et al [1] should be mentioned as well; it deals with some important analytical solutions within the linear polar elasticity for fibre-reinforced solids.

Adopting the framework of Spencer and Soldatos, Lasota [3] develops a finite element formulation and implementation aimed at solving large strain polar elasticity problems. He also proposes a specific simplified strain energy description.

Various finite element formulations for generalised continuum theories were presented in the literature in the last years. Two-dimensional formulations of the linear micropolar theory are proposed in [49], [50], [51], [52]. Planar elements for micropolar elastoplasticity are introduced

in [53], [54] and (within the micromorfic theory) in [55],[55]. Three-dimensional formulations are developed in [56], [57], [58] for micropolar and in [59] for micromorphic framework.

Within the CST framework, linear elastic [60], [61], [62]   and elastoplastic [63] formulations can be mentioned in a non-exhaustive list. Among them, [60] and [62] are of our special interest since they represent two possible finite element approaches to CST: a straightforward displacement based approach and an alternative penalty approach. The former approach implies the use of C1 continuity elements [62] (based on continuity of displacements and their derivatives) due to the presence of second-order derivatives of displacements in the main equations. Such approach is chosen in the present work as well. The latter approach applies C0 continuity elements while introducing rotations as independent variables and then imposing the rotation/displacement dependency as constraint using Lagrange multipliers [60]. With the exception of [49], all the aforementioned models do not include anisotropy, and only one formulation [58] is fully non-linear and three-dimensional.

The aim of the present work is to progress further in understanding and application of the polar elasticity and hyperelasticity for fibre-reinforced solids. The emphasis is on verification and enhancement of both the constitutive model and its FEM implementation.

3. Preliminary study: specimens with thick fibres

In this section, experiments and computational simulations for the specimens with comparatively thick fibres are described. Results and overview presented in this section were published earlier in [5].

While material properties of most fibre composites are linear elastic and the theory of linear elasticity is well known and widely used for any types of anisotropic materials under small strain conditions, large strains induced in elastomers make the stress-strain analyses much more difficult and not yet fully managed. Although first applicable isotropic hyperelastic models were formulated in the forties and fifties of the last century [64], [65], their broader practical application has not started before the nineties, when the power of computers has enabled to solve more complex non-linear problems. However, there is still a lack of criteria for assessment of the risk of failure of isotropic elastomers [66] , [67], [67].

Even more difficulties arise when anisotropy is to be added to the theory as in the case of fibre reinforced elastomers. Constitutive formulations for strongly anisotropic solids [68], [69], [69] are being widely used and implemented into commercial finite element packages. Experience with their practical application in hyperelasticity cases and with identification of their parameters is not sufficient. This section presents results of simulations of basic mechanical tests of fibre composites with elastomer matrix using FEM and their experimental validation.

The experiments and computational simulations of composite material with hyperelastic matrix and steel fibres carried out in the work of Lasota and Burša [7] brought motivation for the following tests and computations. Two computational models of different levels are used for the simulations. The first one is the bimaterial model, which includes 3D geometry modelling of both matrix and fibres. The second one is the unimaterial model in which the fibre and matrix materials are not distinguished, but the reinforcing effect of fibres is described by an anisotropic hyperelastic constitutive model with polynomial strain energy density function. The simulations show that both models give nearly the same results in case of tension tests, while in case of bending tests the results differ substantially: the unimaterial model was unsuccessful, the discrepancy with the test was around 50 %. The authors assumed that the reason of this discrepancy is that the unimaterial model did not incorporate bending stiffness of the reinforcing fibres but their tensile stiffness only. In order to verify this suggestion, the following tests were carried out for the rubber specimens reinforced with textile fibres. Given that the textile fibres are perfectly flexible, the expectation is that the unimaterial model will give better agreement with bending experiments; this is described in the next paragraphs.

21

3.1. Experimental methods

Uniaxial tension tests of composite specimens with a rubber matrix and single family of textile fibres in the middle layer of the specimen are carried out. Four groups of specimens with different declination of fibres were tested: 0°, 30°, 45°, 90°. All the specimens had dimensions approximately 110×22×2.5 mm and diameter of the fibres 0.8 mm. All the specimens were loaded in cycles with different amplitudes to evaluate Mullins effect [71]. The upper extreme value of total elongation of the specimen is nearly 20 mm, with the exception of 0° declination (longitudinal fibres), where the elongation had to be several times lower because of the much higher stiffness of the specimen. Tension tests were realized using universal testing machine ZWICK Z020-TND. Elongation in the middle region of the specimen was recorded by extensometers (**Fig. 3.1**); the distance between extensometer levers was 20 mm.

A particular feature of the tension tests with specimens with declined fibres is that the dimensions of specimens strongly affect the results. Stress-strain curves would be different for the specimens with the same angle of declination but different width to length ratio. Due to the technical limitations of the experiment, longer specimens could not be used. It means that the regions of the specimen that contain fibres clamped on one edge affect the results drastically. The size of the region that contains only fibres free on the both ends is similar to that of the boundary regions with clamped fibres.
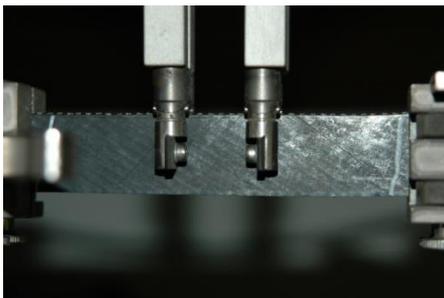
Fig. 3.1. Tension test of fibre composite with rubber matrix
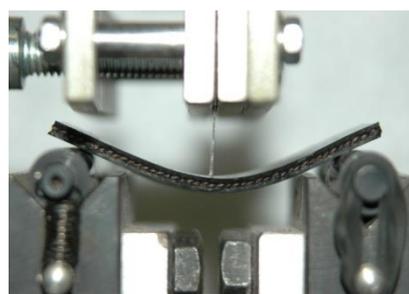
Fig. 3.2. Bending test of fibre composite with rubber matrix

Bending tests were realized also with the ZWICK testing machine as a three point bending. Also pure rubber specimens were tested. Specimens had dimensions approximately 60×20×2.5 mm and diameter of the fibres approximately 0.8 mm. The distance between supports was 50 mm.

During the test each specimen was placed in the test preparation and pushed against its middle part (**Fig. 3.2**). The dependency between the force and the middle deflection was recorded.

Experiments with pure rubber were carried out as well in order to determine material constants for the chosen hyperelastic potential of the matrix. They included uniaxial and equibiaxial tension tests of rubber specimens. As the parameters of the textile fibres are rather uncertain and were not known, their stiffness was identified on the basis of the tension test of the composite specimen with fibres in longitudinal direction.

3.2. Methods of computational simulations

Material of the specimens shows large strains and incompressibility (due to rubber) and a substantial anisotropy (due to fibres).

Rubber matrix of the specimen is characterized by large reversible deformations. Its behaviour is approximated as so called hyperelastic. Constitutive modelling in this case is based on the concept of strain energy density function (strain energy potential). Strain energy potential has to be a function of the strain measures and satisfy certain mathematical requirements such as continuity and polyconvexity. Stress-strain relations are derived from this potential. Commonly, the strain energy potential for isotropic hyperelastic material is based on strain invariants.

For rubber-like materials, a phenomenological polynomial form of the strain energy density W is widely used. Its isovolumic part is based on the first and second deviatoric invariants I_1 and I_2 and volumetric part on the third invariant $J = \lambda_1 \lambda_2 \lambda_3$ representing the volume ratio; it is given by the following formula:

$$W = \sum_{i+j=1}^{3} c_{ij} (I_1 - 3)^i (I_2 - 3)^j + \sum_{k=1}^{N} \frac{1}{d_k} (J - 1)^{2k} , \qquad (3.1)$$

where c_{ij}, d_k are material parameters.

In our case, given that the local tensile strains do not exceed 40% in all tests, the simplest neo-Hooke model can be used for rubber matrix:

$$W = \frac{\mu}{2} (I_1 - 3) + \frac{1}{d} (J - 3)^2 , \qquad (3.2)$$

where $I_1 = \lambda_1^2 + \lambda_2^2 + \lambda_3^2 -$ first invariant of the right Cauchy-Green deformation tensor.

To model the behaviour of the given specimens, we need to account for the material anisotropy. As the specimens contain one family of fibres, they have a single preferred direction. In this direction the stiffness of the material is defined by the stiffness of fibres. The fibres are uniformly distributed not throughout the thickness but only in the middle layer of the specimen (with approximately constant spacing). Continuum approach based on assumption of affine deformation, i.e. perfect bonding between matrix and fibres, will be used for constitutive modelling. It takes into account contribution of both constituents: fibres and rubber.

Specimens for bending simulations were modelled using a three-layer model with the middle layer being anisotropic hyperelastic and two others being isotropic hyperelastic. In contrast, specimens for tension simulations (with the exception of 0 deg. case) were modelled as homogeneous, using anisotropic hyperelastic material model. It has been proved that for uniaxial tension both the models gave the same results for all fibre declinations except for 0°. In this case all fibres are clamped between jaws on both ends which makes the specimen much stiffer and the deformation of the rubber layer between the jaws and the middle layer reinforced with fibres becomes decisive. Therefore the same three-layer model as for bending was used for tension with longitudinal fibres.

Strain energy potential used for anisotropic hyperelastic materials consists of isotropic and anisotropic parts. The anisotropic part includes strain invariant I_4:

$$I_4 = ACA, \qquad (3.3)$$

where A is unit vector characterising the preferred direction in the undeformed configuration and C is right Cauchy-Green deformation tensor, given by squared stretch ratios in the principal coordinate system:

$$C = \begin{pmatrix} \lambda_1^2 & 0 & 0 \\ 0 & \lambda_2^2 & 0 \\ 0 & 0 & \lambda_3^2 \end{pmatrix}. \qquad (3.4)$$

If XY coordinate plane coincides with the specimen's middle plane, the fibre vector has coordinates $(cos\,\alpha, sin\,\alpha, 0)$ where α defines the fibre declination angle. Accordingly, invariant I_4 (representing stretch of fibres) is given by:

$$I_4 = \lambda_1^2 \cos^2 \alpha + \lambda_2^2 \sin^2 \alpha. \qquad (3.5)$$

Anisotropic hyperelastic strain energy potential (volume-preserving part) can be given by polynomial form:

$$W = \sum_{i=1}^{3} a_i \left(I_1 - 3\right)^i + \sum_{j=1}^{3} b_j \left(I_2 - 3\right)^j + \sum_{k=2}^{6} c_k \left(I_4 - 1\right)^k . \tag{3.6}$$

Constants for potential (3.6) are being determined from the characteristics of constituents (rubber and fibres).

The isotropic part of potential (3.6) can be set in the form of neo-Hooke model for an incompressible rubber:

$$W_{iso} = \frac{\mu}{2}\left(I_1 - 3\right). \tag{3.7}$$

Material constant μ for rubber was determined on the basis of the stress-strain curves obtained from two sets of experiments: uniaxial tension and equibiaxial tension of rubber specimens. Approximation of response curves was performed employing the least squares method.

The anisotropic part of potential (6) reflects the characteristics of composite in the preferred direction. It was set as follows:

$$W_a = c_2 \left(I_4 - 1\right)^2 . \tag{3.8}$$

Consequently, potential (6) acquires the form

$$W = \frac{\mu}{2}\left(I_1 - 3\right) + c_2 \left(I_4 - 1\right)^2 . \tag{3.9}$$

The recent studies of our team on specimens with steel fibres [7] have shown substantial discrepancies between the computational and experimental results. There were two main reasons identified by the authors: first, the anisotropic hyperelastic constitutive model used could not account for the bending stiffness of steel fibres and second, the presence of Mullins effect in rubber. Therefore in the present study textile fibres (with zero bending stiffness) and rubber with low Mullins effect are used, thus minimizing the possible causes of errors.

Specific type of rubber was chosen on the basis of preliminary uniaxial tension tests with different rubbers used typically for production of car tyres. From its loading and unloading curves it is clear that Mullins effect does not exceed 10 % of engineering stress for this type of rubber. Consequently, its influence on the results was neglected in this study.

3.3. Results and discussion

In this section results of experiments and the corresponding computational simulations are presented.

3.3.1. Uniaxial tension

The figures below present results of uniaxial tension tests and their simulations. In all the figures the abscissa represents elongation of the middle part of the specimen with original length of 20 mm. Tests were carried out with three groups of specimens: two specimens with 0° fibre declination, three specimens with 45° fibre declination and five specimens with the declination of 90°. Material constants used in Eq. (3.9) were set as follows: $\mu = 1,2$ MPa, $c_2 = 60$ MPa. While the simulations have been done only under monotonous loading (without unloading), all the experiments were carried out in several cycles so that some amount of hysteresis and Mullins effect can be seen.
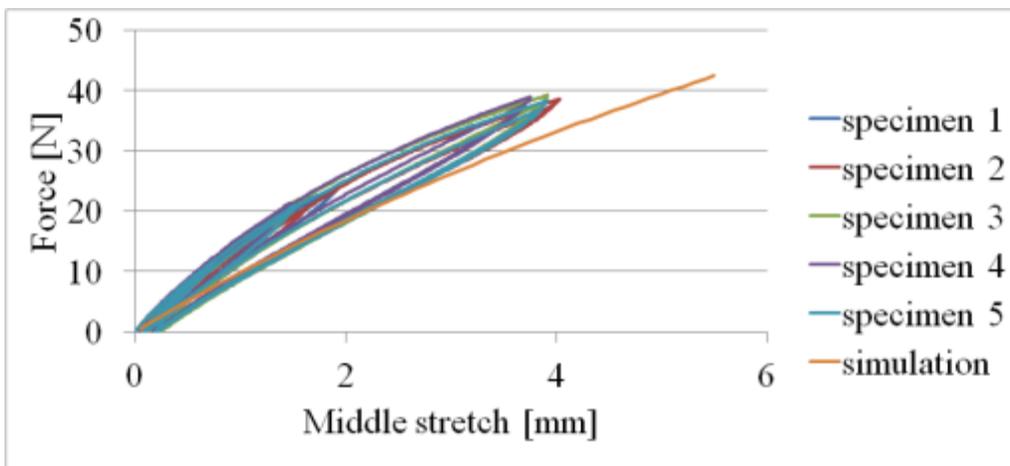
Fig. 3.3. Results of the tension test and its simulation for 90° declination of fibres.
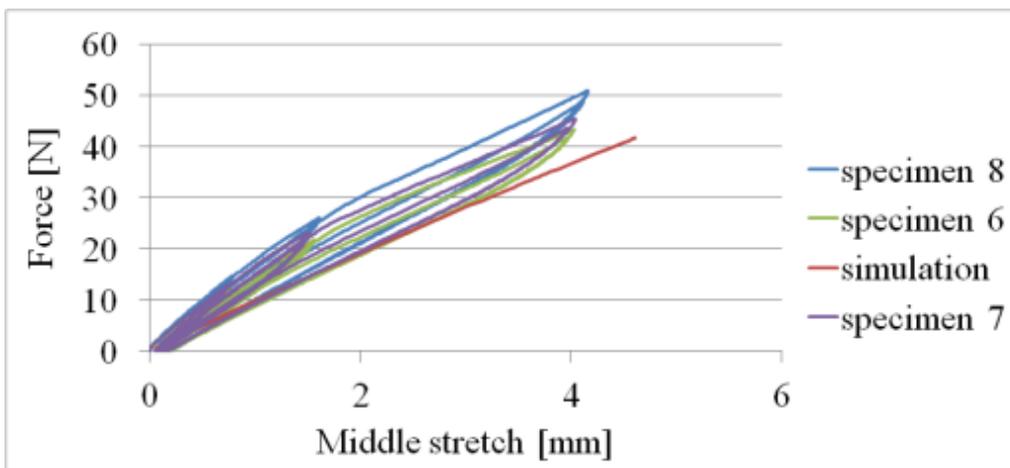
Fig. 3.4. Results of the tension test and its simulation for 45° declination of fibres.
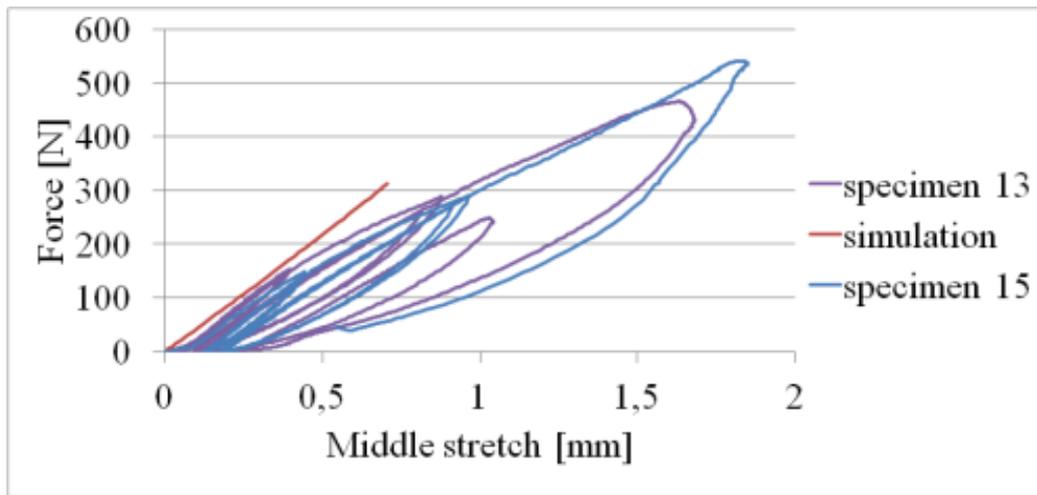
Fig. 3.5. Results of the tension test and its simulation for 0° declination of fibres.

As it was shown in [7], the bimaterial model (which includes models of geometry of both matrix and fibres) can be successfully replaced with the unimaterial one in the case of tension load. It results in a substantial reduction of computational time.

It is evident from **Fig. 3.3-3.5** that simulations are in good agreement with the tests for all fibre declinations. The case of 0° fibre declination needs a particular explanation of the experimental and computationally obtained curves presented in **Fig. 3.5** . The specimen was modelled as a three-layer sandwich with upper and bottom rubber layers (using the isotropic hyperelastic potential) and a fibre-reinforced middle layer (using the potential (3.9)).   The specimen elongation during the experiment is mainly due to the shear in rubber layers between the jaws. The aim of numerical simulation was to determine material constant c_2 representing the stiffness of fibres in (3.9). The potential (3.9) was employed in the computational model; accordingly, constant c_2 was varied until an acceptable agreement between the simulation and the experimental response was reached.

Different situation occurs when the fibres clamped on both ends absent (due to the geometry of specimen and angle of fibre declination). The value of c_2 can be set very high, for only shear strain in matrix is substantial, not the fibre elongation. A very high c_2 corresponds to almost inextensible fibres. If no fibres are clamped on both specimen ends in the experiment, the overall elongation of the specimen occurs almost purely due to shear in the matrix between the inclined fibres. So in this case the behaviour of fibre composite is almost identical with the response of that with inextensible fibres.

3.3.2. *Results of bending simulations*

The figures below present results of bending tests and their simulations. The tests were carried out with three groups of three specimens each: for 45° and 90° declination of fibres and for pure rubber. The same material parameters were set as for the tension test simulations.
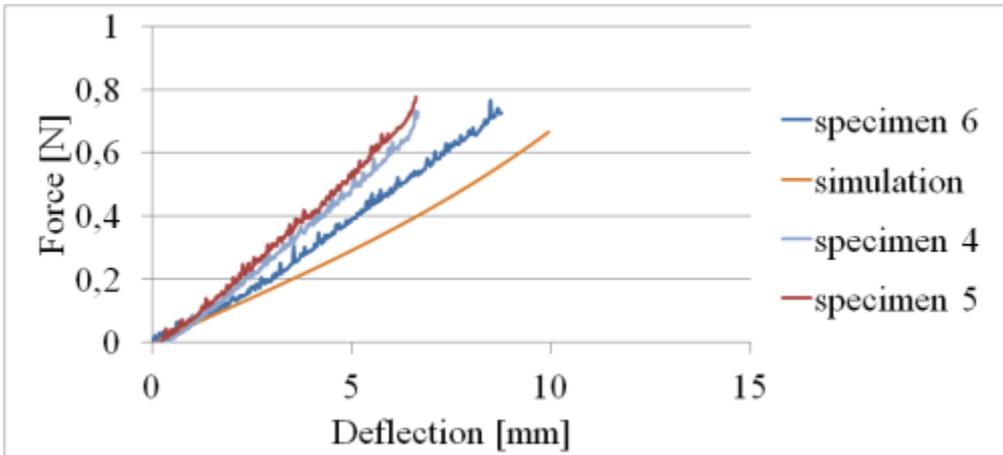
Fig. 3.6. Results of the bending test and its simulation for 45° declination of fibres.
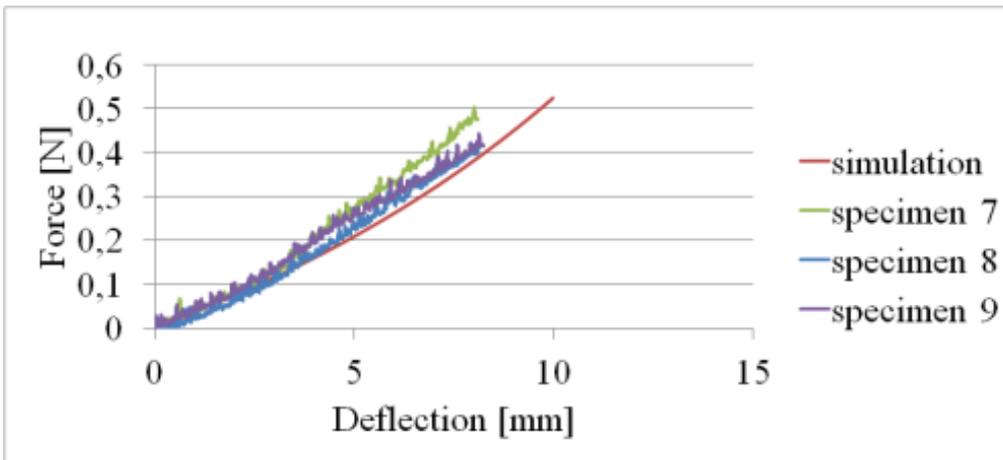
Fig. 3.7. Results of the bending test and its simulation for 90° declination of fibres.
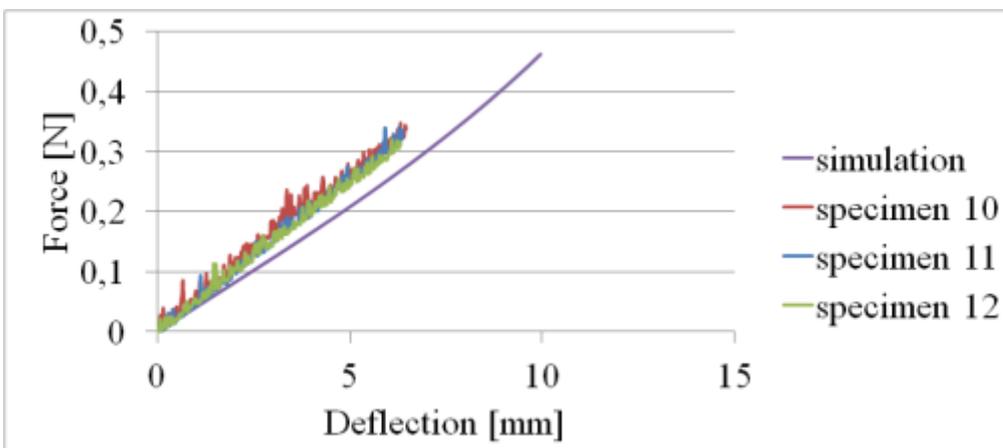
Fig. 3.8. Results of the bending test and its simulation. Specimens made of pure rubber.

In contrast with the previous chapter, for bending tests simulations the value of c_2 shows a great influence on the results. As it was expected, the stiffening effect of the fibres with 90° fibre declination is negligible (also, the results for these specimens are very close to those obtained for pure rubber).

As a result of the tests and simulations carried out it is verified that anisotropic hyperelastic constitutive model (in polynomial form) is able to simulate credibly results of tension and bending tests of fibre composites showing large strains under the following conditions: elastomer matrix shows negligible Mullins effect; bending stiffness of fibres is negligible. This result supports the earlier suggestion that in the case of not infinitely thin fibres the main reason of discrepancy between the unimaterial model and experiment lies in inability of the model to account for the bending stiffness and size effect of fibres.

4. Effective anisotropic constants within simplified mechanics of materials

In this section, the well known "rule of mixtures" approach is recapitulated for the approximate derivation of effective constants within the classical linear elastic mechanics.

It is done in order to proceed to apply a similar simplifying approach of mechanics of materials to include the additional parameter within the linear couple stress theory.

4.1. Effective properties of fibre composite within the linear elasticity

We review now the derivation of the effective material properties within the framework of linear elastic mechanics of materials. Specifically, long fibre composites are still considered. Assumptions and simplifications used in linear elastic mechanics of materials are employed. This approach sets the relationships between the effective properties and properties of the constituents. Engineering constants of an equivalent homogeneous material are derived using characteristics of the given composite and its components - volume fraction and geometric arrangement of fibres, matrix and fibre properties..

Elementary models employ representative volume element (RVE) based on the following simplifications:

- RVE consists of fibre and matrix ;
- both fibre and matrix materials are linear elastic and isotropic;
- RVE geometry does not change in the 3rd direction;
- area fractions in the direction of fibres represent volume fractions;
- strains and stresses due to the Poisson's ratio mismatch at the fibre-matrix interface are neglected;
- the actual fibre arrangement in space (hexagonal, tetragonal, random) is of no consequence;
- the round fibre is replaced with rectangular block with the same volume fraction;
- perfect bonding at fibre/matrix interface is assumed;
- cross-sections of both the matrix and fibre remain planar under any deformation;
- the composite is macroscopically homogeneous and transversely isotropic.

For the load acting in longitudinal direction (**Fig.4.1**) we replace the RVE containing fibre and matrix elements by a respective volume element of an equivalent homogeneous material (EVE).

When describing the material properties of transversely isotropic solid, here and further the following notation is used: subscript "*T*" refers to either x_2 or x_3 direction, subscript "*1*" refers to the x_1 direction – direction of fibres.
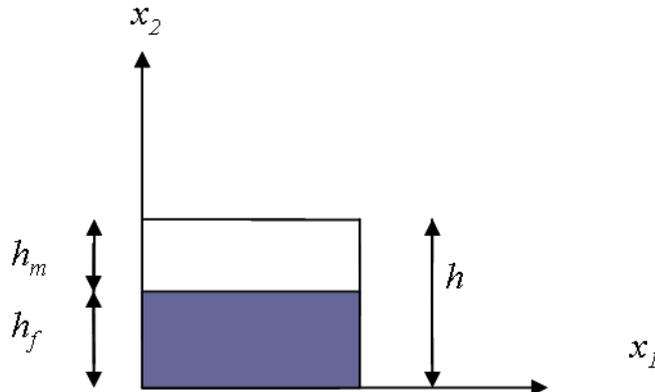
Fig. 4.1. RVE

4.1.1. Effective longitudinal modulus

A uniform state of stress within each material (fibre, matrix and equivalent material) is considered below.

The relations used for a composite under tension in the direction of fibres (x_1) are

$$\varepsilon_1^{\ f} = \varepsilon_1^{\ m} = \hat{\varepsilon}_1 \tag{4.1}$$

$$\frac{S^f}{S} = \psi^{\ f}$$
$$\frac{S^m}{S} = \left(1 - \psi^{\ f}\right) \tag{4.2}$$

where $\varepsilon_1^{\ f}$, $\varepsilon_1^{\ m}$ and $\hat{\varepsilon}_1$ are average strains in the 1st direction in the fibre, matrix and composite, respectively. S^f, S^m, S are, respectively, the areas of the fibre block in the RVE, matrix block in the RVE, and the area of the EVE at which the stress is applied.

The strain energy of the composite must be equal to the strain energy of the homogeneous effective material.

31

$$W_{RVE} = W_{EVE} \tag{4.3}$$

Since the elongation in this case is the same for both constituents in the RVE as well as for the EVE, it is enough to consider the static equilibrium of forces. From the equality of forces acting on the RVE and EVE and using Hooke's law the conventional rule of mixtures can be obtained:

$$\sigma_1{}^f S^f + \sigma_1{}^m S^m = \hat{\sigma}_1 S , \tag{4.4}$$

$$E_1 = E^f \psi^f + E^m \left(1 - \psi^f\right), \tag{4.5}$$

E_1 is the effective longitudinal Young's modulus (in x_1 direction).

Rule of mixtures obtained for the effective Young's modulus in the fibre direction is generally rather accurate and is used in design computations.

4.1.2. Effective transverse modulus

Within the simplified approach, the geometrical compatibility relation is used for load acting in the transversal direction x_2 (see **Fig. 4.1**) of the RVE:

$$\Delta \hat{l}_2 = \Delta l_2{}^f + \Delta l_2{}^m \tag{4.6}$$

where $\Delta \hat{l}_2$, $\Delta l_2{}^f$, $\Delta l_2{}^m$ are the elongations of the EVE and elongations of the fibre block and matrix block in the RVE, respectively, in the x_2 direction.

The simplifying assumption used here is the equality of stresses:

$$\sigma_2{}^f = \sigma_2{}^m = \hat{\sigma}_2 \tag{4.7}$$

With it, and with the Hooke's law, the so called "Inverse Rule of Mixtures" can be obtained from the consideration of the strain energy equality between RVE and EVE:

$$\frac{1}{E_T} = \frac{\psi^f}{E^f} + \frac{1 - \psi^f}{E^m} \tag{4.8}$$

4.1.3. Effective longitudinal shear modulus

To obtain effective in-plane shear modulus G_{IT}, we use the following geometrical relation

$$\hat{\gamma}_{12} = \int_0^h \gamma_{12}(x_2)\,dx_2 \tag{4.9}$$

where $\hat{\gamma}_{12}$ is the shear strain of the resulting EVE and $\gamma_{12}(x_2)$ is the varying shear strain in the RVE section.

Taking into account the assumptions presented above in this section, this relation can be rewritten as

$$\hat{\gamma}_{12} = \psi_f \gamma_{12}{}^f + \psi_m \gamma_{12}{}^m \tag{4.10}$$

We use the equality of the strain energies in the RVE and EVE, where

$$W_{EVE} = \frac{1}{2} h \hat{\tau}_{12} \hat{\gamma}_{12} \tag{4.11}$$

and

$$W_{RVE} = \frac{1}{2}\left(h_f \tau_{12}{}^f \gamma_{12}{}^f + h_m \tau_{12}{}^m \gamma_{12}{}^m \right). \tag{4.12}$$

Where h, h_f and h_m are heights of the RVE, fibre block and matrix block in RVE, respectively (**Fig. 4.1**).

With the assumption of equal stresses in the fibre and matrix $\sigma_{12}{}^f = \sigma_{12}{}^m = \hat{\sigma}_{12} = \sigma_{12}$ and using Hooke's law we obtain

$$W_{EVE} = \frac{1}{2} h \frac{\sigma_{12}{}^2}{G_{1T}} \tag{4.13}$$

$$W_{RVE} = \frac{1}{2} \sigma_{12}{}^2 \left(h_f \frac{1}{G^f} + h_m \frac{1}{G^m} \right) \tag{4.14}$$

After substituting (4.13, 4.14) into equality (4.3) one obtains the effective modulus

$$G_{1T} = \left(\frac{\psi_f}{G^f} + \frac{\psi_m}{G^m} \right)^{-1} \tag{4.15}$$

If the fibre material stiffness is significantly higher than that one of the matrix then the following rough approximation is adopted

$$G_{1T} = \frac{G^m}{\psi_m} = \frac{G^m}{1 - \psi_f} \tag{4.16}$$

4.1.4. Effective major Poisson ratio

The straightforward way to derive the effective Poisson's ratio is as follows. First we use the major definition of Poisson's ratio:

$$\nu_{1T} = \frac{-\varepsilon_2}{\varepsilon_1}, \tag{4.17}$$

where ν_{1T} is the effective Poisson's ratio, ε_1, ε_2 are the strains in the EVE. Poisson's ratios for both isotropic phases are

$$\nu^f = \frac{-\varepsilon_2{}^f}{\varepsilon_1{}^f}, \tag{4.18}$$

$$\nu^m = \frac{-\varepsilon_2{}^m}{\varepsilon_1{}^m}. \tag{4.19}$$

We employ the relation:

$$\varepsilon_2 = \psi_f \varepsilon_2{}^f + \psi_m \varepsilon_2{}^m. \tag{4.20}$$

Consequently, we have

$$\nu_{1T} = \frac{\psi_f \varepsilon_1{}^f \nu_f + \psi_m \varepsilon_1{}^m \nu_m}{\varepsilon_1} \tag{4.21}$$

Since the given elongation in x_1 is known and $\varepsilon_1{}^f = \varepsilon_1{}^m = \varepsilon_1$, we obtain

$$\nu_{1T} = \psi_f \nu_f + \left(1 - \psi_f\right)\nu_m \tag{4.22}$$

In the chapters 8 and 9 of this work, the effective elastic constants for transversely isotropic material are employed without the connection to any specific fibre arrangement in a real composite, only with the purpose of numerical analysis and model verification. Therefore the choice of the material parameters was largely arbitrary, as long as they satisfy the given kinematic constraints (such as incompressibility etc.). In chapters 8 and 9 the convergence of numerical solution is of essence. Therefore the assigned sets of constants should be examined

for applicability: whether they permit numerical stability of the solution. In Li and Barbic [72] the relevant topic is investigated. The authors develop an approach for setting the material constants which insure stability of a subsequent numerical modelling. As a result, certain requirements to the engineering constants are introduced in order to ensure a positive-definite elasticity tensor. For transversely isotropic material, there are only five independent material constants, E_1, E_T, v_{1T}, v_{TT} and G_{1T}. The recommendations for the Poisson's ratios and the proposed formula for the shear modulus are as follows [72]:

$$
\begin{aligned}
v_{1T}{}^2 &< 0.25\frac{E_1}{E_T}, \\
v_{TT} &< 0.5, \\
G_{1T} &= \frac{\sqrt{E_1 E_T}}{2\left(1+\sqrt{v_{1T} v_{T1}}\right)}.
\end{aligned}
\tag{4.23}
$$

4.2.   The inclusion of the fibre bending stiffness parameter

Here we consider modelling of fibre as a beam. Such approach was employed by Fleck and Shu in [31] for the case of microbuckling problem in a composite under compression. In [31] the authors consider the fibres to behave as Timoshenko beams on a microscale which corresponds to the general Cosserat theory material description on a macroscale: the rotation angle of the fibre is independent.

They consider both matrix and fibre elements to behave as Timoshenko beams, undergoing bending, axial extension, and shear deformation.

In the present work, a somewhat different approach is being taken: the constraint Cosserat theory which envolves presence of the couple stress components, but no additional degree of freedom in a homogenized medium. The rotation at any given material point is linked to the derivatives of displacements, as in classical elasticity description. On a substructure scale, such assumption roughly corresponds to the fibre being regarded as a simple beam. Shear deformation of the fibre is neglected, and the cross-section is assumed to remain planar and normal to the fibre axis. To justify this approach, throughout this work the fibres in the composite are considered to be very stiff compared to the matrix material.

The defining geometric relations of the constrained Cosserat theory link the rotational degrees of freedom of the continuum to the displacements derivatives, making thus the rotations dependent. For a two-dimensional case it can be written in the following simple way:

$$\theta_3 = \frac{1}{2}\left(u_{2,1} - u_{1,2}\right)$$
(4.24)

For the present example of fibre-reinforced composite we distinguish between macro-scale and substructure scale. In the previous formula θ_3, u_1, u_2 are characteristics of the point in the homogenised continuum, meaning that they refer to the macro-scale description.

Small linear strains and reinforcement in x_1 only are considered here and further.

4.2.1. Effective constant for the equivalent material

Generally the notation for couple stress components acting on the plane is as shown below:
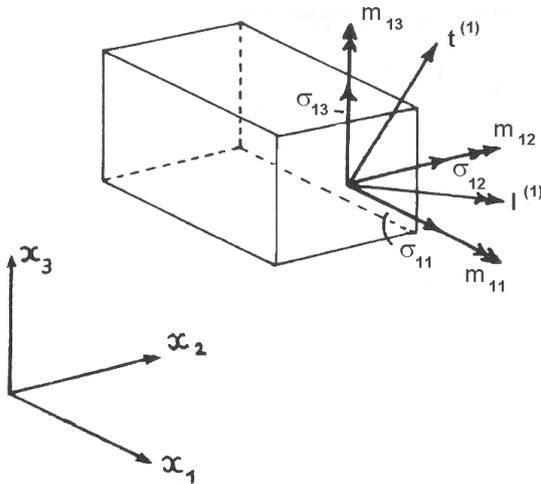
Fig. 4.2. RVE (a, b) (taken from [21])

But in this section only m_{13} is considered (plain strain problem for the unidirectional material). Presently, let us focus on a two-dimensional representative element of the composite, similar to that specified above (**Fig. 4.1**) but with consideration of fibre bending stiffness. We consider the RVE consisting of a fibre element and matrix element; fibre is regarded as a simple beam; matrix material is assumed to be significantly softer. Such approach implies inextensibility of fibres, or the problem formulation in which fibre elongation is negligible.

Below we consider a general stress state of the composite. In **Fig. 4.3** below, the stress components acting on fibre and matrix elements represent an average of the actual stress distribution.
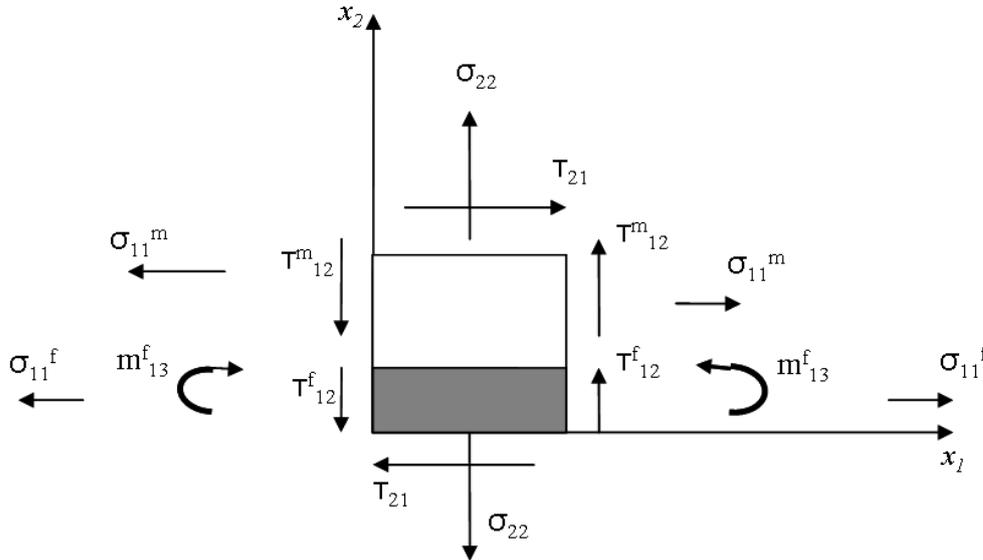
Fig. 4.3. RVE at a substructure scale: resultant loads for each constituent (matrix in the upper part and fibre in the lower part)

The actual stress distribution in the fibre cross-section (**Fig. 4.4**) is linked to the resultant loads in **Fig. 4.3** as follows (by averaging the function throughout the fibre element height):

$$m_{13}{}^f = \frac{1}{h^f} \int_0^{h^f} \tilde{\sigma}_{11}{}^f x_2 dx_2 \tag{4.25}$$

$$\tau_{12}{}^f = \frac{1}{h^f} \int_0^{h^f} \tilde{\tau}_{12}{}^f dx_2 \tag{4.26}$$

$$\sigma_{11}{}^f = \frac{1}{h^f} \int_0^{h^f} \tilde{\sigma}_{11}{}^f dx_2 \tag{4.27}$$
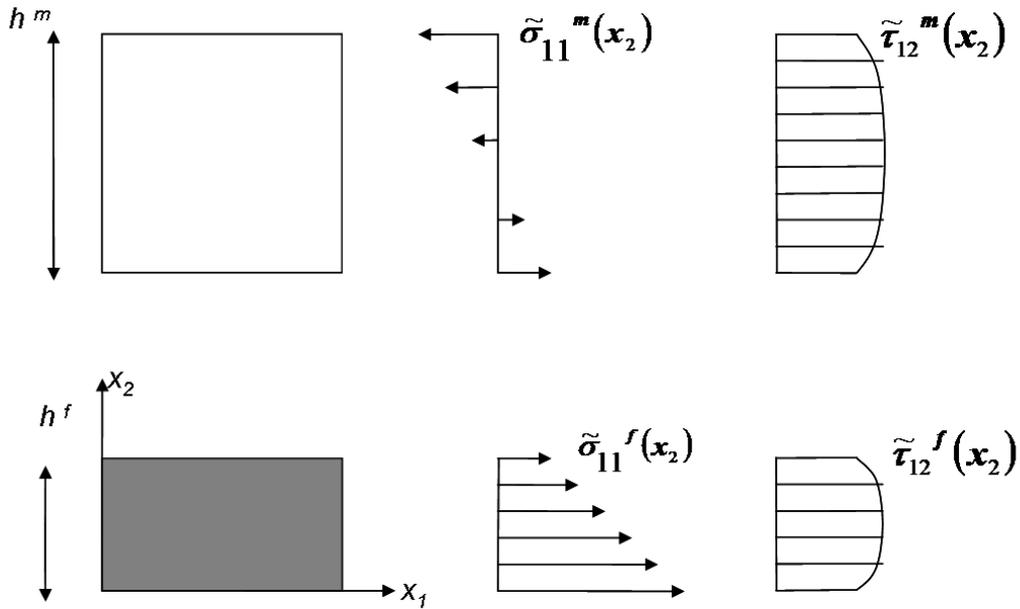
Fig. 4.4. Substructure scale: distributed load for the constituents

If we focus on the normal stress distribution $\tilde{\sigma}_{11}^{f}(x_2)$ acting in the fibre cross-section, we can see that it contains a constant part which corresponds to the resulting traction σ_{11}^{f} and another linear part which corresponds to resulting couple stress m_{13}^{f} (see **Fig. 4.5**)
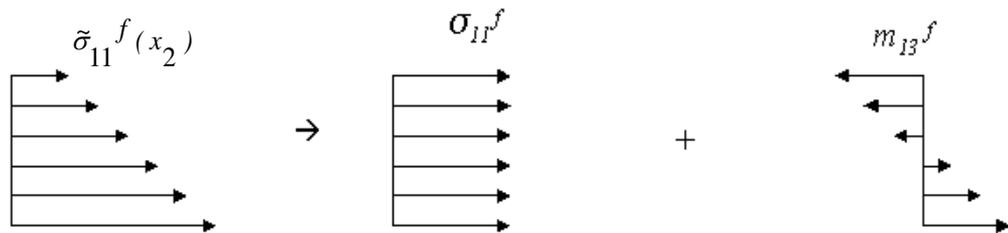
Fig. 4.5. The normal stress distribution and the resulting loads

Now we can transform the real stresses to the equivalent homogenised cell below (**Fig. 4.6**) (by averaging the function throughout the whole representative element hight **h**):

$$m_{13} = \frac{1}{h}\left(\int_{0}^{h^f} \tilde{\sigma}_{11}^{f} x_2 dx_2 + \int_{h^f}^{h} \tilde{\sigma}_{11}^{m} x_2 dx_2 \right) \tag{4.28}$$

$$\tau_{12} = \frac{1}{h}\left(\int\limits_{0}^{h^f} \tilde{\tau}_{12}{}^f dx_2 + \int\limits_{h^f}^{h} \tilde{\tau}_{12}{}^m dx_2 \right) \qquad (4.29)$$

$$\sigma_{11} = \frac{1}{h}\left(\int\limits_{0}^{h^f} \tilde{\sigma}_{11}{}^f dx_2 + \int\limits_{h^f}^{h} \tilde{\sigma}_{11}{}^m dx_2 \right) \qquad (4.30)$$
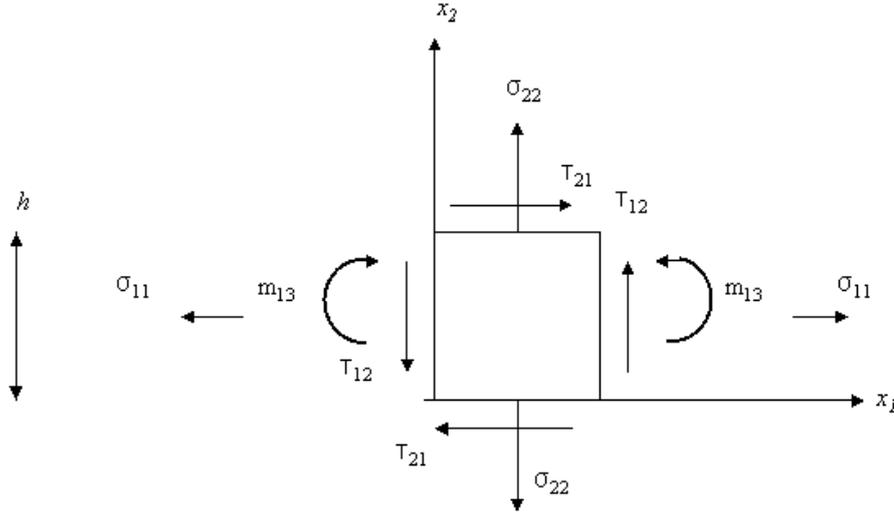
Fig. 4.6. EVE (macro-scale)

The equivalent strains can be obtained by averaging as well, similarly to the equivalent stresses depicted above. In a current desciption, we accept that on the substructure scale the fibres behave as simple beams; on a macro scale (**Fig. 4.6** above) when we consider an equivalent element of the homogenised continuum, the only independent degrees of freedom are displacements.

A more complicated model of the unit cell is used by Fleck and Shu in [31]. There the fibre element is modelled as Timoshenko beam experiencing both bending and shear deformation. Such behaviour on a substructure scale corresponds to the general Cosserat theory with presence of the additional degree of freedom - rotation in the point.

4.2.2. Example

An illustrative example similar to that mentioned in [31] is presented below.

Now we expand the two-dimensional representation to the three-dimensional one. The fibre has a certain shape of the cross-section, and we consider a representative volume element with the associated notation „RVE", containing a fibre element embedded into a matrix block. We also consider an equivalent homogeneous block of material with the associated notation „EVE". The working assumption is that the overall bending moment acting on the block is the same for these two models:

$$M_{13}{}^{EVE} = M_{13}{}^{RVE} \tag{4.31}$$
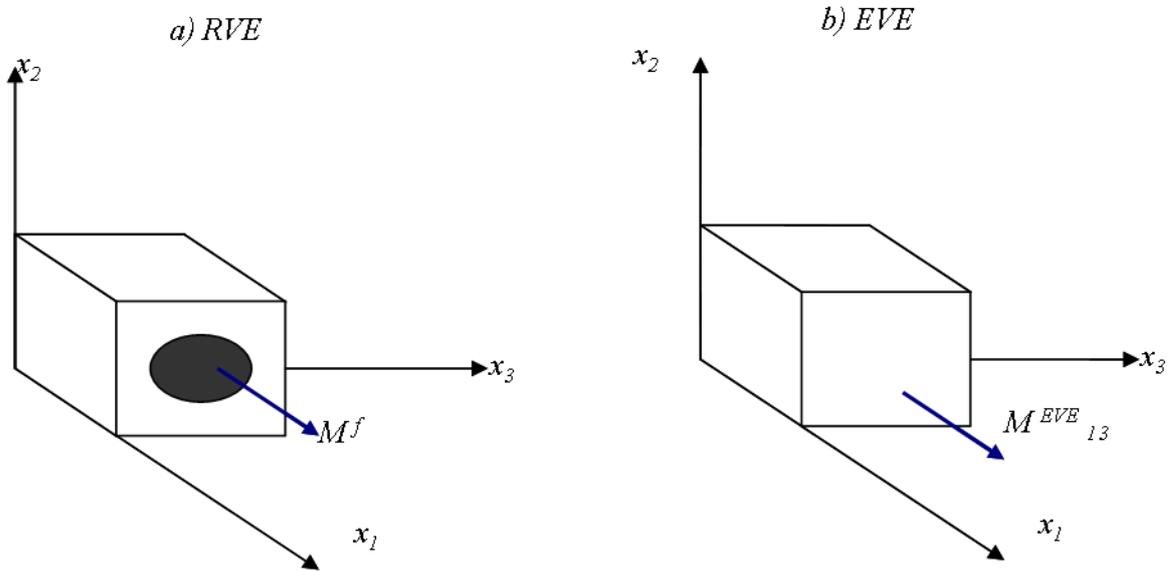
Fig. 4.7 RVE and EVE (3D)

If we consider the bending contribution of the normal stresses in the matrix negligible, the cumulative bending moment in the cross-section on **Fig. 4.7 (a)** equals to the bending moment in the fibre cross-section

$$M_{13}{}^{RVE} = M^{f} \tag{4.32}$$

Since we consider the representative element of the equivalent homogeneous material (EVE) in **Fig. 4.7 (b)** to be under uniform shear stress and uniform couple-stress loading, we can state that

$$M_{13}{}^{EVE} = m_{13}S , \tag{4.33}$$

where S is the area of couple-stress action (the whole cross-section).

$$m_{13} = \frac{M^f}{S}.$$ (4.34)

If we consider fibre with curvature k_f, the second moment of the cross-section J_f and volume fraction ψ_f then the following is true

$$m_{13} = \frac{E_f J_f \psi_f}{S_f} k_f.$$ (4.35)

where the expression $\dfrac{E_f J_f \psi_f}{S_f}$ is a material constant for EVE, linking the couple stress and associated fibre curvature. This expression is obtained from the RVE properties. This is a very rough approach, mainly for illustration purpose.

Fleck and Shu in [31] obtain this relation for the case of microbuckling (caused by initial alignment imperfections of fibre), and for the round shape fibre the formula is $m_{13} = \dfrac{E_f \psi_f d^2}{16} k_f$, where d is the fibre diameter.

We use a condition of equality of the bending moments in the cross-section to obtain effective properties of the equivalent homogeneous unit cell. This is a simplified approach. The general approach should consider the equality of the strain energies.

4.2.3. Notes on the constitutive model

Here and below a two-dimensional problem is considered for simplicity.

The general definition of the rotation vector in the point is

$$\theta_i = \frac{1}{2} \epsilon_{ijk} u_{k,j}$$ (4.36)

Within a two-dimensional problem only one component (4.24) of the rotation vector is used:

$$\theta_3 = \frac{1}{2}(u_{2,1} - u_{1,2})$$

Throughout this work, the following kinematic tensor quantities are used ([2], [6]) for the general case of large strains:

$$G_{iJ} = \frac{\partial(F_{iR} A_R)}{\partial X_J}, \tag{4.37}$$

$$\Lambda_{RS} = F_{iR} G_{iS}, \tag{4.38}$$

with A being fibre direction unit vector.

The tensor quantity G can be decomposed as follows [6]:

$$G_{iR} = k_{iR} + \frac{\partial A_i}{\partial X_J}, \tag{4.39}$$

where the tensor quantity k was introduced by Soldatos [6] as "curvature-strains" of the fibre:

$$k_{iR} = u_{i,RP} A_P + u_{i,P} A_{P,R}. \tag{4.40}$$

For the particular case of small strains and initially straight fibres (for instance, $A=(1,0,0)^{\mathrm{T}}$) the components of interest are:

$$\begin{aligned} k_{21} &= u_{2,11}, \\ k_{31} &= u_{3,11}, \end{aligned} \tag{4.41}$$

which are, essentially, curvatures of the implied fibre in two different planes. If the fibre is considered as a simple beam, the above components can be regarded as the curvatures of the beam axis.

We keep in mind that the material model in consideration is based on the assumption of a homogenous anisotropic continuum in which fibres are represented by mathematical curves possessing a certain bending stiffness. The specificity of this continuum is that couple-stress is produced by this curve resisting to bending and therefore is directly related to the above components of the k tensor (4.41) as follows (in linear case) [2]:

$$\begin{aligned} m_{12} &= -d_{31} \cdot k_{31}, \\ m_{13} &= d_{13} \cdot k_{21} \end{aligned} \tag{4.42}$$

The work contribution done by couple stress in the element of such continuum is

$$W = \iiint\limits_V \overline{m}_{12} \cdot d \cdot \frac{\partial \theta}{\partial x_1} dV \quad \text{where } \theta \text{ is the general formula from (4.24).}$$

5. Composites reinforced with fibres resistant to bending: mathematical model for large strains and its implications

5.1. Adopted kinematics and balance laws

We adopt Cartesian coordinate system $Ox_1x_2x_3$. In a conventional manner, a material point with position vector $\mathbf{X}$ in the reference configuration moves to the position $\mathbf{x}$ of the deformed configuration. In the notation applied below, boldface denotes a tensor or vector; uppercase letter and lowercase letter indices are associated with the reference and deformed configurations, respectively. Subscripts vary from one to three and Einstein's summation convention applies for repeated indices unless stated otherwise.

Within the framework of constrained Cosserat theory a quasi-static problem is considered. The spin vector $\boldsymbol{\omega}$ is not independent but related to the displacement rate vector $\boldsymbol{v}$ in the following way:

$$\omega_i = \frac{1}{2}\in_{ijk}\frac{\partial v_k}{\partial x_j},\tag{5.1}$$

where $\in_{ijk}$ represents the Levi-Civita operator. Deformation gradient tensor $\mathbf{F}$ and right Cauchy-Green deformation tensor $\mathbf{C}$ are given by:

$$F_{iR} = \frac{\partial x_i}{\partial X_R},\tag{5.2}$$

$$C_{KL} = F_{iK}F_{iL}.\tag{5.3}$$

For a unidirectional fibre-reinforced composite, unit vector fields $\mathbf{A}(\mathbf{X})$ and $\mathbf{a}(\mathbf{X})$ define fibre directions in reference and deformed configurations, respectively. Conventional kinematics has to be enhanced in order to account for fibre bending stiffness. Adopting theoretical framework proposed in [2], additional second grade kinematical quantities are to be introduced. On the basis of the vector $\boldsymbol{b}$

$$b_i = F_{iR}A_R,\tag{5.4}$$

deformed fibre gradient tensor $\mathbf{G}$ and tensor $\boldsymbol{\Lambda}$ are defined as follows:

$$G_{iJ} = \frac{\partial b_i}{\partial X_J},\tag{5.5}$$

$$\Lambda_{RS} = F_{iR}G_{iS}.\tag{5.6}$$

As we endow the material point with bending stiffness, additional stress measures are to be employed in the form of moments per unit area. These measures are generally referred to as "couple stresses". Cauchy stress tensor is no longer symmetric due to the presence of couple stresses. This interconnection is obvious from the equations of equilibrium (body forces and body couples are absent):

$$\frac{\partial \sigma_{ji}}{\partial x_j} = 0 \quad , \tag{5.7a}$$

$$\frac{\partial m_{ji}}{\partial x_j} + \in_{ijk} \sigma_{jk} = 0 \tag{5.7b}$$

where $\boldsymbol{\sigma}$ and $\boldsymbol{m}$ are Cauchy stress tensor and couple stress tensor, respectively.

For the sake of further computations the stress tensor can be decomposed into symmetric and antisymmetric parts:

$$\sigma_{ij} = \sigma_{(ij)} + \sigma_{[ij]} \tag{5.8}$$

The couple stress tensor can be decomposed into the deviatoric and spherical parts [2]:

$$m_{kl} = \overline{m}_{kl} + \frac{1}{3}\delta_{kl}m_{ii} \tag{5.9}$$
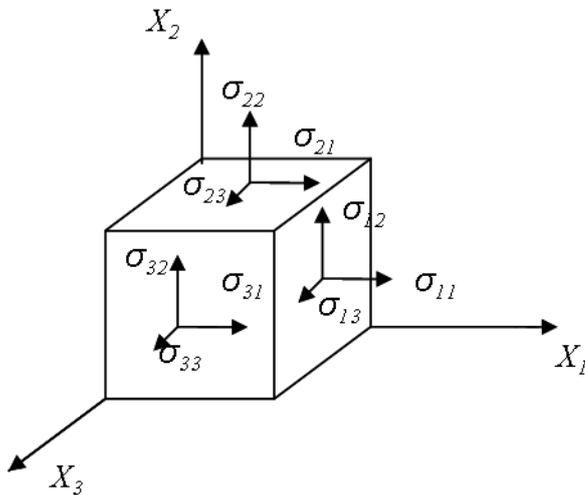
Fig. 5.1. Components of the stress tensor

44
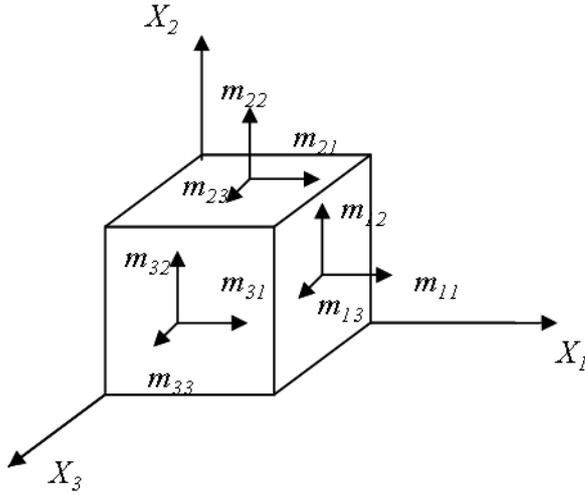
Fig. 5.2. Components of the couple stress tensor

If we assume the elementary volume is transversely isotropic with the direction x_1 representing the direction of reinforcement, the couple stress m_{11} would correspond to the torsion moment acting on the fictitious fibre (and the "twist mode"), m_{23} and m_{32} would correspond to the "splay mode" and, finally, only m_{13} and m_{12} correspond to the bending moment acting on the fibre (m_{13} would cause bending in the x_1x_2 plane, m_{12} would cause bending in the x_1x_3 plane) [2]. For the current model representing the influence of thick and stiff fibres in a unidirectional composite, only the m_{13} and m_{12} components are of interest. Here are mathematical consequences of the chosen constitutive model:

- in the strain energy density an additional deformation invariant is included that reflects the bending mode of deformation of fibres;
- an additional material constant is introduced that corresponds to this invariant (the physical meaning of such constant will be discussed later);
- the resulting stresses and couple stresses are derived by differentiation of the strain energy with respect to the respective deformation measures;
- only those couple stresses that refer to bending moment will be left non-zero.

5.2. Constitutive formulation within couple stress theory

5.2.1. Form of strain-energy density

Conventional form of the strain energy density for hyperelastic materials with one family of fibres is function of the right Cauchy-Green deformation tensor **C** and fibre direction vector **A**.

In order to include the effect of gradients of the deformed fibre direction into the mathematical framework, Spencer and Soldatos [2] proposed the strain energy density being, in addition, a function of tensor $\boldsymbol{\Lambda}$ (introduced by Eq. (5.6)). This function is introduced by means of 33 specific invariants of the above tensors $\mathbf{C}$, $\boldsymbol{\Lambda}$ and vector $\mathbf{A}$ on the basis of canonical forms presented by Zheng [74]. However, these 33 independent invariants lead to excessively complicated constitutive equations. To simplify this theory, Spencer and Soldatos propose to assume that the strain energy depends on one directional derivative of the fibre vector only, namely that in the fibre direction representing the curvature of fibres. This assumption implies the dependence on the tensor $\boldsymbol{\Lambda}$ is replaced by dependence on the vector $\mathbf{K}$ with components $K_R = \Lambda_{RS}A_S$. With this restriction the amount of invariants decreases from 33 to 11 having the following forms and physical dimensions:

$$I_1 = tr\boldsymbol{C}, \; [-]$$

$$I_2 = \frac{1}{2}\left\{(tr\boldsymbol{C})^2 - tr\boldsymbol{C}^2\right\}, \; [-]$$

$$I_3 = det\boldsymbol{C}, \;\; [-]$$

$$I_4 = \boldsymbol{ACA}, \; [-]$$

$$I_5 = \boldsymbol{AC^2A}, \; [-]$$

$$I_6 = \boldsymbol{A\Lambda^T \Lambda A}, \; [m^{-2}] \qquad\qquad (5.10)$$

$$I_7 = \boldsymbol{A\Lambda^T C \Lambda A}, \; [m^{-2}]$$

$$I_8 = \boldsymbol{A\Lambda^T C^2 \Lambda A}, \;\; [m^{-2}]$$

$$I_9 = \boldsymbol{A \Lambda A}, \; [m^{-1}]$$

$$I_{10} = \boldsymbol{AC \Lambda A}, \; [m^{-1}]$$

$$I_{11} = \boldsymbol{AC^2 \Lambda A}. \; [m^{-1}]$$

However, the strain energy density, as function of all the 11 above invariants, still yields excessively complicated constitutive equations.

5.2.2. Constitutive equations for stresses and couple stresses

It should be noted that only the symmetric part of Cauchy stress tensor generates work upon deformation [2]. Analogously, if we decompose couple stress tensor into spherical and deviatoric parts, only its deviatoric components contribute to the energy balance equation. Antisymmetric components of Cauchy stresses can be derived from (5.7b), while spherical components of the couple stresses remain indeterminate within the framework of couple stress theory [75].

Constitutive equations are formulated by Spencer and Soldatos [2] for the symmetric part of Cauchy stress and for the deviatoric part of couple stress as follows:

$$\sigma_{(ij)} = \frac{\rho}{\rho_0}\left[F_{iR}F_{jS}\left(\frac{\partial W}{\partial C_{RS}} + \frac{\partial W}{\partial C_{SR}} \right) + \left(G_{iR}F_{jS} + G_{jR}F_{iS} \right)\frac{\partial W}{\partial \Lambda_{SR}} \right], \qquad (5.11a)$$

$$\overline{m}_{ji} = \frac{2}{3}e_{ikm}\frac{\rho}{\rho_0}\frac{\partial W}{\partial \Lambda_{PR}}F_{mP}\left(F_{jR}b_k + F_{kR}b_j \right) \qquad (5.11b)$$

where $\rho_0/\rho = J$ is volume ratio. The detailed derivation of the equations based on the energy balance equation can be found in [2].

In accordance with equilibrium equations, the anti-symmetric part of the stress is defined by the following equation [6]:

$$\sigma_{[ij]} = \frac{1}{2}\in_{kji}\frac{\partial m_{lk}}{\partial x_l}. \qquad (5.12)$$

5.3. Choice of the specific form of the model – slightly compressible material

5.3.1. Introduction of the modified invariants

To construct computationally applicable strain energy form suited for the rubber-like composites reinforced with stiff fibres, simplifying assumptions were employed by Lasota [3]. The strain energy density W was restricted to be at most quadratic function of the components of Λ. Such assumption, as pointed out in [2], implies that the fibre radius of curvature is large compared to the substructure dimensions (fibre diameters or fibre spacing). To reduce the amount of invariants, the coupling between Λ and C is ignored. For simplicity the strain energy density function is chosen to contain only one additional invariant accounting for the bending stiffness of fibres.

To reduce numerical difficulties in finite element simulation it is advantageous to perform multiplicative decomposition of deformation gradient [76], [3]:

$$\boldsymbol{F} = J^{1/3}\overline{\boldsymbol{F}}, \qquad \Rightarrow \qquad \boldsymbol{C} = J^{2/3}\overline{\boldsymbol{C}}. \qquad (5.13)$$

where $\overline{\boldsymbol{F}}$ and $\overline{\boldsymbol{C}} = \overline{\boldsymbol{F}}^T\overline{\boldsymbol{F}}$ are associated with volume-preserving (distortional) deformation of the material. Tensors $\overline{\boldsymbol{F}}$ and $\overline{\boldsymbol{C}}$ will be referred to as the modified deformation gradient tensor and modified right Cauchy-Green tensor, respectively [76].

Multiplicative decomposition was extended to second gradient kinematics by Lasota [3], as outlined below. First the modified tensor $\overline{\boldsymbol{G}}$ is introduced:

$$\overline{G}_{iJ} = \frac{\partial \overline{b}_i}{\partial X_J} = \frac{\partial \left(\overline{F}_{iR} A_R\right)}{\partial X_J}. \tag{5.14}$$

Modified tensor $\overline{\Lambda}$ is introduced by the formula

$$\overline{\Lambda}_{RS} = \overline{F}_{iR}\overline{G}_{iS}. \tag{5.15}$$

Modified invariants can be introduced on the basis of the above modified tensors. Model, proposed by Lasota, retains for simplicity only few invariants from (5.10) and has the following form:

$$W = k_1\left(\overline{I}_1 - 3\right) + k_2\left(\overline{I}_4 - 1\right)^2 + k_9\overline{I}_9{}^2 + \frac{1}{d}(J-1)^2. \tag{5.16}$$

where

$$\overline{I}_1 = \overline{C}_{AA} = J^{-2/3}C_{AA}, \tag{5.17}$$

$$\overline{I}_4 = A_B\overline{C}_{CB}A_C = J^{-2/3}A_BC_{CB}A_C, \tag{5.18}$$

$$\overline{I}_9 = A_B\overline{\Lambda}_{CB}A_C = J^{-2/3}\left(A_B\Lambda_{CB}A_C - \frac{1}{3}I_4G_{kO}F_{Ok}^{-1}\right). \tag{5.19}$$

In (5.16) invariant $\overline{I}_9$ is present in square due to the requirement of the energy density W being an even function of tensor $\overline{\Lambda}$.

In the present work the form of the energy density is modified and the invariant $\overline{I}_6$ is included instead of the invariant $\overline{I}_9$ in the following way:

$$\overline{I}_6 = A_B\overline{\Lambda}_{OB}\overline{\Lambda}_{OC}A_C = J^{-4/3}\Big(A_B\Lambda_{OB}\Lambda_{OC}A_C -$$
$$-\frac{1}{3}F_{OK}^{-1}G_{KO}A_LC_{LR}\left(A_S\Lambda_{RS}F_{OK}^{-1}G_{KO} + A_N\Lambda_{RN} - \frac{1}{3}G_{BC}F_{CB}^{-1}A_OC_{OR}\right)\Big), \tag{5.20}$$

$$W = k_1\left(\overline{I}_1 - 3\right) + k_2\left(\overline{I}_4 - 1\right)^2 + k_3\overline{I}_6 + \frac{1}{d}(J-1)^2. \tag{5.21}$$

Through the invariant $\overline{I}_6$ the energy potential relates directly to the fibre curvature and serves to introducing the bending mode of fibre deformation into the model; the previously used invariant $\overline{I}_9$ equals to zero in the pure bending deformation.

Similarly to model eq. (5.16) formulated by Lasota, the anisotropic term *(I₄-1)* can occur in *W* only through its squares [77] to ensure positive strain energy contribution when the fibres are compressed. The strain energy density must be at least quadratic in the components of either **F** or **G** [46]. The coefficients represent material parameters: k_1 is related to properties of the matrix (neo-Hooke model), k_2 and k_3 relate to the tensile and bending stiffness of the medium in the direction of reinforcement, respectively; *d* relates to the material compressibility.

The invariant $\bar{I}_6$ relates directly to the fibre curvature and serves to introduce bending mode of fibre deformation into the model, as it will be illustrated by the linearised case, while the previously used invariant $\bar{I}_9$ contributes to the so called "splay mode" of fibre deformation [2] and not to the bending mode. Another advantage of the choosing $\bar{I}_6$ over $\bar{I}_9$ is due to the fact that – within the linear beam theory – the presence of $\bar{I}_6$ yields a simple relation between the curvature of the beam (and the underlying fibres) and the couple stresses contributing to the bending moment in the beam cross-section (see Section 4.4). Another important reason for modifying the form of energy density function is that the coefficient k_9 from (5.16) does not appear in the corresponding constitutive equations for couple stresses [2] in linearised form.

Let's now introduce symmetric Kirchhoff (force, i.e. classical) stress $\tau_{(ij)}$ and deviatoric Kirchhoff couple stress $\bar{\mu}_{ij}$:

$$
\begin{aligned}
\tau_{(ij)} &= J\sigma_{(ij)} \\
\bar{\mu}_{ij} &= J\bar{m}_{ij}.
\end{aligned}
\tag{5.22}
$$

According to (5.11a, b) and (5.21), the constitutive equations acquire the form:

$$
\begin{aligned}
\tau_{(ij)} = 2F_{iR}F_{jS}J^{-2/3}&\left[k_1\left(\delta_{SR} - \frac{1}{3}C^{-1}_{RS}C_{AA} \right) + 2k_2\left(\bar{I}_4 - 1\right)\left(A_R A_S - \frac{1}{3}C^{-1}_{RS}A_B C_{CB}A_C \right) + \right. \\
&\left. + \frac{1}{d}(J - 1)C^{-1}_{RS}J^{-3/2} \right] + k_3\left[F_{iR}F_{jS}\left(\frac{\partial \bar{I}_6}{\partial C_{RS}} + \frac{\partial \bar{I}_6}{\partial C_{SR}} \right) + \left(G_{iS}F_{jR} + G_{jS}F_{iR} \right)\frac{\partial \bar{I}_6}{\partial \Lambda_{RS}} \right].
\end{aligned}
\tag{5.23a}
$$

$$
\bar{\mu}_{ji} = \frac{2}{3}e_{ikm}k_3 \frac{\partial \bar{I}_6}{\partial \Lambda_{PR}} F_{mP}\left(F_{jR}b_k + F_{kR}b_j \right).
\tag{5.23b}
$$

5.3.2. Correlation between the invariants and deformation modes of fibres

For the purpose of elucidation it makes sense to trace the correlation between the additional invariants included in the strain energy function, the resulting constitutive equations and the corresponding physical meaning. It is done below for the case of energy function (5.21) and small strain conditions (within linearised theory).

Here we evoke the notation employed in [2]. In the general case of the theory presented in [2] a complete list of 33 invariants is introduced denoted as I_1 - I_{33} (such notation is different from and not consistent with that employed in eq. (5.10) above). The invariant $A\Lambda^T\Lambda A$ can be expressed via some of those 33 invariants as follows [2]:

$$A\Lambda^T\Lambda A = I_{21} - I_{22} + 2I_{27}. \tag{5.24a}$$

$$I_{21} = A\Lambda_S^{\ 2}A \ , \tag{5.24b}$$

$$I_{22} = A\Lambda_a^{\ 2}A , \tag{5.24c}$$

$$I_{27} = A\Lambda_S\Lambda_a A \ , \tag{5.24d}$$

where Λ_S and Λ_a are the symmetric and antisymmetric parts of tensor Λ. The expression $A\Lambda^T\Lambda A$ corresponds to the invariant denoted as I_6 in (5.10).

In order to verify the formulas employed in the present work, we establish relations between alternative notations used for the following material parameters:

- k_3 parameter from (5.21) represents additional bending stiffness of the homogenised material with respect to the reinforced direction within the large strain framework;

- parameters b_5, b_6, b_7 below refer also to the additional bending stiffness; they represent coefficients in the linear combination of general invariants [2] as shown in (5.24a) and further, in the expression for the strain energy function);

- d_{31} is the additional bending stiffness parameter that refers to the influence of fibres (it links directly the respective couple stress and fibre curvature as shown below)

The general form of strain energy density formulated in Section 9 of [2] contains, among others, the following members:

$$W = ... + \tilde{b}_5 I_{21} + \tilde{b}_6 I_{22} + \tilde{b}_7 I_{27}. \tag{5.25}$$

For comparison, in the present work we choose the additional term of the strain energy density to be $k_3 I_6$ (before multiplicative decomposition of the deformation gradient):

$$W = ... + k_3 I_6.$$

It means that the constant k_3 relates to $\tilde{b}_5, \tilde{b}_6, \tilde{b}_7$ in the following way:

$$\begin{aligned} \tilde{b}_5 &= k_3, \\ \tilde{b}_6 &= -k_3, \\ \tilde{b}_7 &= 2k_3. \end{aligned} \tag{5.26}$$

In this case it holds in accordance with [2]

$$d_{31} = \frac{1}{3}\left(\tilde{b}_5 - 3\tilde{b}_6 + 2\tilde{b}_7\right), \tag{5.27}$$

And the linearised relations for the nonzero couple stresses are given as follows [2]:

$$\begin{pmatrix} m_{12} \\ m_{13} \end{pmatrix} = \begin{pmatrix} -d_{31} & 0 \\ 0 & d_{13} \end{pmatrix} \begin{pmatrix} \partial^2 u_3 / \partial x_1^2 \\ \partial^2 u_2 / \partial x_1^2 \end{pmatrix} \tag{5.28}$$

which correspond to the "bending mode of deformation". Consequently, the addition of the invariant I_6 (or its modified form $\bar{I}_6$) to the strain energy density function serves to account for the strain energy accumulated in the composite due to bending of fibres of the substructure.

5.4. Identification of material parameters for the simple beam case

Generally, two main classical approaches exist for determination of the effective overall properties of the heterogeneous materials – average-field theory and homogenization theory (multiscale perturbation method) [79]. Within the average–field theory the effective properties are determined as relations between the volume averages of the microstresses and microstrains within periodically repeated RVE.

In case of a strictly periodic fibre arrangement the unit cell serves as a representative of material (RVE). If the substructure possesses symmetry, it can be used as well in the relevant boundary value problem.

Classical homogenization techniques are based on Cauchy description at both micro- and macro-scales. Classical theory holds an assumption that the size of the microstructural components is negligible with respect to the macrostructure. In the present work, such

assumption is not sustained: the so called "polar theory" [6] employed here for constitutive modelling of fibre composites becomes relevant when the fibre thickness becomes comparable to the size of the composite structure.

The applicable scheme of determination of the effective material constants for the specific new model is the matter of the current and future studies. Considerations of low computational cost and sufficient simplicity are essential. As a result, new homogeneous model with the effective material properties should correctly mimic the response of the given composite under both tension and bending loads.

5.4.1. Couple stress theory for the planar problem

For illustration, let us consider an elementary volume in equilibrium for a planar problem (**Fig. 5.3**). In accordance with balance equations (5.7b) the following holds in the given undeformed coordinates:

$$-\sigma_{13} + \sigma_{31} + \frac{\partial m_{12}}{\partial X_1} + \frac{\partial m_{22}}{\partial X_2} + \frac{\partial m_{32}}{\partial X_3} = 0 \qquad (5.29)$$
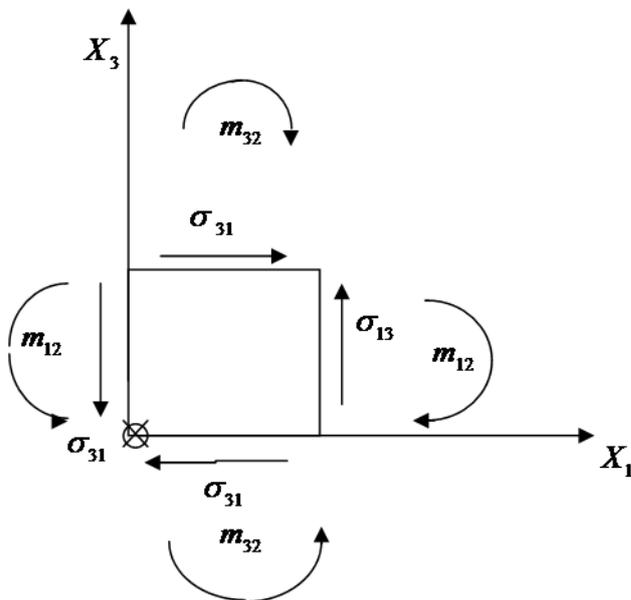
Fig. 5.3 Positive directions of shear stresses and couple stresses in a planar problem

Let us consider a beam undergoing pure bending around X_2 axis. **Fig.5.4** presents schematically inner resultants acting in the section of the beam and depicts (for the given coordinate system) normal stress distribution contributing to a positive value of the classical moment M_2 and positive direction of the couple stresses.
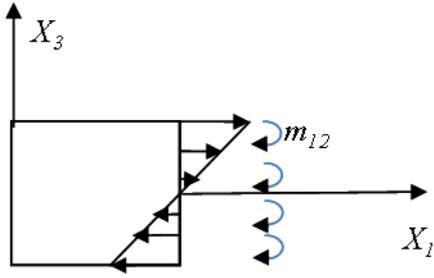
Fig. 5.4. Stress and couple stress distribution in pure bending.

For the case of small linear strains, we operate with displacements u_i and rotations

$\theta_i = \dfrac{1}{2} \in_{ijk} \dfrac{\partial u_k}{\partial x_j}$ instead of displacement rates and spins.

The overall bending moment in the beam cross-section in the chosen coordinate system can be calculated as

$$M_2{}^{full} = \iint\limits_S \left(\sigma_1 x_3 + m_{12}\right) dx_2 dx_3, \tag{5.30}$$

$$M_2{}^{full} = M_2 + \iint\limits_S m_{12} dx_2 dx_3, \tag{5.31}$$

where double integration is done throughout the cross section S.

5.4.2. Discrepancy between heterogeneous and homogeneous models in bending

Let us consider linear elastic behaviour of a composite beam with one family of fibres aligned along the beam axis. Such a specimen can be modelled as a heterogeneous structure characterized by elastic constants of constituents and a specific arrangement and size of fibres. Also, it can be modelled using a homogenized anisotropic (transversely isotropic) hyperelastic or even linear elastic model. In this case the tensile stiffness of the specimen in the preferred direction is uniformly "smeared-out" throughout the section of the model. The corresponding elastic modulus in the direction of fibres can be obtained by the rule of mixtures:

$$E_{\text{hom}} = \left(1 - \psi_f\right) E_m + \psi_f E_f, \tag{5.32}$$

where ψ_f is the volume fraction of fibres. As it can be seen from (5.32), the homogeneous model is characterized by elastic constants of constituents and their volume fractions only, with no regard to disposition and distribution of fibres in the given composite.

Let us compare the pure bending behaviour of these two beam models. If the heterogeneous model is subjected to bending along the fibres, we can express the overall bending moment in the section as $M_2 = D_{het} k^{pure}$, where $k^{pure} = -\dfrac{\partial^2 u_3}{\partial x_1^2}$ is the curvature of the beam, D_{het} is the bending stiffness of the model along the preferred direction:

$$D_{het} = E_m J_m + E_f J_f \ , \tag{5.33}$$

where J_m and J_f are overall moments of inertia of the sections of matrix and fibres, respectively, with respect to the principal central axis of the whole beam section.

If the homogeneous model is subjected to bending along the direction of the reinforcement, we can express the overall bending moment in the section as $M_2 = D_{hom} k^{pure}$, where D_{hom} is the bending stiffness of the homogeneous model:

$$D_{hom} = E_{hom} J \tag{5.34}$$

where J is the moment of inertia of the whole cross-section of the beam.

If we substitute E_{hom} from (5.32) we obtain

$$D_{hom} = \left(\left(1 - \psi_f\right)E_m + \psi_f E_f\right)J \tag{5.35}$$

If we compare (5.33) and (5.35) it is obvious that the homogenized model cannot successfully simulate bending behaviour of the heterogeneous model. The bending stiffness D_{hom} takes into account volume fraction of fibres and properties of the constituents only but does not include moments of inertia of constituents. By replacing the heterogeneous model with a transversely isotropic homogeneous one we preserve the same tensile stiffness but not the same bending response, as illustrated in **Fig. 5.5**.
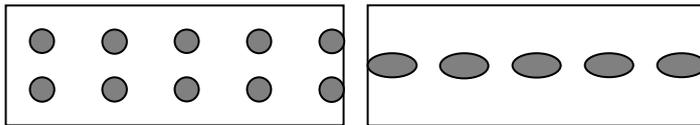
Fig. 5.5a, b Sections of the models with the same value of D_{hom} but different D_{het}

54

Bending stiffness D_{hom} can be larger or smaller than the actual stiffness D_{het} of the corresponding heterogeneous model, depending on the distribution of the fibres with respect to the neutral plane (middle plane in case of symmetrical cross-section). A homogeneous model which describes bending behaviour in better accordance with the heterogeneous one can be formulated using couple stress theory.

5.4.3. Parameter k_3 for the fibre reinforced incompressible material

We continue to consider a beam reinforced by parallel fibres subjected to pure bending with respect to X_2 axis (**Fig. 5.6**). For simplicity, material incompressibility is assumed.
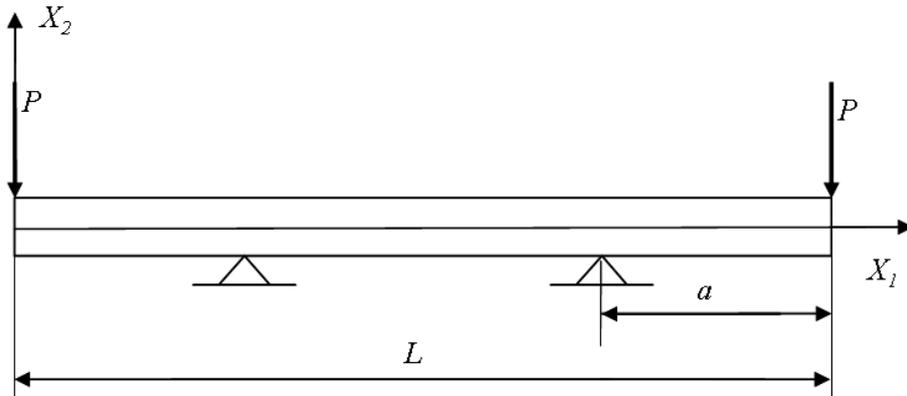
Fig. 5.6. The beam in the reference configuration

In the case when fibres are initially aligned along the X_1 direction, it holds from eq. (5.14, 5.15) in general:

$$A = \begin{pmatrix} 1 \\ 0 \\ 0 \end{pmatrix} \tag{5.36}$$

$$F = \begin{pmatrix} 1 + \dfrac{\partial u_1}{\partial X_1} & \dfrac{\partial u_1}{\partial X_2} & \dfrac{\partial u_1}{\partial X_3} \\ \dfrac{\partial u_2}{\partial X_1} & 1 + \dfrac{\partial u_2}{\partial X_2} & \dfrac{\partial u_2}{\partial X_3} \\ \dfrac{\partial u_3}{\partial X_1} & \dfrac{\partial u_3}{\partial X_2} & 1 + \dfrac{\partial u_3}{\partial X_3} \end{pmatrix} \tag{5.37}$$

$$b = \begin{pmatrix} 1 + \dfrac{\partial u_1}{\partial X_1} \\ \dfrac{\partial u_2}{\partial X_1} \\ \dfrac{\partial u_3}{\partial X_1} \end{pmatrix} \tag{5.38}$$

55

Overall bending moment M^{full} acting in the cross-section of the model is given by Eq. (5.31). The constitutive relations for an incompressible material given in the general form are

$$\sigma_{(ij)} = \left[F_{iR}F_{jS}\left(\frac{\partial W}{\partial C_{RS}} + \frac{\partial W}{\partial C_{SR}} \right) + \left(G_{iR}F_{jS} + G_{jR}F_{iS} \right)\frac{\partial W}{\partial \Lambda_{SR}} \right] + p\delta_{ij},$$

$$\overline{m}_{ji} = \frac{2}{3} e_{ikm} \frac{\partial W}{\partial \Lambda_{PR}} F_{mP}\left(F_{jR}b_k + F_{kR}b_j \right)$$

$$(5.39a, b)$$

where p is hydrostatic pressure. In this case it holds for the energy density

$$W = \frac{\mu}{2}\left(I_1 - 3 \right) + k_2\left(I_4 - 1 \right)^2 + k_3 I_6 \qquad (5.40)$$

where unmodified invariants I_1, I_4, I_6 can be used.

Let us linearise constitutive relations (5.39a, b) for the case of small strains. The basic assumption is that all partial derivatives of displacements are much smaller than one. If we follow the notation of [2] we can state that all $\dfrac{\partial u_i}{\partial x_j}$ are of the order of magnitude $O(e)$. Consequently the strain energy density W has to be of the order $O(e^2)$ and the terms of higher order can be discarded.

Symmetric stresses have to be of order $O(e)$. If we leave out higher order terms in (5.39a), the following expression is left:

$$\sigma_{(ij)} = \frac{\partial W}{\partial C_{ij}} + \frac{\partial W}{\partial C_{ji}} + \delta_{ij} p. \qquad (5.41)$$

It should be noted that if no volumetric deformation occurs, and we use strain energy density function such as (5.40), in which no coupling between C and Λ is present, the symmetric stresses (5.41) do not depend on the fibre curvature. Therefore the expressions for normal stresses are identical with those in the classical (Cauchy) theory of transversely isotropic materials. If we compute $\sigma_{(11)}$ for the case of bending of the beam along the fibre direction using (5.40) and (5.41) and then linearise to the order of magnitude $O(e)$, we obtain

$$\sigma_{(11)} = \left(3\mu + 8k_2 \right)\varepsilon_{11} + p, \qquad (5.42)$$

where ε_{11} is tensile strain and $\left(3\mu + 8k_2 \right)$ is equivalent of Young's modulus of the material in the preferred direction. We can rewrite it as

$$\sigma_{(11)} = E_{hom}\varepsilon_{11} + p \tag{5.43}$$

If shear is absent and plane X_1 X_2 coincides with the neutral plane of the beam, the longitudinal strain ε_{11} is expressed via curvature k as $\varepsilon_{11} = k^{pure} \cdot X_3$, where $k = -\dfrac{\partial^2 u_3}{\partial x_1^2}$. Then we can rewrite Eq. (5.43) as

$$\sigma_{(11)} = E_{hom}k^{pure}X_3 + p \tag{5.44}$$

Now let us consider deviatoric couple stresses. For the given problem we have

$$I_6 = \Lambda_{11}^2 + \Lambda_{21}^2 + \Lambda_{31}^2 \tag{5.45}$$

$$\frac{\partial I_6}{\partial \Lambda_{i1}} = 2\Lambda_{i1}, \tag{5.46}$$

Relation (5.6) gives

$$\Lambda_{31} = F_{13}\frac{\partial^2 u_1}{\partial X_1^2} + F_{23}\frac{\partial^2 u_2}{\partial X_1^2} + F_{33}\frac{\partial^2 u_3}{\partial X_1^2}. \tag{5.47}$$

If we assume small strains and consider only bending with respect to axis X_2, it holds

$$\Lambda_{31} = F_{33}\frac{\partial^2 u_3}{\partial X_1^2} \approx \frac{\partial^2 u_3}{\partial X_1^2} \tag{5.48}$$

Employing relations (5.11b) and (5.48) and leaving out the higher order terms we obtain:

$$\overline{m}_{12}^{\ lin} = -\frac{8}{3}k_3\Lambda_{31} = -\frac{8}{3}k_3\frac{\partial^2 u_3}{\partial X_1^2} \tag{5.49}$$

Using the notion of curvature k^{pure} introduced above we can reformulate (5.49) as

$$\overline{m}_{12}^{\ lin} = \frac{8}{3}k_3 k^{pure} \tag{5.50}$$

Employing Eqs. (5.31), (5.44), (5.50) we obtain

$$M_2^{full} = \iint\limits_{S}\left(E_{hom} \cdot X_3^2 + \frac{8}{3}k_3\right)k^{pure}dX_2dX_3. \tag{5.51}$$

As the curvature and the material parameters for the polar anisotropic beam model are assumed to be constant throughout the cross-section, the following is valid:

$$M_2^{full} = E_{hom}k^{pure} \cdot \iint\limits_{S} X_3^2 dX_2dX_3 + \frac{8}{3}k_3 k^{pure} \cdot \iint\limits_{S} dX_2dX_3. \tag{5.52}$$

The bending moment then equals

$$M_2^{full} = D_{hom}^{full} \cdot k^{pure} \tag{5.53}$$

where the D_{hom}^{full} can be identified as the bending stiffness of the beam model:

$$D_{hom}^{full} = E_{hom}J \ + \frac{8}{3} \cdot k_3 \cdot S, \tag{5.54}$$

where S is the beam cross-section area.

The constant k_3 is then determined from the condition $D_{hom}^{full} = D_{het}$ as

$$k_3 = \frac{3}{8}\frac{E_m J_m + E_f J_f - E_{hom}J}{S} = \frac{3}{8}\frac{D_{het} - D_{hom}}{S} \tag{5.55}$$

D_{het} is the bending stiffness of the heterogeneous specimen along the preferred direction: it is calculated by using all geometrical information of fibres (volume fraction and second moments of fibres with respect to the axis). D_{hom} is the bending stiffness of the homogeneous model: the only geometrical input is the volume fraction of fibres. The constant k_3 is then calculated in order to correct the difference between D_{het} and D_{hom}. Thus we obtain D_{hom}^{full}. Having computed k_3 for the case of fibres aligned along x_1 , we then can use it for problems with the different fibre angle (but the same fibre arrangement) by changing the vector A. Thus, the enhanced bending characteristics of the specimen are covered by the vector A (present in invariant I_6) and the constant k_3 in the constitutive model (5.40).

This formula is analogous to the rule of mixture in application to the bending stiffness. The effective bending stiffness of the initial heterogeneous model is "smeared out" uniformly throughout the section of the homogeneous model by means of the couple stress theory.

A somewhat similar approach to representing flexural rigidity of a beam with pronounced substructural size effects has been taken, for instance, in [27] for the case of microscale problems and in [81] within investigation of the microstructure design of cellular solids .

We can see from (5.55) that the material constant k_3 is directly related to the difference between D_{hom} (which can be described as the bending stiffness generated by the averaged tensile stiffness of the structure throughout the cross-section) and D_{het} which is the actual bending stiffness of the heterogeneous block resulting from the specific fibre arrangement. It follows that constant k_3 approaches zero if the distribution of fibres throughout the cross-section tends to be more and more uniform; consequently the polar theory problem transits to the conventional theory.

The formula (5.55) stems from the requirement of the equivalence of the bending moment occurring in two models: homogeneous polar model (or couple stress theory model) and the

heterogeneous model (model with explicitly defined substructure). The same formula can be obtained if, instead of the moment equivalence, strain energy equivalence is required (with respect to the strain energy of the beam per unit length in both models).

5.4.4. Parameter k_2 derivation

The material parameter k_2 can be determined under condition that the tensile force P in the direction of fibres remains the same in both the homogenous and heterogeneous models under uniaxial tension

$$P^{het} = P^{hom}. \tag{5.56}$$

Consider $A = \begin{pmatrix} 1 \\ 0 \\ 0 \end{pmatrix}$ and uniaxial tension in the direction X_1. We consider small tensile strains in

the fibre direction, therefore linearised constitutive equations can be used. $\sigma_{ij} = 2F_{ik}F_{jl}\dfrac{\partial W}{\partial C_{kl}}$ is a

general constitutive relation for incompressible hyperelastic material (hydrostatic pressure is

absent). The strain energy density is given by equation $W = \dfrac{\mu}{2}(I_1 - 3) + k_2(I_4 - 1)^2$. The right

Cauchy-Green deformation tensor is $C = \begin{pmatrix} \lambda_1^2 & 0 & 0 \\ 0 & \lambda_2^2 & 0 \\ 0 & 0 & \lambda_3^2 \end{pmatrix}$ and the incompressibility condition

$\lambda_1 \lambda_2 \lambda_3 = 1$ holds, where $\lambda_1, \lambda_2, \lambda_3$ are principal stretch ratios.

Consequently, we can write that

$$\sigma_{11}^{hom} = \mu\left(2\lambda^2 - \frac{1}{\lambda}\right) + 4k_2\left(\lambda^4 - \lambda^2\right) \tag{5.57}$$

where $\lambda = \lambda_1$ is the stretch ratio in the direction of fibres.

For small strains it takes the form

$$\sigma_{11}^{hom} = (3\mu + 8k_2)\cdot \varepsilon_{11} = E_1^{hom}\cdot \varepsilon_{11}. \tag{5.58}$$

The tensile force acting in the cross section will be

$$P^{hom} = \int_S \sigma_{11}^{hom} dS = S \cdot \sigma_{11}^{hom} = S \cdot (3\mu + 8k_2) \cdot \varepsilon_{11} \,, \tag{5.59}$$

where S is the cross section area. As to the heterogeneous model, the tensile force in the linearised case is as follows

$$P^{het} = \int_S \sigma_{11}^{het} dS = S \cdot ((1 - \psi_f) \cdot E_m + \psi_f \cdot E_f) \cdot \varepsilon_{11} \tag{5.60}$$

where ψ_f is the fibre volume fraction, E_m, E_f are matrix and fibre moduli of elasticity, respectively. Consequently, we obtain the condition (5.56) in the form

$$(3\mu + 8k_2) \cdot \varepsilon_{11} = ((1 - \psi_f) \cdot E_m + \psi_f \cdot E_f) \cdot \varepsilon_{11} \tag{5.61}$$

and it follows

$$k_2 = \frac{1}{8}((1 - \psi_f) \cdot E_m + \psi_f \cdot E_f - 3\mu). \tag{5.62}$$

5.5. Numerical examples

The new finite element code developed in Matlab software by Lasota [3] is used below for computations within polar theory, and Ansys software is used for computations within conventional theory. The new code has been undergoing changes and modifications; the modifications introduced by me included:

- the change of the constitutive model and all the related finite element equations in accordance with (5.21, 5.23a, b);
- reformulation of code equations in the matrix form instead of index form which reduced the computational time substantially.

The main specific features of the FEM formulation for the couple stress framework are outlined below. More detailed derivation can be found in [3].

5.5.1. FEM formulation outline

With couple stresses the principle of virtual work can be rewritten into the form

$$\int_V \left(\tau_{(ji)} \frac{\partial \delta v_i}{\partial x_j} + \frac{1}{2} \in_{ilk} \bar{\mu}_{ji} \frac{\partial^2 \delta v_k}{\partial x_j \partial x_l} \right) dV = 0. \tag{5.63}$$

60

where $\delta\boldsymbol{v}$ is virtual displacement rate field.

Due to presence of the gradients of strain in the variational formulation, a need arises for higher orders of continuity in the interpolation functions. Namely, so called complete C_1 element shape functions are to be employed. Displacement field and virtual displacement rate field within the element are approximated in the following manner:

$$u_i(\xi) = N^a(\xi)u_i^a + O^a(\xi)\alpha_i^a + P^a(\xi)\beta_i^a + Q^a(\xi)\gamma_i^a, \qquad (5.64)$$

$$\delta v_i(\xi) = N^a(\xi)\delta v_i^a + O^a(\xi)\delta a_i^a + P^a(\xi)\delta b_i^a + Q^a(\xi)\delta g_i^a \qquad (5.65)$$

where ξ_i are normalized local coordinates: $-1 < \xi_i < 1$ (natural coordinates); u_i^a can be regarded as nodal displacements, and $\alpha_i^a, \beta_i^a, \gamma_i^a$ as nodal slopes in directions ξ_1, ξ_2, ξ_3 respectively; superscript indices identify the node number. Virtual rates of nodal displacements and slopes are denoted as $\delta v_i^a, \delta a_i^a, \delta b_i^a, \delta g_i^a$ in (5.65). N, O, P, Q are Hermite polynomials [78] satisfying the following conditions: $N^a(\xi)$ takes the value of 1 at node a and zero at all the other nodes within the element; its derivatives $\dfrac{\partial N^a(\xi)}{\partial \xi_i}$ are zero at all nodes; $O^a(\xi)$, $P^a(\xi)$, $Q^a(\xi)$ take zero value at all nodes, while their derivatives $\dfrac{\partial O^a(\xi)}{\partial \xi_1}$, $\dfrac{\partial P^a(\xi)}{\partial \xi_2}$, $\dfrac{\partial O^a(\xi)}{\partial \xi_3}$ take the value of 1 at node a and zero at all the others; the derivatives with respect to the other ξ_i are zero at all nodes.

In order to proceed with discretization let us convert derivatives into the weak form (5.63) to the reference coordinates X_i, thus obtaining

$$\int_V \left(\tau_{(ij)} \frac{\partial \delta v_i}{\partial X_M} F_{Mj}^{-1} + \frac{1}{2} \in_{ikl} \bar{\mu}_{ji} F_{Mj}^{-1} \left(F_{Nk}^{-1} \frac{\partial^2 \delta v_l}{\partial X_M \partial X_N} - F_{No}^{-1} F_{Pk}^{-1} \frac{\partial \delta v_l}{\partial X_N} \frac{\partial F_{oP}}{\partial X_M} \right) \right) dV = 0. \qquad (5.66)$$

Using eq. (5.65) and element connectivity and utilizing the fact that $\delta v_i^a, \delta a_i^a, \delta b_i^a, \delta g_i^a$ are arbitrary everywhere except for the boundary surface, we obtain four systems of nonlinear equations. Integration is performed using a standard Gauss quadrature scheme.

These nonlinear systems are to be solved using Newton-Raphson iterative procedure. After their linearisation, the following four linear systems with respect to unknown increments of displacements Δu_i^a and increments of slopes $\Delta\alpha_i^a, \Delta\beta_i^a, \Delta\gamma_i^a$ are considered:

$$K_{aibk}^{uu}\Delta u_k^b + K_{aibk}^{u\alpha}\Delta\alpha_k^b + K_{aibk}^{u\beta}\Delta\beta_k^b + K_{aibk}^{u\gamma}\Delta\gamma_k^b = R_i^a$$

$$K_{aibk}^{\alpha u}\Delta u_k^b + K_{aibk}^{\alpha\alpha}\Delta\alpha_k^b + K_{aibk}^{\alpha\beta}\Delta\beta_k^b + K_{aibk}^{\alpha\gamma}\Delta\gamma_k^b = S_i^a \qquad (5.67)$$

$$K_{aibk}^{\beta u}\Delta u_k^b + K_{aibk}^{\beta\alpha}\Delta\alpha_k^b + K_{aibk}^{\beta\beta}\Delta\beta_k^b + K_{aibk}^{\beta\gamma}\Delta\gamma_k^b = T_i^a$$

$$K_{aibk}^{\gamma u}\Delta u_k^b + K_{aibk}^{\gamma\alpha}\Delta\alpha_k^b + K_{aibk}^{\gamma\beta}\Delta\beta_k^b + K_{aibk}^{\gamma\gamma}\Delta\gamma_k^b = U_i^a$$

As an illustrative example, let us consider a fibre reinforced thin rectangular plate with two rows of unidirectional fibres (cross-section is schematically presented in **Fig. 5.4a**) undergoing four-point bending (**Fig. 5.6**). As the fibre diameter is comparable to the dimensions of the specimen, size effect is to be expected. The given specimen is modelled in three different ways:

- via a heterogeneous FE model with explicitly modelled fibres embedded in matrix;

- via equivalent homogeneous transversely isotropic FE model in accordance with the classical elasticity (later referred to as classical model);

- via equivalent homogeneous transversely isotropic FE model in accordance with the couple stress theory and formulations given in sections *5.1, 5.2, 5.3* (later referred to as CST model).

5.5.2. A thin composite plate with 0 degrees fibre declination: four-point bending

Let us consider a fibre reinforced nearly incompressible rectangular plate with the dimensions *40x2x1mm* (length x height x width) with two rows of unidirectional fibres along its length. Fibre diameter is *d=0.1mm*, distance from the middle plane to fibre centre is *c=0.35 mm*, the fibre spacing in each row is *s=0.2mm*. Material constants of the constituents include elastic modulus E_f*=2100 MPa* and Poisson's ratio v_f*=0.3* of fibres and matrix parameters for neo-Hooke material law *μ=2 MPa, d=0.0001MPa⁻¹*. The strain energy potential for the rubber matrix is given as follows

$$W = \frac{\mu}{2}(I_1 - 3) + \frac{1}{d}(J - 1)^2 \qquad (5.68)$$

The classical model with fibre direction defined by vector *A* (1,0,0) is based on the strain energy density

$$W = \frac{\mu}{2}(I_1 - 3) + k_2(I_4 - 1) + \frac{1}{d}(J - 1)^2 \qquad (5.69)$$

Then it holds for stress

$$\sigma_{ij} = 2F_{ik}F_{jl}\frac{\partial W}{\partial C_{kl}}$$

<div align="right">(5.70)</div>

The shear modulus μ is the same as used for matrix in the heterogeneous model. For the given problem with linear elastic fibres under small strains, the constant k_2 can be calculated from the condition of the same average tensile stiffness of the heterogeneous and homogeneous models in the preferred direction (see *5.4.4.*) as $k_2 = \frac{1}{8}\left((1-\psi_f)\cdot E_m + \psi_f \cdot E_f - 3\mu\right) = 18.244\,\text{MPa}$.

In the CST model a new term I_6 is added related to the curvature of the deformed fibres. The corresponding hyperelastic anisotropic potential is as follows:

$$W = \frac{\mu}{2}\left(\bar{I}_1 - 3\right) + k_2\left(\bar{I}_4 - 1\right)^2 + k_3\bar{I}_6 + \frac{1}{d}\left(J - 1\right)^2$$

<div align="right">(5.71)</div>

The objective of setting all the constants is to simulate correctly both tensile and bending behaviour of the given heterogeneous model.

According to (5.55) and the given data we set the constant $k_3 =2.1718\,N$. Constants μ and k_2 are the same as in the classical model used above. Boundary conditions prescribed for the respective finite element model in the new code are outlined below. Only a quarter of the plate (**Fig. 5.7**) is modelled due to the symmetries of the problem. Displacements and displacement derivatives (slopes) are prescribed in accordance with the problem setting and code requirements in the following way:
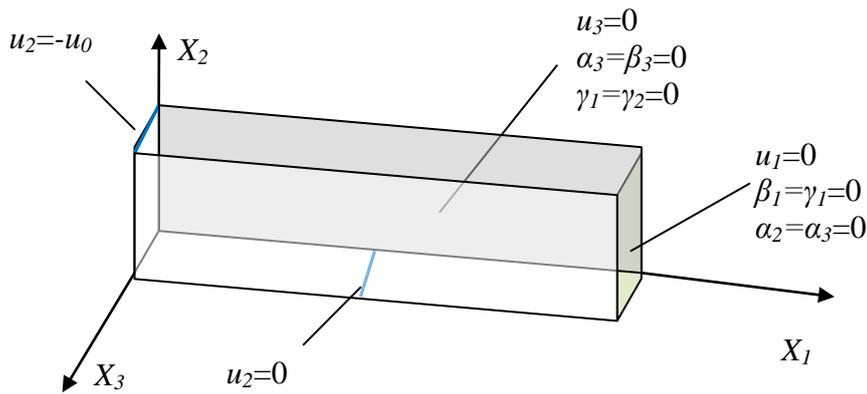
Fig. 5.7 Boundary conditions (slopes and displacements prescribed)

Here the displacements within the element are approximated in the following manner:

$$u_i(\xi) = N^a(\xi)u_i^a + O^a(\xi)\alpha_i^a + P^a(\xi)\beta_i^a + Q^a(\xi)\gamma_i^a, \tag{5.72}$$

$$\alpha_i^a = \frac{\partial u_i^a}{\partial X_1},$$

$$\beta_i^a = \frac{\partial u_i^a}{\partial X_2}, \tag{5.73}$$

$$\gamma_i^a = \frac{\partial u_i^a}{\partial X_3}$$

where ξ_i are normalized local coordinates: $-1 < \xi_i < 1$ (natural coordinates); u_i^a can be regarded as nodal displacements, and $\alpha_i^a, \beta_i^a, \gamma_i^a$ as nodal slopes in directions ξ_1, ξ_2, ξ_3 respectively; superscript indices identify the node number. *N, O, P, Q* are Hermite polynomials.

Results of all the three simulations are compared in **Fig. 5.8.**
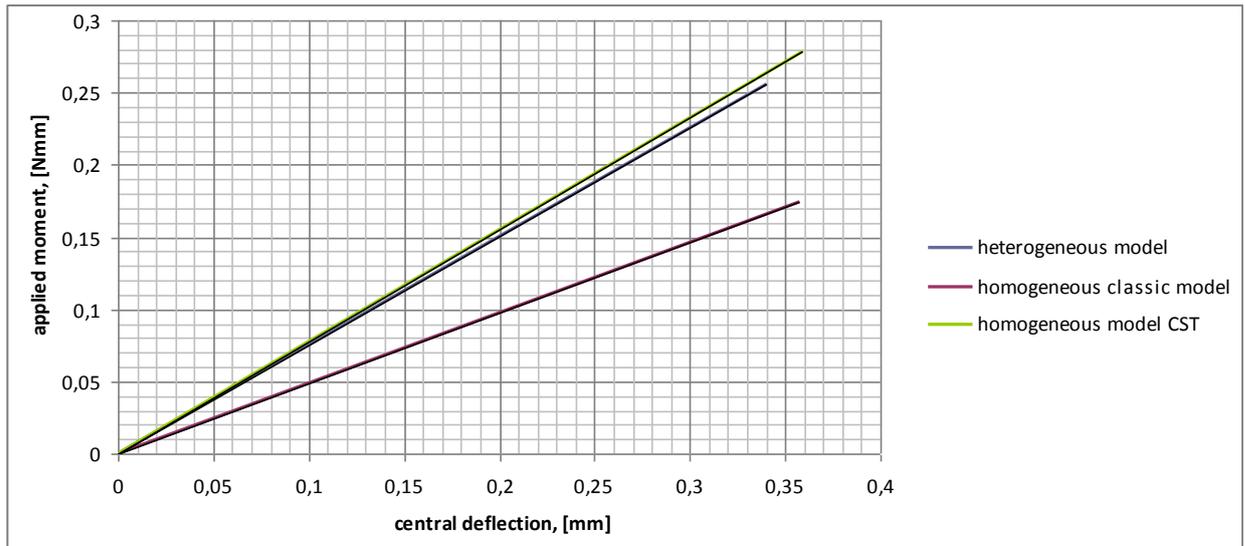
Fig. 5.8 Comparison of FE simulations of 4-point bending using different constitutive models.

5.5.3. A thin composite plate with 30 degrees fibre declination: four-point bending

The example above is a standard linear problem which can be solved analytically with respect to the deflection which can be assumed constant throughout the plate thickness. This simplicity occurs due to the fibres being aligned along the X_1 axis. In the present example, we consider the case when the fibres have 30 degrees declination angle which renders the problem unsolvable analytically. Dimensions of the composite structure are given as follows: *240x25.4x5,8 mm.*

Fibre diameter is $d=0.45mm$, distance from the middle plane to fibre centre is $c=1.45$ mm, the fibre spacing in each row is $s=1mm$.

Material constants of the constituents include elastic modulus $E_f=2100$ MPa and Poisson ratio $v_f=0.3$ of fibres and matrix parameters for neo-Hooke material law $\mu=2$ MPa, $d=0.0001MPa^{-1}$. The plate is loaded as shown in **Fig.5.6.**

The constant k_3 is determined using (5.55) on the basis of the corresponding representative periodic element containing two fibres in the cross-section (**Fig.5.9**).
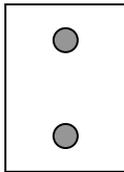
Fig. 5.9 Representative periodic element

The values of the material parameters obtained for the expression (5.71) are as follows: k_2 $=12.75$ MPa, k_3 $=-25.27$ $Pa·m^2$. Negative value of the constant k_3 indicates that the bending stiffness of the classical homogeneous model, generated by the averaged tensile stiffness of the heterogeneous plate, is higher than the actual plate's bending stiffness. So the CST model is constructed by augmenting the classical model with the additional term that, roughly speaking, subtracts the excessive bending stiffness without affecting the tensile properties of the model in any way (which are in complete agreement with the heterogeneous structure already). Importantly, the fibre direction unit vector is now defined as $(0.866, 0, 0.5)^T$
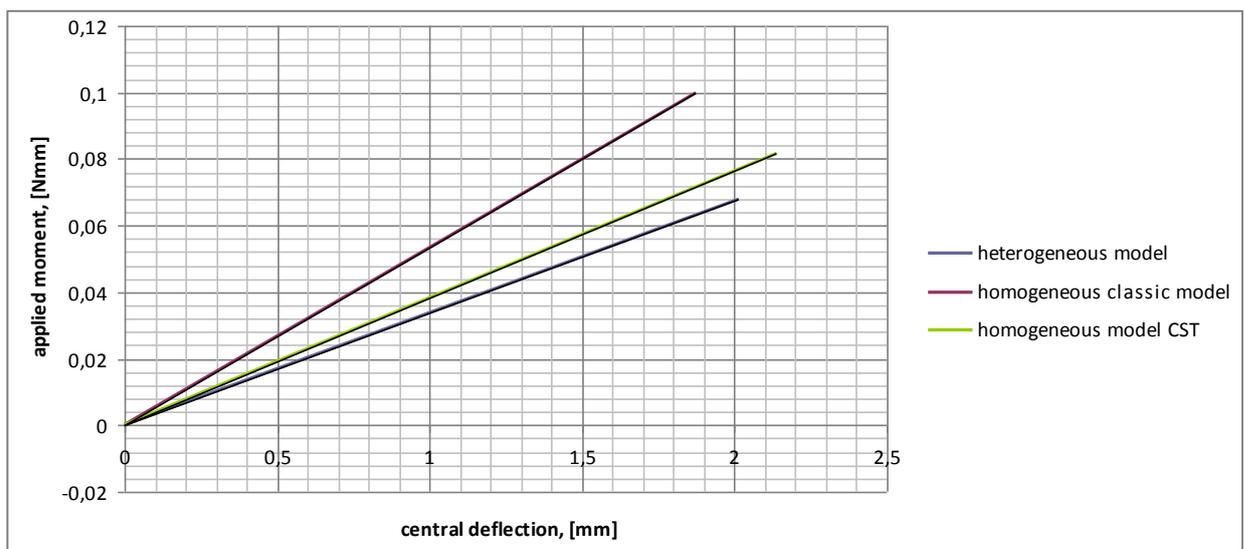
Fig. 5.10. Comparison of FE simulations of 4-point bending using different constitutive models for the case of fibre declination angle of 30 degrees.

6. An exact solution of the boundary problem for the thick polar material plate for the linearised case

In this section, thick fibre-reinforced plate under certain boundary conditions is considered. Polar theory equations are employed in linear formulation. The solution of the plane strain boundary problem of polar elasticity for the static and dynamic flexure of a thick laminated plate has been recently derived by Farhat and Soldatos in [1]. The authors take into account the contribution of the couple stresses with the help of one extra elastic modulus. In the present study, after reproduction of the solution presented in [1] for the case of static flexure of a single-layer plate, the solution is extended to different boundary conditions with three extra elastic moduli in the model. In this chapter some new numerical results are presented which complement those in [1].

6.1. Problem setting

Let us consider a planar boundary problem: a thick transversely isotropic plate, infinite in the x_3 direction, subjected to certain boundary conditions corresponding to the plane strain. In this case, the displacements are functions of only two coordinates

$$
\begin{aligned}
u_1 &= u_1(x_1, x_2), \\
u_2 &= u_2(x_1, x_2), \\
u_3 &= 0.
\end{aligned}
\tag{6.1}
$$

The following equations in terms of displacements u_1, u_2, obtained by Spencer and Soldatos [2] for the case of the plane strain problem of the plate with the fibres initially aligned with x_1 direction, will be further employed:

$$
\begin{aligned}
c_{11}\frac{\partial^2 u_1}{\partial x_1^2} + (c_{12}+c_{66})\frac{\partial^2 u_2}{\partial x_1 \partial x_2} + c_{66}\frac{\partial^2 u_1}{\partial x_2^2} + c_2\frac{\partial^4 u_1}{\partial x_1^2 \partial x_2^2} + c_3\frac{\partial^4 u_2}{\partial x_1^3 \partial x_2} + c_1\frac{\partial^4 u_2}{\partial x_1 \partial x_2^3} &= 0, \\
c_{66}\frac{\partial^2 u_2}{\partial x_1^2} + (c_{12}+c_{66})\frac{\partial^2 u_1}{\partial x_1 \partial x_2} + c_{22}\frac{\partial^2 u_2}{\partial x_2^2} - c_1\frac{\partial^4 u_2}{\partial x_1^2 \partial x_2^2} - c_2\frac{\partial^4 u_1}{\partial x_1^3 \partial x_2} - c_3\frac{\partial^4 u_2}{\partial x_1^4} &= 0.
\end{aligned}
\tag{6.2}
$$

where c_{ii} represent stiffness matrix components from classical elasticity, and c_i are elastic moduli that characterise the substructure (c_1, c_2 correspond to the resistance to "splay" mode deformation of fibres and c_3 - to "bending" mode deformation, also see (6.9)).

These equations are derived from the equilibrium equations of couple stress theory and linearised constitutive relations for the case of small strains. Constitutive equations of couple

stress theory for small strains are given in [2]. The relations for the symmetric part of the stresses are given in the form of the generalized Hooke's law for transversely isotropic materials:

$$
\begin{pmatrix} \sigma_{11} \\ \sigma_{22} \\ \sigma_{33} \\ \sigma_{(12)} \end{pmatrix} = \begin{pmatrix} c_{11} & c_{12} & 0 \\ c_{12} & c_{22} & 0 \\ c_{12} & c_{23} & 0 \\ 0 & 0 & c_{66} \end{pmatrix} \begin{pmatrix} \varepsilon_{11} \\ \varepsilon_{22} \\ 2\varepsilon_{12} \end{pmatrix}
$$
(6.3)

where ε_{11}, ε_{22}, ε_{12} are the only non zero strain tensor components conventionally derived as

$$
\varepsilon_{ij} = \frac{1}{2}\left(\frac{\partial u_i}{\partial x_j} + \frac{\partial u_j}{\partial x_i} \right)
$$
(6.4)

The theory employed in the present paper assumes that the rotation vector $\boldsymbol{\omega}$ is not independent but related to the displacement vector $\boldsymbol{u}$ in the following way:

$$
\omega_i = \frac{1}{2}\in_{ijk} \frac{\partial u_k}{\partial x_j}.
$$
(6.5)

The components of the symmetric and antisymmetric parts of the stress are denoted as $\sigma_{(ij)}$ and $\sigma_{[ij]}$ respectively so that

$$
\sigma_{ij} = \sigma_{(ij)} + \sigma_{[ij]}.
$$
(6.6)

The linearised relations for the nonzero couple stresses are given as follows [2]:

$$
\begin{pmatrix} m_{23} \\ m_{13} \end{pmatrix} = \begin{pmatrix} d_{11} & d_{33} & 0 \\ 0 & 0 & d_{31} \end{pmatrix} \begin{pmatrix} \partial\varepsilon_{11}/\partial x_1 \\ \partial\varepsilon_{22}/\partial x_1 \\ \partial^2 u_2/\partial x_1^2 \end{pmatrix}
$$
(6.7)

And the antisymmetric part of the stress tensor can be expressed in this case as:

$$
2\sigma_{[21]} = \frac{\partial m_{13}}{\partial x_1} + \frac{\partial m_{23}}{\partial x_2}.
$$
(6.8)

The constants c_1, c_2, c_3 in (6.2) are related to the physical constants in (6.7) as follows:

$$
c_1 = \frac{1}{2}d_{33}, \; c_2 = \frac{1}{2}d_{11}, \; c_3 = \frac{1}{2}d_{31}
$$
(6.9)

Let us examine the order of the system of differential equations (6.2). With the substitution $u_{2,1} = \tilde{u}_2(x_1, x_2)$, the system (6.2) can be written in the following alternative form:

$$\begin{cases} u_{2,1} = \tilde{u}_2(x_1, x_2), \\ c_{11}\dfrac{\partial^2 u_1}{\partial x_1^2} + (c_{12} + c_{66})\dfrac{\partial \tilde{u}_2}{\partial x_2} + c_{66}\dfrac{\partial^2 u_1}{\partial x_2^2} + c_2\dfrac{\partial^4 u_1}{\partial x_1^2 \partial x_2^2} + c_3\dfrac{\partial^3 \tilde{u}_2}{\partial x_1^2 \partial x_2} + c_1\dfrac{\partial^3 \tilde{u}_2}{\partial x_2^3} = 0, \\ c_{66}\dfrac{\partial \tilde{u}_2}{\partial x_1} + (c_{12} + c_{66})\dfrac{\partial^2 u_1}{\partial x_1 \partial x_2} + c_{22}\dfrac{\partial^2 u_2}{\partial x_2^2} - c_1\dfrac{\partial^3 \tilde{u}_2}{\partial x_1 \partial x_2^2} - c_2\dfrac{\partial^4 u_1}{\partial x_1^3 \partial x_2} - c_3\dfrac{\partial^3 \tilde{u}_2}{\partial x_1^3} = 0 \end{cases} \quad (6.10)$$

The system is of the 6th order with respect to the coordinate x_1 and requires 6 boundary conditions applied at the plate ends:

$$\begin{cases} \sigma_1(0, x_2) = 0, \\ u_2(0, x_2) = 0, \\ m_{13}(0, x_2) = 0, \\ \sigma_1(L, x_2) = 0, \\ u_2(L, x_2) = 0, \\ m_{13}(L, x_2) = 0. \end{cases} \quad (6.11)$$

If the solution is sought in the form

$$\begin{aligned} u_1 &= f_1(x_2)\cos\left(\frac{\pi x_1}{L}\right), \\ u_2 &= f_2(x_2)\sin\left(\frac{\pi x_1}{L}\right), \end{aligned} \quad (6.12)$$

then with the substitution $f_2{}' = \tilde{f}$ the system (6.2) yields the following set of equations:

$$\begin{cases} f_2{}' = \tilde{f}_2, \\ k_1 f_1 + k_2 \tilde{f}_2 + k_3 f_1{}'' + k_4 \tilde{f}_2{}'' = 0, \\ k_5 f_2 + k_6 f_1' + k_7 \tilde{f}_2{}' = 0 \end{cases} \quad (6.13)$$

which is clearly a system of the 4th order with respect to x_2. Consequently, the lateral boundary conditions for the present problem are set as follows:

$$\begin{cases} u_1(x_1, h/2) = 0, \\ u_2(x_1, h/2) = -u_0 \sin(\pi x_1 / L), \\ u_1(x_1, -h/2) = 0, \\ u_2(x_1, -h/2) = 0. \end{cases} \quad (6.14)$$

$u_1=0$

x_2

$u_2=-u_0 \sin(\pi x_1/L)$

h

x_1

$u_1=0$

$u_2=0$

L
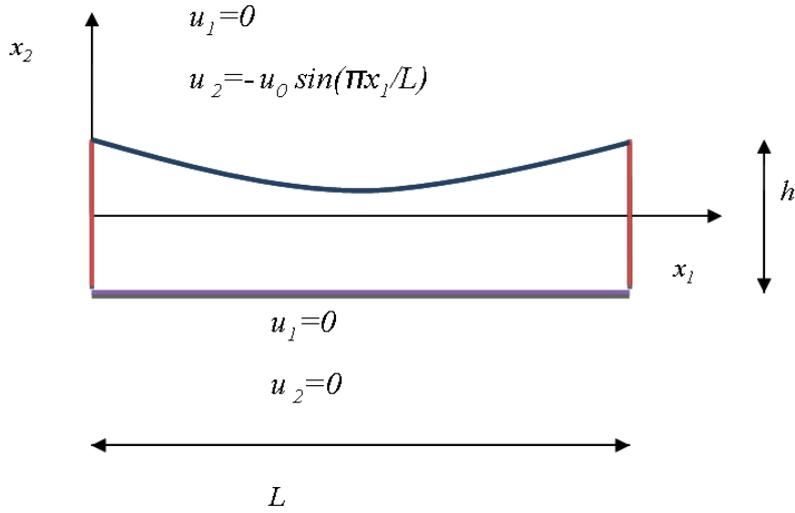
Fig. 6.1 Displacement boundary conditions

6.2. Solution

We make use of the method of the boundary problem solution in [1] for the case of static flexure of a single-layered plate and extend it to different boundary conditions (**Fig. 6.1**) and additional components of the model (terms with coefficients c_1, c_2 in the system (6.10)).

For a plate under the above specified load, the solution in the following form can be used:

$$u_1 = f_1(x_2)\cos\left(\frac{\pi x_1}{L}\right),$$
$$u_2 = f_2(x_2)\sin\left(\frac{\pi x_1}{L}\right) \tag{6.15}$$

where

$$f_1(x_2)= a_i e^{\mu_i x_2},$$
$$f_2(x_2)= \bar{a}_i e^{\mu_i x_2}. \tag{6.16}$$

The presence of constants c_1, c_2 relates to the splay modes of fibre deformation and c_3 relates to the bending mode [2]. The presence of these constants in the equations (6.10) is dependent on the choice of relevant invariants in the form of the polynomial strain energy density function.

6.3.   Results

The elastic constants for the transversely isotropic material are set as follows: $E_L = 40\ E_T$, $G_{LT} = 0.5E_T$, $G_{TT} = 0.2\ E_T$, $v_{TT} = v_{LT} = 0.25$.

Adopting notation from [1] we set

$$d_{31} = c_{11}\ \tilde{\lambda}\ hL \tag{6.17}$$

where $\tilde{\lambda}$ is a non-dimensional parameter related to intrinsic material length parameter (for more details see [1]).

Each of the remaining moduli can be set in the similar manner ($d_{11} = c_{11}\tilde{\lambda}_1\ hL$, $d_{33} = c_{11}\tilde{\lambda}_2\ hL$), although the definition of these moduli is out of the scope of this study.

The constants c_1, c_2, c_3 are then defined in accordance to (6.9).

In the **Table 6.1** the results of calculations are presented for the plate of the length L and thickness $h=0,25L$.

For each calculation only one additional elastic modulus is considered nonzero, the other additional moduli are omitted from the model (i.e., not present in the system (6.10)). Thus we have obtained a quantitative estimation of the influence of each of the additional elastic moduli as presented in **Table 6.1**.

Table 6.1. Through-thickness distribution of u_1

x_2/h	$u_1(0,x_2)/u_0$ $c_1=c_2=c_3=0$	$u_1(0,x_2)/u_0$ $c_1=c_2=0,$ $c_3\neq0$ $\tilde{\lambda}=0.01$	$u_1(0,x_2)/u_0$ $c_3=c_2=0,$ $c_1\neq0$ $\tilde{\lambda}_1=0.01$	$u_1(0,x_2)/u_0$ $c_1=c_3=0,$ $c_2\neq0$ $\tilde{\lambda}_2=0.001$
0.4	−0.013948196	−0.005908389	−0.013918808	−0.02828146
0.3	−0.0205631560	−0.00859638	−0.021534995	−0.02764271
0.2	−0.023533576	−0.0097066	−0.02552476	−0.027067310
0.1	−0.02465696	−0.0100383	−0.027351710	−0.02657205
0	−0.0247528504	−0.0099579	−0.02774786	−0.026155487
-0.1	−0.02407952	−0.00958854	−0.026954455	−0.0258163
-0.2	−0.0224657	−0.00887389	−0.024801370	−0.025553716
-0.3	−0.01922424	−0.0075502366	−0.02065144	−0.025366720
-0.4	−0.0128034	−0.00501168	−0.013191293	−0.025238771

7. Application of polar elasticity to bending of a thick plate under small strains.

To gain a better understanding of the additional constant and the role of couple stress in polar theory [2], we focus on exact analytical (polar elasticity) solutions for the problem of pure bending of thick infinite plates. The solution is done for a transversely isotropic material under small strain assumption.

The section is organized in the following manner: in 7.1 the displacement solution is derived for a transversely isotropic thick plate under pure bending (and the conventional – Cauchy theory of elasticity); in 7.2 the solution is derived for the case of longitudinal modulus being a periodic function of position in transversal direction; in 7.3 the first problem is analyzed on the basis of couple stress theory. In 7.4 solutions of all the three models, taken with the matching effective properties and the same effective load, are compared.

7.1. Homogeneous material (conventional theory of elasticity)

Let us consider a rectangular plate subjected to a known bending moment M_3 (**Fig. 7.1**). The material is transversely isotropic and characterized by the following constants related to conventional linear elasticity theory: E_1, E_2, v_{1T}, $v_{23} = v_{32} = v_{TT}$, G_{1T}. The isotropic plane of the material is X_2X_3. This model is referred to as the EC (effective classical) model below.
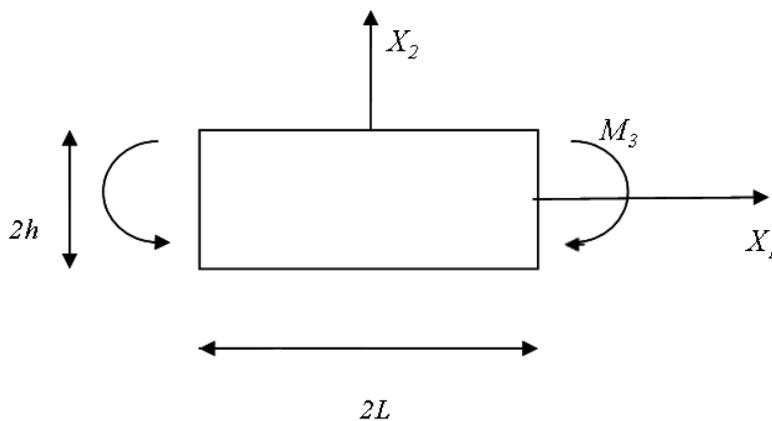
Fig. 7.1. A thick plate with infinite length in X_3 direction

The following boundary conditions have to hold for the tractions t_1 and t_2

on the faces defined by: $\qquad X_2 = \pm h \qquad => \qquad t_2 = 0$

$$X_1 = \pm L \quad \Rightarrow \quad \int_{-h}^{h} t_1 dX_2 = 0 \tag{7.1}$$

$$\int_{-h}^{h} t_1 X_2 dX_2 = M_3$$

Equilibrium equations (with negligible volume loads) must be satisfied as well:

$$\frac{\partial \sigma_{ji}}{\partial X_j} = 0 \quad , \tag{7.2}$$

The following stress distribution satisfies both (7.1) and (7.2):

$$\sigma_{22} = 0, \quad \sigma_{11} = \alpha X_2, \quad \sigma_{12} = 0. \tag{7.3}$$

The stress distribution throughout the plate thickness is the same at any cross-section (**Fig. 7.2**).
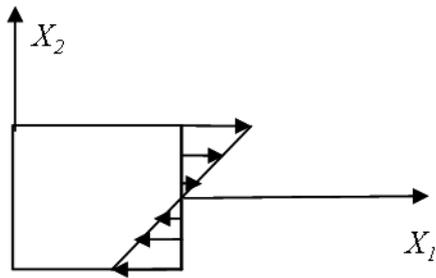
Fig. 7.2. Normal stress distribution throughout the plate thickness

Under plane strain conditions ($\varepsilon_3=0$) and for stresses in the form (7.3) the constitutive equations yield:

$$\varepsilon_1 = \frac{1 - v_{T1} v_{1T}}{E_1} \sigma_1$$

$$\varepsilon_2 = \frac{-v_{1T}(1 + v_{TT})}{E_1} \sigma_1 \tag{7.4}$$

By integrating (7.4) we obtain

$$u_1 = \int \varepsilon_1 dX_1 + g_1(X_2)$$

$$u_2 = \int \varepsilon_2 dX_2 + g_2(X_1) \tag{7.5}$$

$$\begin{cases} u_1 = \dfrac{1-\nu_{T1}\nu_{1T}}{E_1}\alpha X_1 X_2 + g_1(X_2) \\ u_2 = \dfrac{-\nu_{1T}(1+\nu_{TT})}{2E_1}\alpha X_2{}^2 + g_2(X_1) \end{cases} \tag{7.6}$$

With the additional condition of zero shear strain

$$\frac{\partial u_1}{\partial X_2} + \frac{\partial u_2}{\partial X_1} = 0 \tag{7.7}$$

we find that

$$\frac{1-\nu_{T1}\nu_{1T}}{E_1}\alpha X_1 + g_1{}'(X_2) + g_2{}'(X_1) = 0 \tag{7.8}$$

and

$$\begin{cases} g_2{}'(X_1) = -\dfrac{1-\nu_{T1}\nu_{1T}}{E_1}\alpha X_1 + c, \\ g_1{}'(X_2) = -c, \end{cases} \tag{7.9}$$

$$\begin{cases} g_2(X_1) = -\dfrac{1-\nu_{T1}\nu_{1T}}{2E_1}\alpha X_1{}^2 + cX_1 + c_1, \\ g_1(X_2) = -cX_2 + c_2, \end{cases} \tag{7.10}$$

where the constants c_1, c_2, c are set to zero (c_1, c_2 refers to rigid body translation, c to the rigid body rotation). The final solution in displacements then acquires the form

$$\begin{cases} u_1 = \dfrac{1-\nu_{T1}\nu_{1T}}{E_1}\alpha X_1 X_2, \\ u_2 = \dfrac{-\nu_{1T}(1+\nu_{TT})}{2E_1}\alpha X_2{}^2 - \dfrac{1-\nu_{T1}\nu_{1T}}{2E_1}\alpha X_1{}^2. \end{cases} \tag{7.11}$$

7.2. Heterogeneous material with periodic properties

We still consider a plate subjected to a known bending moment M_3 (**Fig. 7.3**)
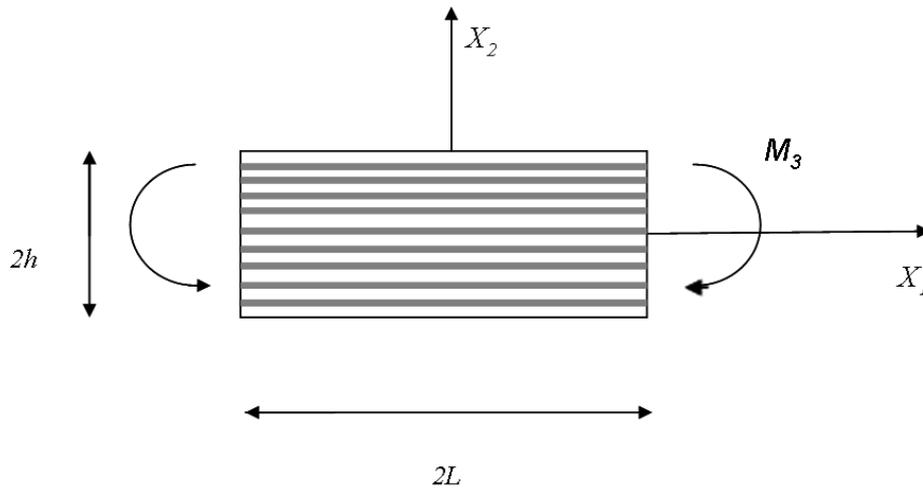
Fig. 7.3. Composite plate pure bending

The Young's modulus is changing throughout the plate thickness, its distribution in x_2 direction is given using cosinus function, as shown on the **Fig.7.4** while it is independent of x_1 coordinate.
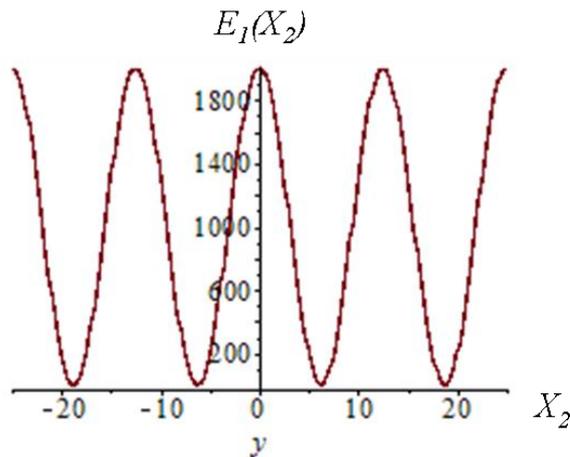
Fig. 7.4. Young's modulus throughout the plate thickness

Such periodically changing stiffness can be regarded as an approximation of a composite reinforced by fibres aligned with x_1 direction. This model is referred to as the PS (periodical stiffness) model.

Thus the material is also transversely isotropic, characterized by the following parameters:

$$E_1 = E_0 + \tilde{E} \cos(\frac{\pi N}{h} X_2), \ E_2 = \left(\frac{N}{2h} \int_0^{2N/h} \frac{dX_2}{E_1(X_2)} \right)^{-1}, \ \nu_{1T}, \ \nu_{TT}, \ G_{1T}.$$

The same boundary conditions (7.1) and equilibrium equations (7.2) must be satisfied. In order to ensure pure bending, the applied normal stress at the ends of the plate must accommodate to the strain distribution $\varepsilon_1 = kX_2$, where the curvature is introduced as $k = -u_{2,11}$. The curvature can be defined in relation to the load as follows:

$$M_3 = \frac{k}{1-\nu_{T1}\nu_{1T}} \int_{-h}^{h} E_1 X_2^2 \, dx_2 \tag{7.12}$$
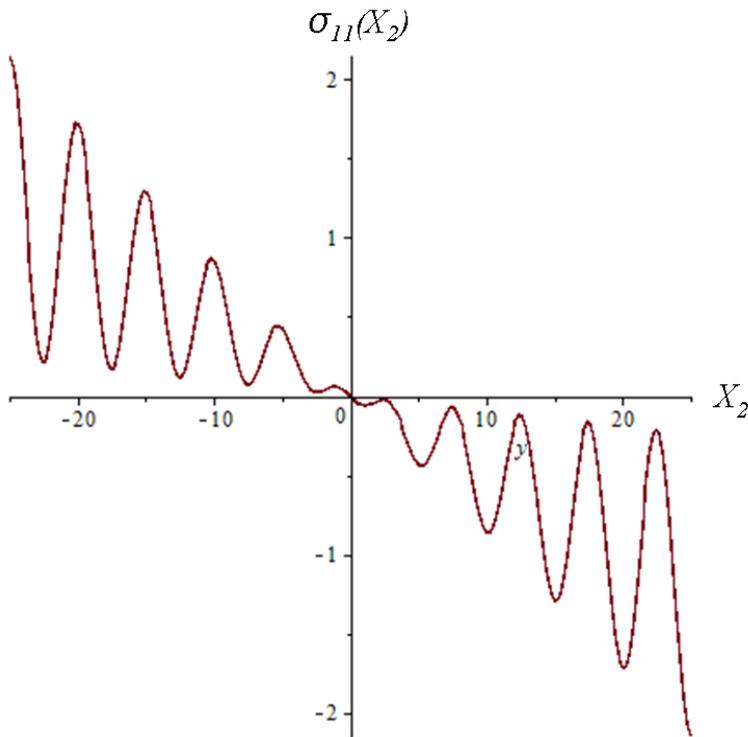
Fig. 7.5. Normal stress distribution throughout the plate thickness

Thus the stresses are

$$\sigma_{22} = 0,$$

$$\sigma_{11} = \frac{E_0 + \tilde{E}\cos(\dfrac{\pi N}{h} X_2)}{1-\nu_{1T}\nu_{T1}} kX_2, \tag{7.13}$$

$$\sigma_{12} = 0.$$

The distribution of normal stress σ_{11} is shown in Fig. 7.5. By integrating strains we arrive to the displacement solution, where σ_{11} is the expressed above function of x_2.

The displacements are presented as functions of the stress distribution and the curvature.

$$\begin{cases} u_1 = kX_1X_2, \\ u_2 = \dfrac{-\nu_{1T}\left(1+\nu_{TT}\right)}{E_1}\int \sigma_{11}dX_2 - \dfrac{1}{2}kX_1{}^2, \end{cases} \qquad (7.14)$$

Following the logics of the previous section and the Hooke's law relations for plane strain (7.4) the solution has final form

$$\begin{cases} u_1 = kX_1X_2, \\ u_2 = \int\limits_0^X \varepsilon_2 dX_2 - \dfrac{1}{2}kX_1{}^2. \end{cases} \qquad (7.15)$$

7.3. Homogeneous material (polar theory of elasticity)

Now let us consider pure bending of the plate with the additional elastic constant d_{31} indicative of the bending stiffness of the substructure. The loading conditions stay the same as on the **Fig. 7.1.** Such model we refer to as the EP (effective polar) model.

 The boundary conditions on the faces are as follows in this case:

$$X_2 = \pm h: \ t_2 = 0$$
$$X_1 = \pm L: \ \int\limits_{-h}^{h} t_1 dX_2 = 0 \qquad (7.16)$$
$$\int\limits_{-h}^{h} t_1 X_2 dX_2 + \int\limits_{-h}^{h} m_{13} dX_2 = M_3$$

where the couple stress [2] m_{13} is introduced.

Equilibrium equations in the polar theory for the present case are augmented by the equation connecting the antisymmetric shear stress and the couple stress:

$$\frac{\partial \sigma_{ji}}{\partial X_j} = 0 \ ,$$

$$2\sigma_{[21]} = \frac{\partial m_{13}}{\partial X_1}.$$

(7.18)

where equation (6.6) holds again for the symmetric and antisymmetric parts of the stress tensor. The following stress and couple stress distribution satisfies both (7.16) and (7.18) (also see **Fig. 7.6**):

$$\sigma_{22} = 0, \quad \sigma_{21} = 0$$
$$\sigma_1 = \alpha X_2, \quad \sigma_{12} = 0$$
$$m_{13} = const = \beta$$

(7.19)
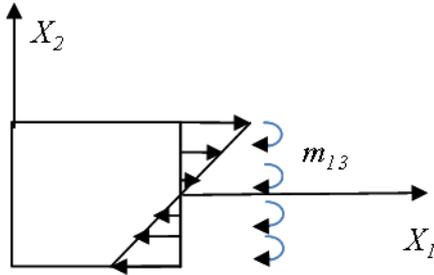
Fig. 7.6 Distribution of the non-zero stress and couple stress components in a section of the plate

The strain-stress relations hold in the form of (7.4) with the additional equation [2]:

$$m_{13} = d_{31}u_{2,11}$$

(7.20)

which can be rewritten here as

$$u_{2,11} = \frac{\beta}{d_{31}}$$

(7.21)

From the integration of (7.4) and zero shear condition (7.7) we obtain the displacement solution identical with (7.11):

$$\begin{cases} u_1 = \dfrac{1 - v_{T1}v_{1T}}{E_1}\alpha X_1 X_2 \\[2mm] u_2 = \dfrac{-v_{1T}\left(1 + v_{TT}\right)}{2E_1}\alpha X_2{}^2 - \dfrac{1 - v_{T1}v_{1T}}{2E_1}\alpha X_1{}^2 \end{cases}$$

(7.22)

If we now insert the second equation of (7.22) into (7.21) we can see that this solution is valid only if

$$-\frac{1-v_{T1}v_{1T}}{E_1}\alpha = \frac{\beta}{d_{31}} \quad . \tag{7.23}$$

So (7.23) is the result of requirement of zero shear strain (20). It means that for the given material constant d_{31} the applied stress parameter α and the applied couple stress value β must relate via (7.23) in order to ensure pure bending.

As this section shows, it can be concluded that the displacement solution in the form of (7.22) for the pure bending problem is valid for

a)   transversely isotropic plate (d_{31}=0) under end loading $\sigma_{11} = \alpha X_2$ or

b)   transversely isotropic polar material plate (d_{31}≠0) under the end loading $\sigma_{11} = \alpha X_2$ and

$m_{13} = const = \beta$ under condition of validity of eq. (7.23).

It can be verified that the units of the elastic constant d_{31} correspond to Newtons [N].

7.4.   Comparison summary

To briefly illustrate the differences in the equivalent models, a summary of the models presented in chapters 7.1 and 7.3 is presented below (not the periodic structure acc. chapter 7.2) for comparison.

classical (EC)　　　　　periodic (PS)　　　　　couple stress (EP)
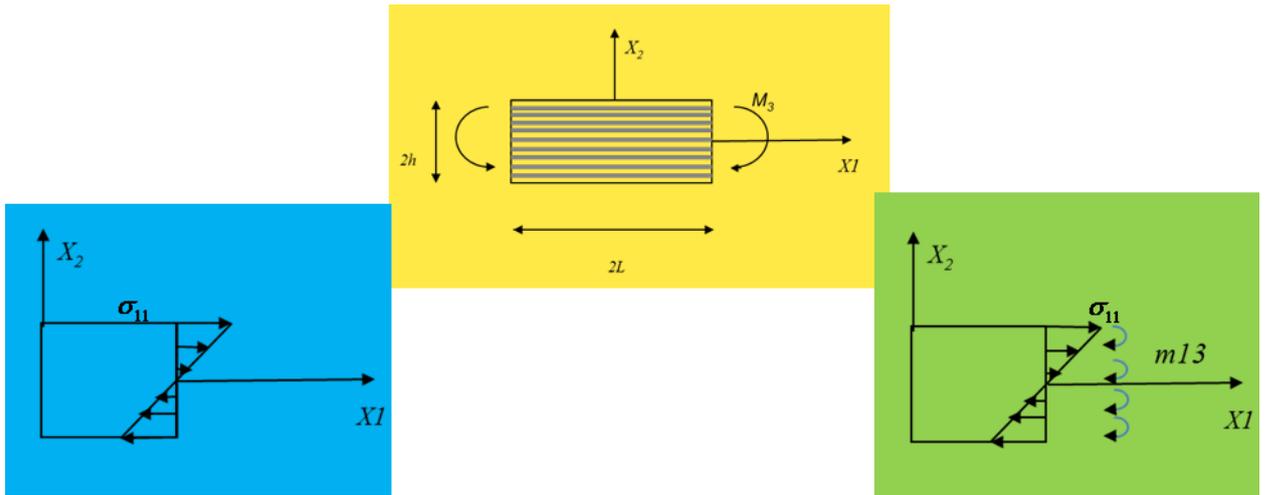
$$\int_{-h}^{h} \sigma_{11} X_2 dx_2 = M_3$$

$$\int_{-h}^{h} \sigma_{11} X_2 dX_2 + \int_{-h}^{h} m_{13} dX_2 = M_3$$

Fig. 7.7. Comparison of the models. Bending moment

The heterogeneous plate (PS model) under pure bending can be modelled as effective classical (EC) homogenous model (option 1) or effective polar (EP) homogeneous model (option 2). The overall applied bending moment in all the cases has the same value, but the stress distribution is different.

In the 1st model the moment is transferred to the material by tensile stress only, and in the *2nd* model the moment is transferred by tensile stress as well as couple stress. While normal stress is related to the extension or compression of the fibre, Couple stress is directly related to the fibre curvature only.
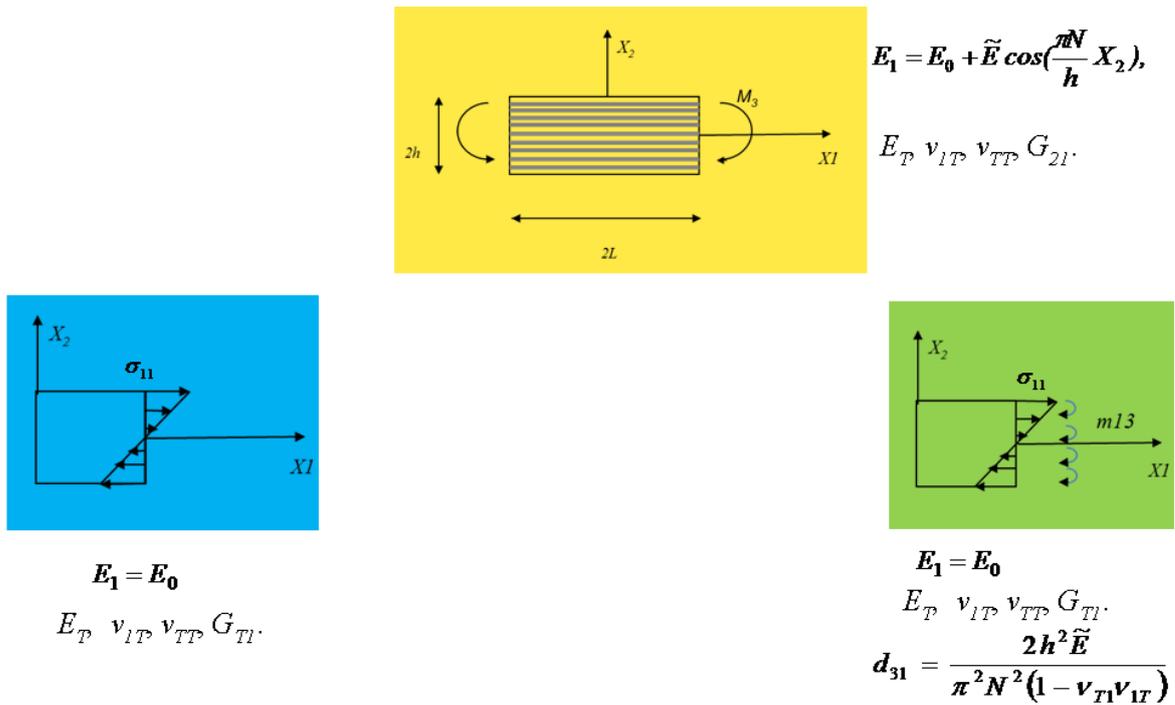
Fig. 7.8. Comparison of the models. Material parameters

In order to compare the above 3 models, the equivalent effective material parameters must be defined. We start with the heterogeneous (periodic) model: E_1 is the function of x_2, the rest of parameters are constants. Its periodically changing stiffness can be regarded as an approximation of the fibre reinforced composite.

For the EC homogeneous model the E_1 is defined by averaging, and the rest of the constants are the same.

For the EP homogeneous model, all the constants are identical to the classical, but the additional parameter is present. Bending stiffness parameter d_{31} serves as a correction parameter which ensures that the overall bending stiffness of the plate in the EP model equals that one of the PS model.

Even without going into detail, we can see that characteristics of the heterogeneous model are more comprehensively accounted for in the *2nd* (EP) model: particularly, the amplitude E wave is not present in the 1st model in any way, since it has no effect on the averaged modulus. Also the number N which is indicative of the number of fibres can not be included in the 1st model.

7.5. Discussion

On the basis of the previous developments we compare the solutions of the three corresponding models under the given value of the applied bending moment. The model from the Section 7.2 is taken as a reference model. Its periodically changing stiffness can be regarded as an approximation of the fibre reinforced composite. This model is referred to as the PS (periodical stiffness) model. If we try to replace the PS model with a homogeneous one, we can do it in two ways. Firstly, the model from the Section 7.1, taken with the corresponding properties, can serve this goal. This model we refer to as the EC (effective classical) model. Secondly, the model from the Section 7.3, further called the EP (effective polar) model, can simulate the given problem. The goal is to compare the results from two of the alternative homogeneous models (ES and EP) with the PS model and to evaluate their accuracy under varying N which can be regarded as analogous to the nominal number of fibres per height in a unidirectional fibre composite. The properties of both the homogeneous models are set as effective (averaged) properties of the PS model. In addition, the bending stiffness parameter in the EP model is set as

$$d_{31} = \frac{2h^2 \tilde{E}}{\pi^2 N^2 \left(1 - \nu_{T1}\nu_{1T}\right)}$$ and serves as a correction parameter which ensures that the overall

bending stiffness of the plate in the EP model equals that one of the PS model. All models are loaded at both ends of the plate by two equilibrated couples with magnitude (per unit width) of *M=-500 N* inducing the same bending moment in all sections along the plate length. The dimensions are: *2L=200* mm (length of the plate), *2h=50* mm (thickness).

The material properties set in the computations are listed in **Table 7.1**.

Table 7.1. Material parameters used in the models of thick plate

	PS model	EC model	EP model
E_1, MPa	$1000 + 999\,cos(\dfrac{\pi N}{h}X_2)$	1000	1000
E_T, MPa	44,71	44,71	44,71
v_{T1}	0,3	0,3	0,3
v_{TT}	0,3	0,3	0,3
d_{31}, MPa·mm^2			8690 for N=4 1390 for N=10
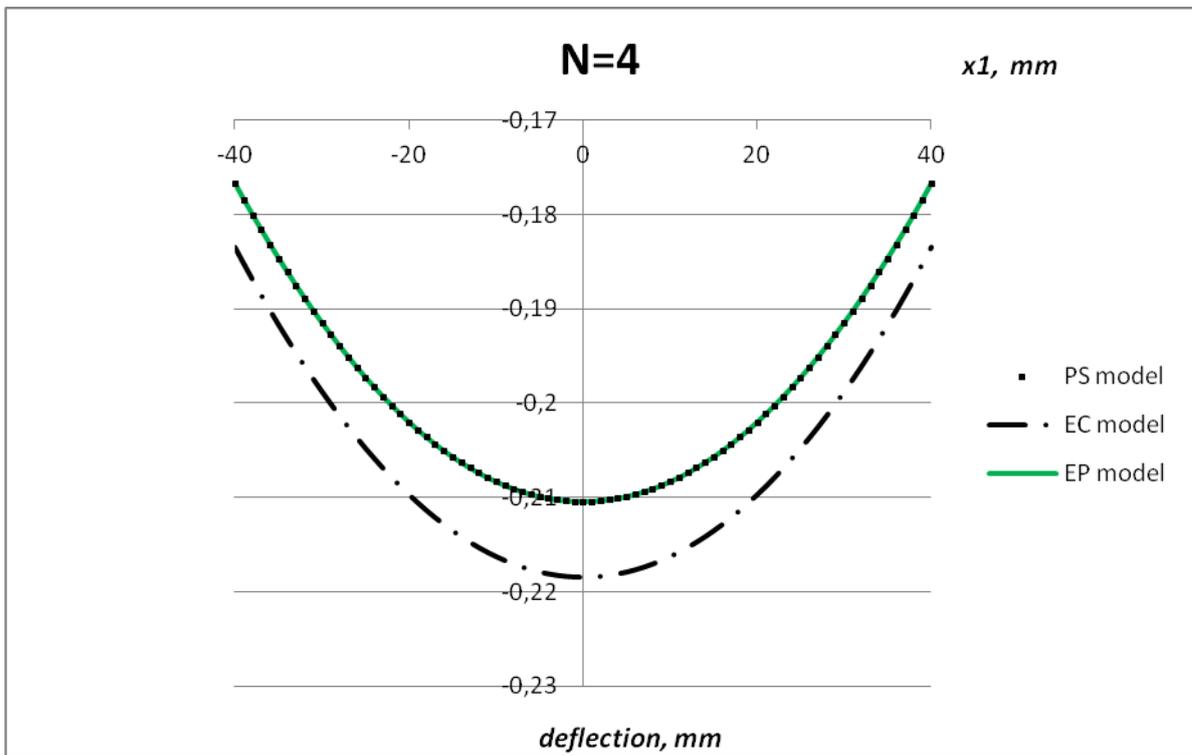
Fig. 7.9. Plate deflection for different models and 4 fibres per thickness (N=4)
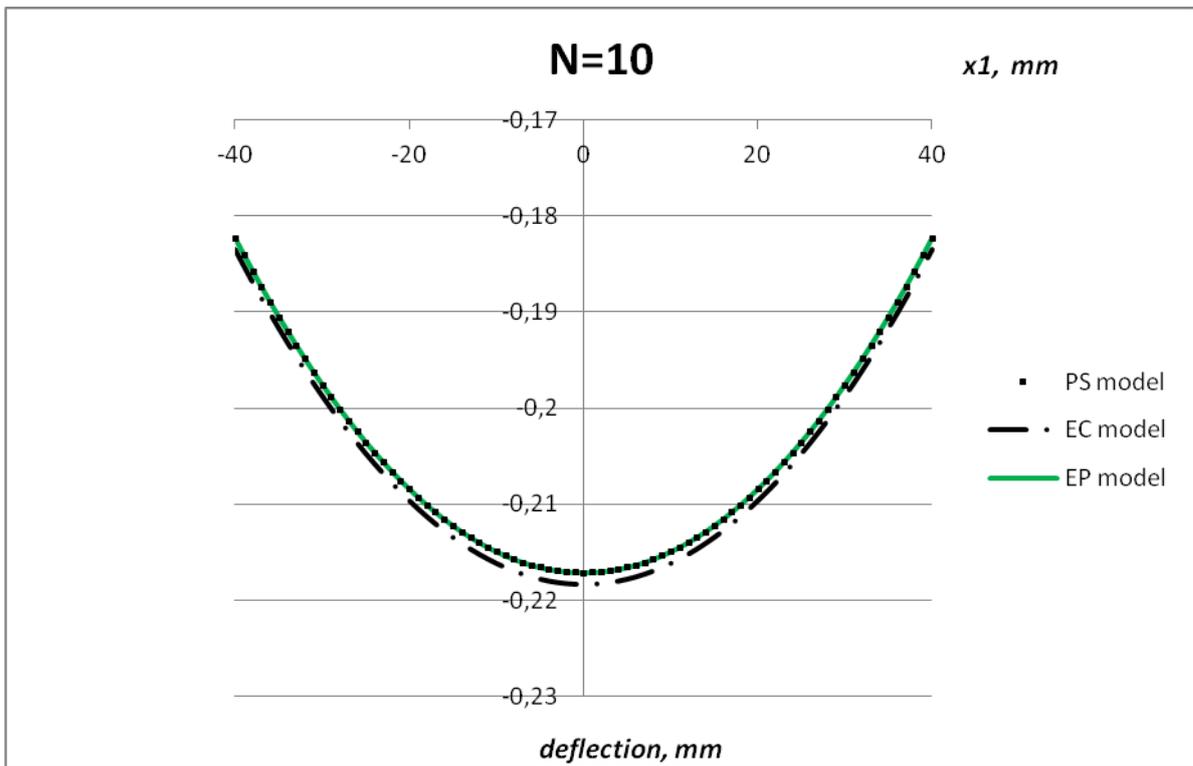
Fig. 7.10. Plate deflection for different models and 10 fibres per thickness (N=10)

The motivation for such comparison sprung from chapter 4 in [2] where the authors consider Euler-Bernoulli beam with the cosinusoidal Young's modulus distribution to point out the inaccuracy of the conventional theory of fibre-reinforced materials in cases where the fibres are not infinitesimally thin.

In polar theory, the length scale can be introduced via the additional elastic constant d_{31}. In the present computations, the formula for d_{31} contains $(h/N)^2$ which is the (squared) dimension of a representative volume unit related to the nominal fibre thickness (similarly to [1], [85].) Therefore the EP model gives correct results (equal to the PS model) for N=4 while the conventional theory of elasticity (EC model) neglects the bending stiffness of fibres and consequently underestimates the stiffness because the fibre thickness is not negligible. With increasing N the bending stiffness of fibres decreases and the correct solution obtained by both PS and EP models becomes closer to the EC model which gives still the same results independent of the number of fibres (no size effect).

8. Verification of the FEM code based on the exact solutions for small strain problems

Verification is carried out using new exact solutions for the anisotropic couple stress continuum with the incompressibility constraint.

Considerations and techniques employed in Section 6 are used to achieve exact solutions of the linear boundary problems below.

Plane strain boundary problem is solved both analytically and numerically (using the new FEM code). The large strain problem is also examined.

8.1. Large strain framework

The large-strain framework modified by Spencer and Soldatos [2] for couple stress theory and shortly outlined in 5.1 is used in this section. Deformation gradient tensor F and right Cauchy-Green deformation tensor C are conventionally used.

The tensor Λ will be denoted as "curvature tensor" below because it is related to the curvature of fibres and to other derivatives of the deformation gradient tensor F in the deformed configuration (although only some components of this tensor can be interpreted geometrically as fibre curvatures).

For a unidirectional fibre-reinforced composite model, unit vector A(X) defines the fibre direction in the reference configuration.

The basic differential equations of equilibrium of the couple stress theory were introduced in 5.1. and served as a basis for the formulation of FE code by Lasota in [3] based on calculus of variations.

8.1.1. Choice of the specific form of the model – incompressible material

To construct a computationally applicable strain energy density function in a form suitable for the rubber-like composites reinforced with fibres stiff in bending, we choose a strain energy density function that contains only one additional invariant accounting for the bending stiffness of fibres. Here and below the chosen material is considered to be fully incompressible. Therefore the constitutive model differs somewhat from that described in section 5.3, where "nearly incompressible" formulation is outlined. The following invariants are employed from (5.10):

$$I_1 = C_{JJ}, \tag{8.1}$$

$$I_4 = A_J C_{LJ} A_L \tag{8.2}$$

$$I_6 = A_J \Lambda_{OJ} \Lambda_{OL} A_L \tag{8.3}$$

Then the strain energy density has the final form based on [8] and now is modified for material incompressibility:

$$W = k_1(I_1 - 3) + k_2(I_4 - 1)^2 + k_3 I_6 + p(J - 1) \tag{8.4}$$

where p is Lagrange multiplier related to incompressibility and J is the volume ratio.

The coefficients in eq. (8.4) represent material parameters: k_1 is related to properties of the matrix (neo-Hooke model), k_2 and k_3 relate to the tensile and bending stiffness of the material in the direction of reinforcement, respectively.

The specific constitutive equations can be derived for the proposed strain energy density from the general relations [2]:

$$\sigma_{(ij)} = \left[F_{iR} F_{jS} \left(\frac{\partial W}{\partial C_{RS}} + \frac{\partial W}{\partial C_{SR}} \right) + \left(G_{iR} F_{jS} + G_{jR} F_{iS} \right) \frac{\partial W}{\partial \Lambda_{SR}} \right], \tag{8.5a}$$

$$\overline{m}_{ji} = \frac{2}{3} e_{ikm} \frac{\partial W}{\partial \Lambda_{PR}} F_{mP} \left(F_{jR} b_k + F_{kR} b_j \right) \tag{8.5b}$$

where $G_{iJ} = \dfrac{\partial F_{iR} A_R}{\partial X_J}$, $b_i = F_{iR} A_R$.

8.1.2. *Finite element formulation*

As it has been mentioned before, two finite element approaches exist with relation to CST. One of them introduces the rotations as independent variables which enables application of *C0* finite elements. In this case the rotations-displacements dependency is taken into account using penalty term in the virtual work expression. Such approach has been used in [4] which, however, has not yielded successful numerical results.

The present work uses the pure displacement based approach and employs *C1* Hermite elements, as elaborated in Section 5.5.

Displacement vector field and the hydrostatic pressure are taken to be the only fundamental unknowns.

After the linearisation, the following five linear systems with respect to unknown increments of nodal displacements Δu_i^a, increments of nodal slopes $\Delta \alpha_i^a, \Delta \beta_i^a, \Delta \gamma_i^a$ and increments of nodal hydrostatic pressure are considered:

$$K_{aibk}^{uu}\Delta u_k^b + K_{aibk}^{u\alpha}\Delta \alpha_k^b + K_{aibk}^{u\beta}\Delta \beta_k^b + K_{aibk}^{u\gamma}\Delta \gamma_k^b + K_{aib}^{up}\Delta p^b = R_i^a \,,$$

$$K_{aibk}^{\alpha u}\Delta u_k^b + K_{aibk}^{\alpha\alpha}\Delta \alpha_k^b + K_{aibk}^{\alpha\beta}\Delta \beta_k^b + K_{aibk}^{\alpha\gamma}\Delta \gamma_k^b + K_{aib}^{\alpha p}\Delta p^b = S_i^a \,,$$

$$K_{aibk}^{\beta u}\Delta u_k^b + K_{aibk}^{\beta\alpha}\Delta \alpha_k^b + K_{aibk}^{\beta\beta}\Delta \beta_k^b + K_{aibk}^{\beta\gamma}\Delta \gamma_k^b + K_{aib}^{\beta p}\Delta p^b = T_i^a \,, \qquad (8.6)$$

$$K_{aibk}^{\gamma u}\Delta u_k^b + K_{aibk}^{\gamma\alpha}\Delta \alpha_k^b + K_{aibk}^{\gamma\beta}\Delta \beta_k^b + K_{aibk}^{\gamma\gamma}\Delta \gamma_k^b + K_{aib}^{\gamma p}\Delta p^b = U_i^a \,,$$

$$K_{aib}^{pu}\Delta p^b + K_{aib}^{p\alpha}\Delta p^b + K_{aib}^{p\beta}\Delta p^b + K_{aib}^{p\gamma}\Delta p^b + K_{aib}^{pp}\Delta p^b = V^a \,,$$

where R_i^a, S_i^a, T_i^a, U_i^a, V^a are residual vectors components and nodal number *a* changes from 1 to n, coordinate number *k* changes from 1 to 3.

The above finite element formulation refers to the case of purely incompressible material, as is evident from the presence of the hydrostatic pressure parameter. This is the approach alternative to the approach in 4.5.1 for the slightly compressible case where four systems of equations were used. Both approaches have been implemented in Matlab software by Lasota [3].

8.2. Numerical results for linear elastic case

The above solver is based on finite element method (FEM) and applies the polar (couple stress) theory. To test the applicability of this solver, it is applied to two plane strain problems in

the first part of this section. In order to verify the element formulation and the chosen form of strain energy density function, the FEM numerical results are compared with values obtained analytically. Since there are no analytical solutions available for large strain anisotropic polar elasticity, we consider a small strain case here.

8.2.1. *Verification within the small strains range*

Analytical solution of a plane strain boundary problem of polar elasticity for flexure of the thick plate under sinusoidal pressure load (**Fig. 8.1**) has been derived recently by Farhat and Soldatos in [1] the outline of the solution is presented briefly in Appendix**.**

As it is shown in paragraph 5.3.2, for the case of the strain energy density with the additional invariant I_6 and the case of small strains, only two components of the couple stress tensor are non-zero. Here, since the plane strain problem is considered, only one component is left:

$$m_{13} = d_{31} \frac{\partial^2 u_2}{\partial x_1^2},$$

(8.7)

so that

$$\sigma_{[21]} = \frac{1}{2} d_{31} \frac{\partial^3 u_2}{\partial x_1^3}.$$

(8.8)

So the lateral boundary conditions (see (A.11) in Appendix) can be written in the following way:

$$
\begin{cases}
c_{12} \dfrac{\partial u_1}{\partial x_1}\left(x_1, \dfrac{h}{2}\right) + c_{22} \dfrac{\partial u_2}{\partial x_2}\left(x_1, \dfrac{h}{2}\right) = -q_0 \sin\left(\dfrac{\pi x_1}{L}\right), \\[2mm]
c_{66}\left(\dfrac{\partial u_1}{\partial x_2}\left(x_1, \dfrac{h}{2}\right) + \dfrac{\partial u_2}{\partial x_1}\left(x_1, \dfrac{h}{2}\right)\right) + \dfrac{1}{2} d_{31} \dfrac{\partial^3 u_2}{\partial x_1^3}\left(x_1, \dfrac{h}{2}\right) = 0, \\[2mm]
c_{12} \dfrac{\partial u_1}{\partial x_1}\left(x_1, -\dfrac{h}{2}\right) + c_{22} \dfrac{\partial u_2}{\partial x_2}\left(x_1, -\dfrac{h}{2}\right) = 0, \\[2mm]
c_{66}\left(\dfrac{\partial u_1}{\partial x_2}\left(x_1, -\dfrac{h}{2}\right) + \dfrac{\partial u_2}{\partial x_1}\left(x_1, -\dfrac{h}{2}\right)\right) + \dfrac{1}{2} d_{31} \dfrac{\partial^3 u_2}{\partial x_1^3}\left(x_1, -\dfrac{h}{2}\right) = 0,
\end{cases}
$$

(8.9)

And they are satisfied by identifying 4 unknown coefficients (eight coefficients are used overall, but only four of them are independent) in the solution functions $f_1(x_2)$, $f_2(x_2)$ (introduced earlier in (6.15), (6.16)) and then used below in (8.10) (see Appendix for more details):

$$u_1 = a_i e^{\mu_i x_2} cos\left(\frac{\pi x_1}{L}\right),$$

$$u_2 = \bar{a}_i e^{\mu_i x_2} sin\left(\frac{\pi x_1}{L}\right),$$

(8.10)

However, we couldn't use the values in [1] directly for the verification of the code, since it is programmed for the incompressible material model only and the numerical results given in [1] are calculated for a specific material with some compressibility. Therefore we use the solution technique offered in [1] for another linear elastic, transversely isotropic incompressible polar material.

8.2.2. The equivalent linear constitutive law

The FEM code produced by Lasota [3] and modified in the present work is designed to accommodate a certain form of material description. Material must be defined by elastic strain energy density being a function of several invariants. On the other hand, the linear boundary problem described in Section 6 and later in this section requires material law to be presented in the form of the generalised Hooke's law. The aim of this section is to compare analytically obtained solutions (for the linear elastic material) with the FEM obtained solutions (for the hyperelastic material under small strains). Evidently, it has to be the same material (same behaviour described in two different forms). In this paragraph we briefly outline the transition between the nonlinear anisotropic material law (NAML) and the equivalent generalised Hooke's law (EGHL) which describe the same behaviour under small strains.

We start with the conventional elasticity (with no regard for the presence of couple stresses). The given incompressible transversely isotropic material with fibres initially aligned along the x_1 direction is described as follows

$$W = k_1(I_1 - 3) + k_2(I_4 - 1)^2 + p(J - 1),$$

(8.11)

where k_1 is related to properties of the matrix (neo-Hooke model), k_2 relates to the tensile and stiffness of fibres, p plays the role of a Lagrange multiplier. Let us construct equivalent material model within the framework of the Hooke's law.

Shear moduli of the EGHL are $G_{12}=G_{23}=G_{31}=2k_1$. The Young's modulus in the preferred direction is

$$E_1=6k_1+8k_2$$

(8.12)

The relations between elastic constants for the orthotropic material are as follows:

89

$$\frac{v_{21}}{E_2} = \frac{v_{12}}{E_1},$$

$$\frac{v_{31}}{E_3} = \frac{v_{13}}{E_1}, \qquad (8.13)$$

$$\frac{v_{23}}{E_2} = \frac{v_{32}}{E_3}.$$

For the orthotropic material in general, the following relations of Poisson's ratios ensure incompressibility:

$$v_{12} + v_{13} = 1,$$
$$v_{21} + v_{23} = 1, \qquad (8.14)$$
$$v_{32} + v_{31} = 1.$$

In our case (transversely isotropic material) the following is true:

$$v_{1T} = 0.5,$$
$$v_{T1} = \frac{E_T}{E_1} v_{1T}, \qquad (8.15)$$
$$v_{TT} = 1 - v_{T1},$$

where index T denotes transversal directions and index 1 denotes the preferred direction.

So, with G given by $2k_1$, E_1 given by (8.12) and v_{1T} given by (8.15) the two remaining elastic constants (E_T and consequetnly v_{T1}) are to be found from the following relations:

$$\begin{cases} G_{TT} = \dfrac{E_T}{2(1 + v_{TT})}, \\[2mm] v_{T1} = \dfrac{E_T}{E_1} v_{1T}. \end{cases} \qquad (8.16)$$

Then we can say that for the present calculations, the following parameters are further employed: $k_1=1$, $k2= 11.75$, $d=0$ in the large-strain description, and, consequently, the following constants for the equivalent linear elastic material: $G_{1T}=G_{TT}=2$, $E_1=100$, $E_T=7.84$, $v_{1T}=0.5$, $v_{TT}=0.96$.

Now let us consider additional elastic parameters related to couple stress theory. Within the couple stress theory the energy density has the following form with additional parameter k_3:

$$W = k_1\left(\bar{I}_1 - 3\right) + k_2\left(\bar{I}_4 - 1\right)^2 + k_3\bar{I}_6 + \frac{1}{d}\left(J - 1\right)^2, \tag{8.17}$$

where d is incompressibility constant

or an incompressible formulation

$$W = k_1\left(I_1 - 3\right) + k_2\left(I_4 - 1\right)^2 + k_3 I_6 + p(J - 1) \tag{8.18}$$

From the paragraph *5.3.2.* it can be concluded that

$$m_{13} = d_{31}\frac{\partial^2 u_2}{\partial x_1^2}, \tag{8.19}$$

and that for the present form of the strain energy density

$$d_{31} = \frac{8}{3}k_3, \tag{8.20}$$

where $d_{31}=2c_3$ in the governing equations for the linear boundary problem in Appendix.

The material behaviour is characterised by the strain energy density (8.18) with the following constants: $k_1=1$ *MPa*, $k_2=$ *11.75 MPa*, $k_3=$ *30 mPa·mm²*.

The above material parameters correspond (within the small strain range) to the linear constitutive equations (see Appendix) described by means of the following constants: $G_{12}=G_{22}=2$ *MPa*, $E_1=100$ *MPa*, $E_2=7.84$ *MPa*, $v_{12}=0.5$, $v_{23}=0.96$, $c_3=40$ *mPa·mm²*, where the indices denote numbers of axes with 1 denoting the preferred direction.

The boundary condition at the top surface is $\sigma_2\left(x_1, h/2\right) = -q_0 sin\left(\dfrac{\pi x_1}{L}\right)$ where $q_0=0.01$ *N/mm*.

The length L of the plate was 100 *mm*, the height was $h=L/4$. Complete boundary conditions are depicted in **Fig. 8.1**.
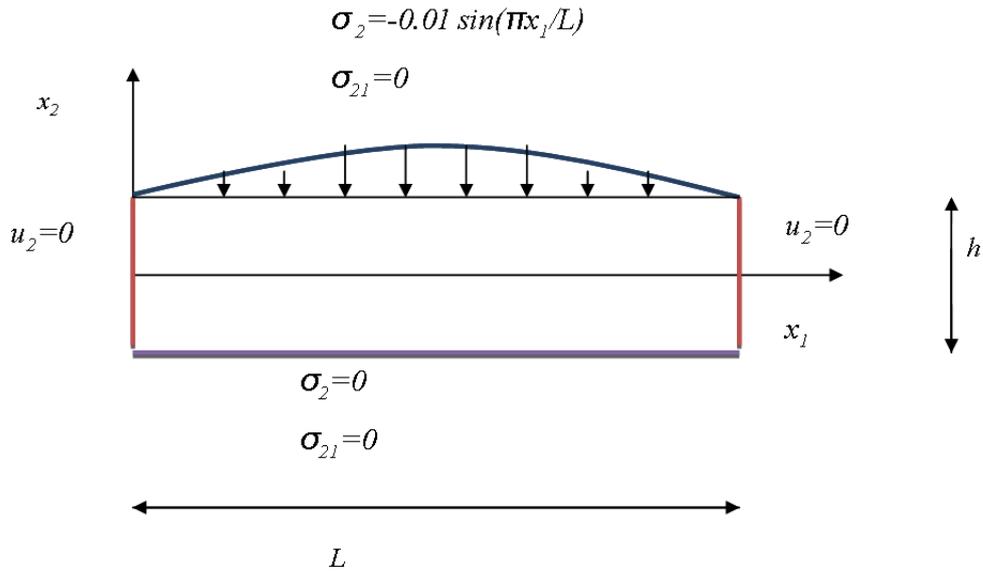
Fig. 8.1. Boundary value problem

The finite element model represents one half of the plate due to its symmetry and employs three dimensional elements. The boundary conditions including nodal forces, slopes and displacements are applied to the surfaces as shown in **Fig. 8.2.**
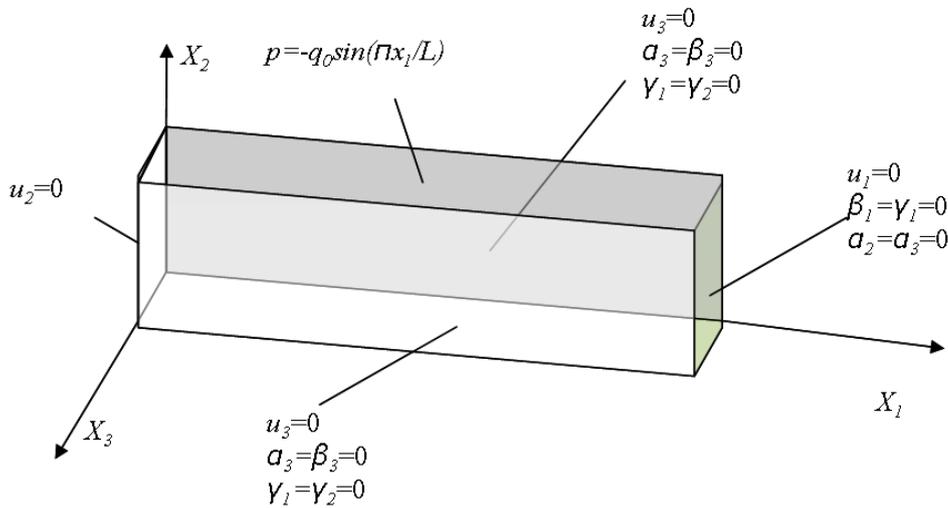
Fig. 8.2. Half of the plate with boundary conditions of the FE model

8.2.3. Results

Numerical and analytical results for the deflection of the top surface of the plate ($x_2=h/2$), the normal stress and the couple stress along the axis x_2 (in the cross-section $x_1=L/2$) are depicted in

92

Figs. 8.3, 8.4, 8.5, respectively. All the FEM results show highly accurate agreement with the exact analytical curves.
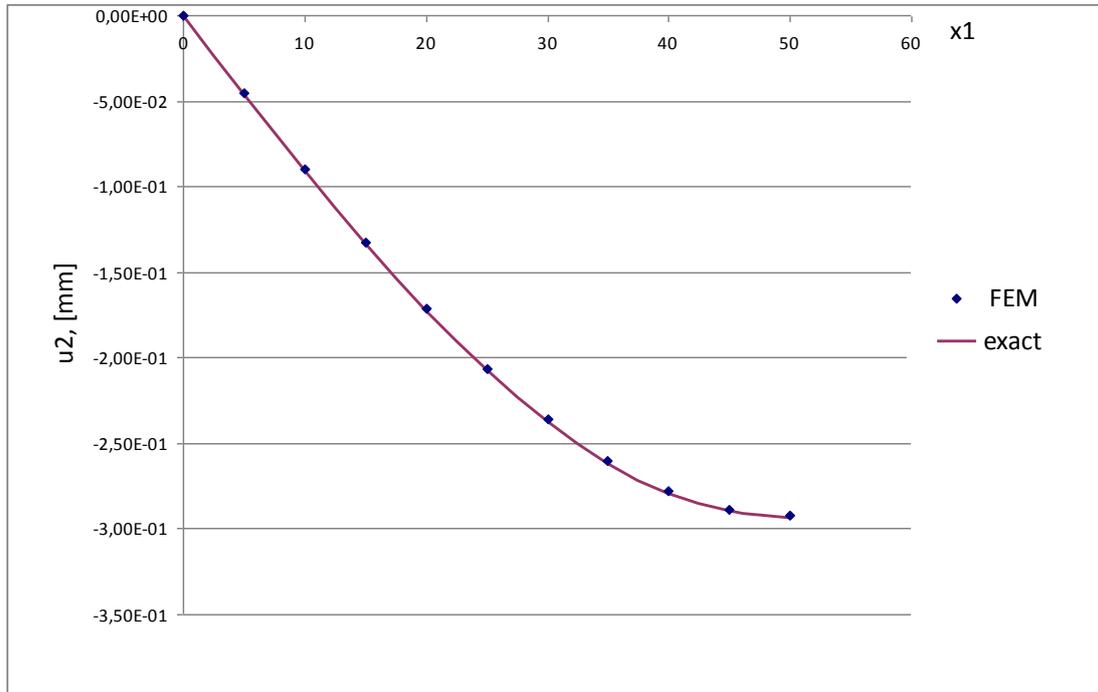
Fig. 8.3. Displacement in x_2 direction computed at the top surface of the plate (results are shown along a half of the plate due to its symmetry)
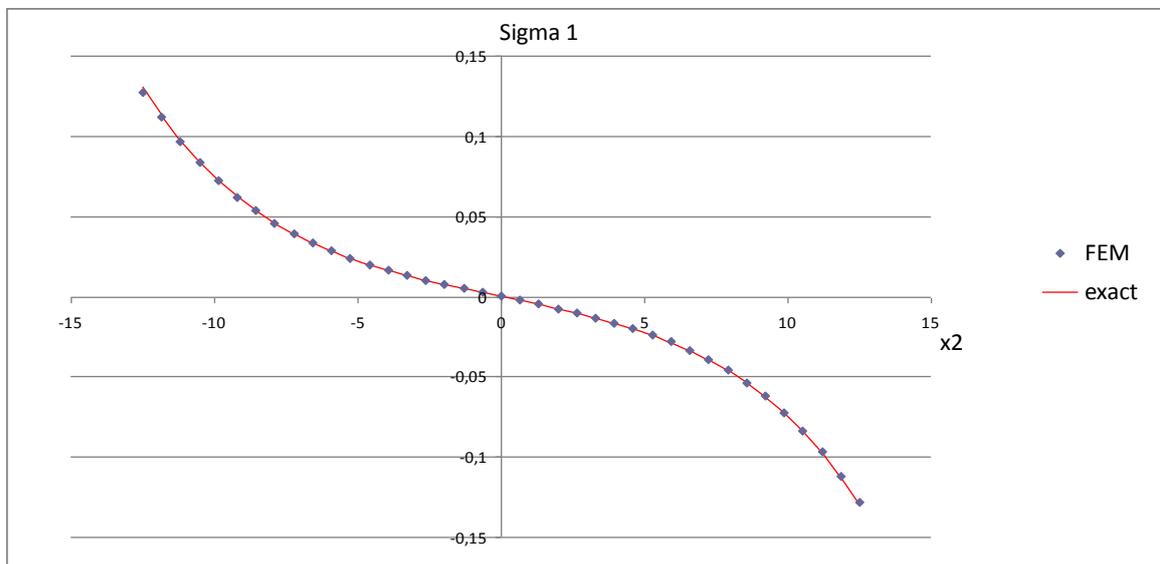
Fig. 8.4. Distribution of first principal stress σ_1 throughout the thickness of the plate in the middle section ($x_1 = L/2$).
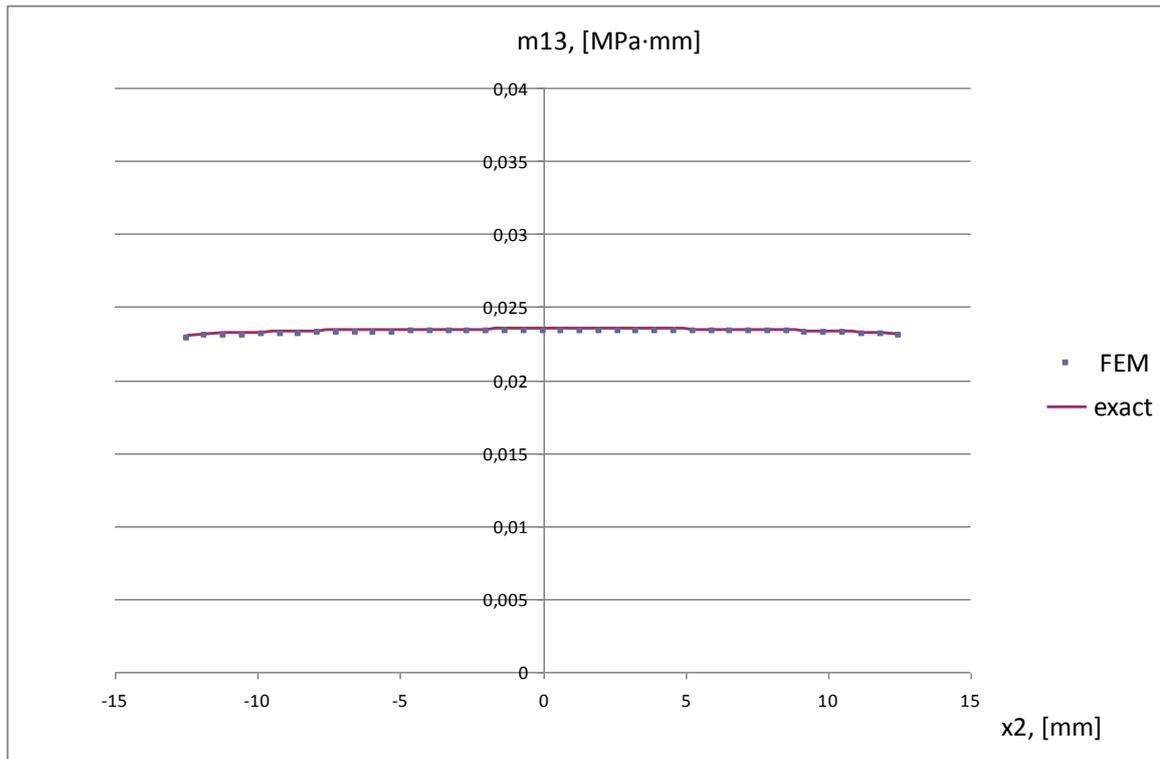
Fig. 8.5. Distribution of couple stress m_{13} throughout the thickness of the plate in the middle section ($x_1 = L/2$).

8.3. Illustrative problem in large strains

The capability of the FEM code to model three-dimensional problems under large strains is demonstrated below.

To illustrate the capability of the FEM code to solve problems under large strains, tension test of a fibre reinforced elastomer specimen loaded in another direction than that of the fibres was chosen. The FEM applications on the basis of both classical elasticity and nonlinear polar theory are compared in this section by means of analyses of stresses and deformations of the specimen.

Let us consider a thin rectangular elastomer specimen reinforced with one family of fibres. The specimen is subjected to uniaxial tension as shown in **Fig.8.6**. The fibre direction corners a general angle with the direction of tension. The material law for the model is chosen in the form (8.18). Two models with the same mesh have been used for FEM computations. The material parameters of the models were set as follows: $k_1=1$ *MPa*, $k_2= 11.75$ *MPa*, $k_3= 0$ for the 1st model, and $k_1=1$ *MPa*, $k_2= 11.75$ *MPa*, $k_3= 0.5$ *MPa·mm²* for the 2nd model. The angle between the principal material direction and tension direction was $\alpha=\pi/4$ in the further analyses.

The 1st model corresponds to the classical theory of elasticity and so the respective problem can be easily solved using commercial FEM code Ansys. The 2nd model incorporates the

94

material constant k_3 related to the intrinsic bending stiffness and the respective problem is solved in the new code presented above. We pay particular attention to the deformed fibre rotation angle in both models (**Fig. 8.7**). We keep in mind that fibres are not present in either geometrical model explicitly, but the effect of their presence is included mathematically in the constitutive law. Consequently, the "deformed fibre rotation angle" is calculated by subtracting the relevant angular positions of the nodes in the deformed and undeformed meshes (**Fig.8.8**).

As expected, the non-zero parameter k_3 influences the response by adding anisotropic bending stiffness to the model (namely, to the implicitly present fibres). From **Fig. 8.7** it can be seen that the deformed fibre rotation angle is higher in the classical ($k_3= 0$) model. The influence was also confirmed by maximum lateral displacements (in x_2 direction) of the specimen being 20 % lower for the non-zero k_3 constant.
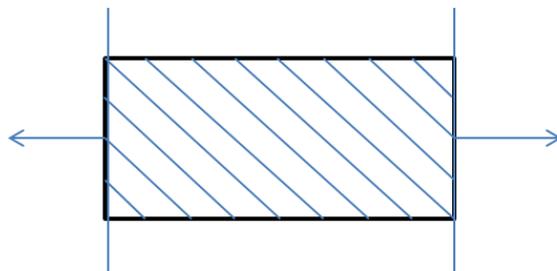
Fig. 8.6. Specimen of fibre reinforced elastomer loaded in tension
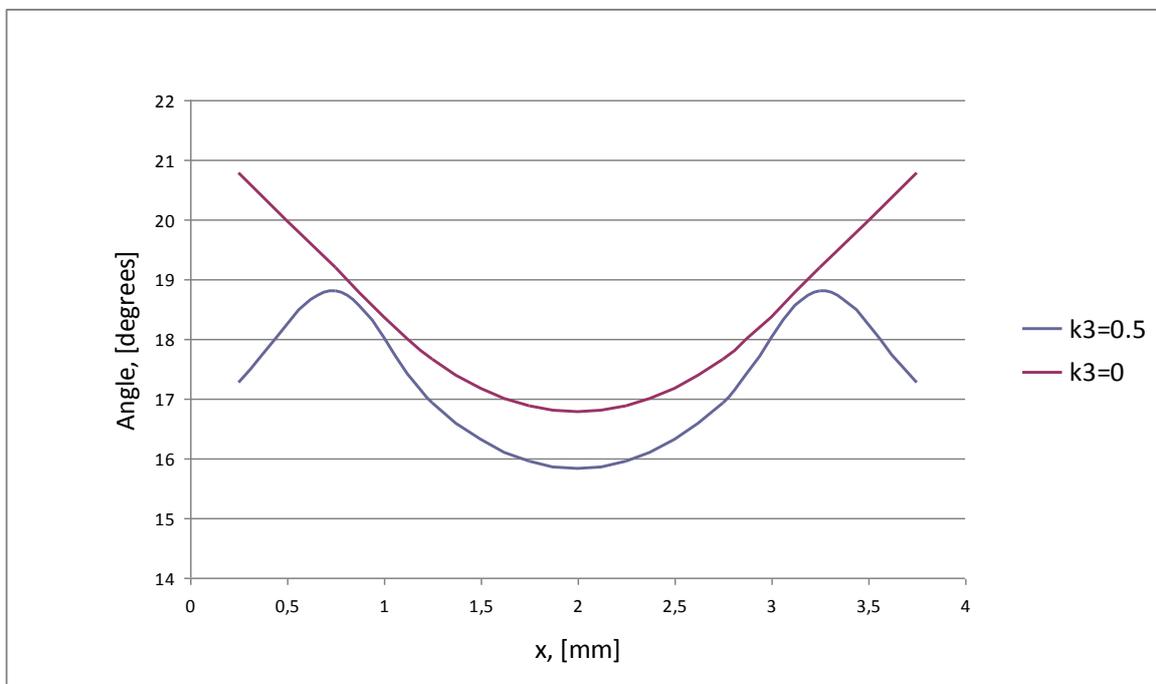
Fig. 8.7. Comparison of the deformed fibre rotation angle in both models under the same load
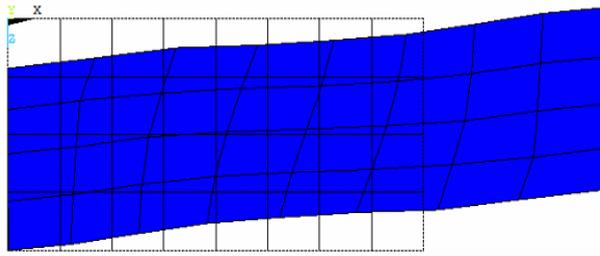
Fig. 8.8. Deformed and undeformed mesh of the fibre reinforced elastomer under tension (k_3=0.5)

In the large strain range no solution enabling us a verification was found in literature, so the presented example illustrates only qualitatively the capability of the code to mimic the bending stiffness of the fibres. When the parameter k_3 is set to zero in the applied material model, it is reduced to a classical (Cauchy) model taking only tension stiffness of the fibres into consideration, i.e. based on the assumption of the infinitesimal diameter of fibres and their uniform distribution. Under these conditions the solution obtained by the new code showed a full agreement with the commercial FEM code ANSYS. Addition of a non-zero value of the k_3 parameter has increased the stiffness of the specimen, demonstrating thus the increased resistance of the specimen against deformation caused by bending stiffness of the fibres.

9. Problems with kinematic constraints: linear elasticity with and without additional bending stiffness

Analytical solutions for small deformations of thick isotropic plates are established in the literature for long. The studies relevant to this work are outlined below.

Extending the study of Srinvas et al [82] by adding the incompressibility constraint, Aimmanee and Batra [83] provide an analytical solution for free vibration of a simply supported rectangular plate. They focus on identifying natural frequencies of a three-dimensional plate, which is out of the scope of this work, but the general logic of their solution is relevant to the present study.

In terms of conventional linear elasticity, the present work extends the study [83] by extending the case to orthotropy, specifically transversal isotropy, the fibre inextensibility constraint while in the same time restricting the case to plane strain and static deformation.

Then the recently introduced polar elasticity for fibre-reinforced solids [1] is employed in this part, the applied material description includes homogeneity, anisotropy and additional intrinsic bending stiffness, corresponding to the contribution of fibres in the equivalent composite.

In terms of polar theory the present study extends the work [1] by adding kinematic constraints of incompressibility and inextensibility to the relevant problem. The work [1] itself can be regarded as a polar elasticity generalization of the classical elasticity approach of [84]. Pagano in [84] derives elasticity solutions for cylindrical bending of orthotropic laminates. The scheme of his solutions is adopted in the present work with appropriate modifications, related to the introduced kinematic constraints.

With regard to the kinematic constraints in polar elasticity problems, some other recent works have to be mentioned. Incompressibility and inextensibility constraints have been applied to the problem of large strain hyperelastic deformation of a transversely isotropic block [46] and azimuthal shear of a transversely isotropic tube [85].

9.1. Restrictions on elastic constants outgoing from the kinematic constraints

The restrictions on Poisson's ratios for isotropic and transversely isotropic incompressible materials are established for long, but here they are derived again in order to reiterate the mathematical logics behind such restrictions. The aim is to outline how introducing a kinematic

constraint yields the restrictions for material constants, and how the corresponding Lagrange multipliers (e.g., hydrostatic pressure or an arbitrary tension in the direction of reinforcement) appear in the constitutive equations based on the generalized Hooke's law.

For all the cases, the hydrostatic pressure can be expressed, by definition, as

$$P = -\frac{1}{3}\left(\sigma_{11} + \sigma_{22} + \sigma_{33}\right) \tag{9.1}$$

9.1.1. Isotropic case

First, let us consider the isotropic case of an incompressible material

From the generalised Hooke's law we know

$$\begin{pmatrix} \sigma_{11} \\ \sigma_{22} \\ \sigma_{33} \\ \sigma_{23} \\ \sigma_{13} \\ \sigma_{12} \end{pmatrix} = \frac{E}{(1+v)(1-2v)} \begin{pmatrix} 1-v & v & v & 0 & 0 & 0 \\ v & 1-v & v & 0 & 0 & 0 \\ v & v & 1-v & 0 & 0 & 0 \\ 0 & 0 & 0 & 1-2v & 0 & 0 \\ 0 & 0 & 0 & 0 & 1-2v & 0 \\ 0 & 0 & 0 & 0 & 0 & 1-2v \end{pmatrix} \begin{pmatrix} \varepsilon_{11} \\ \varepsilon_{22} \\ \varepsilon_{33} \\ \varepsilon_{23} \\ \varepsilon_{13} \\ \varepsilon_{12} \end{pmatrix} \tag{9.2}$$

Let us introduce $\theta = \varepsilon_{11} + \varepsilon_{22} + \varepsilon_{33}$ representing relative volumetric change.

Then inserting the expressions for normal stresses from (9.2) into (9.1) we obtain the relation for isotropic material:

$$P = -\frac{E}{3(1-2v)}\theta \tag{9.3}$$

We can use an alternative to (9.2) form of Hooke's law

$$\sigma_{ij} = \lambda\theta\delta_{ij} + 2\mu\,\varepsilon_{ij}\ , \tag{9.4}$$

and consequently, alternative form of relation (9.3):

$$P = -\frac{1}{3}\left(3\lambda + 2\mu\right)\theta \tag{9.5}$$

Now we impose the incompressibility constraint

$$\varepsilon_{11} + \varepsilon_{22} + \varepsilon_{33} = \theta = 0 \tag{9.6}$$

Then from (9.3) we have

$$\theta = \frac{1-2v}{E}\left(\sigma_1 + \sigma_2 + \sigma_3\right) = 0 \tag{9.7}$$

and straightforward consequent restriction for Poisson's ratio:

$$\nu = 0.5 \tag{9.8}$$

Alternative form (9.3) of constitutive equations with use of Lame constants gives

$$\varepsilon_1 + \varepsilon_2 + \varepsilon_3 = \frac{1}{3\lambda + 2\mu}(\sigma_1 + \sigma_2 + \sigma_3) = 0 \tag{9.9}$$

and a corresponding restriction

$$\lambda -> \infty \tag{9.10}$$

Then constitutive relations for normal stresses can be rewritten in a new form. Using the example of normal stress σ_1 we can see below how the hydrostatic pressure occurs in the equations.

$$\sigma_{ij} = \frac{\nu E}{(1+\nu)(1-2\nu)}\theta\delta_{ij} + 2G\varepsilon_{ij} \tag{9.11}$$

we insert $\theta = \theta(P)$ using (9.3)

$$\sigma_{11} = -\frac{3\nu}{1+\nu}P + 2G\varepsilon_{11} \ , \tag{9.12}$$

since $\nu = 0.5$, it holds

$$\sigma_{11} = -P + 2G\varepsilon_{11}. \tag{9.13}$$

Similarly, other normal stresses are derived.

Now, by carrying out same steps for (9.4) Lame form, we will obtain same result with alternative constants. The Hooke's law transforms as follows:

$$\sigma_{ij} = \lambda\theta\delta_{ij} + 2\mu\ \varepsilon_{ij} \ , \tag{9.14}$$

$$\sigma_{11} = \lambda\theta + 2\mu\ \varepsilon_{11}, \tag{9.15}$$

we insert $\theta = \theta(P)$ using (9.5) and obtain

$$\sigma_{11} = -\frac{3\lambda}{3\lambda + 2\mu} P + 2\mu\, \varepsilon_{11}\,, \tag{9.16}$$

since $\lambda -> \infty$,

$$\sigma_{11} = -P + 2\mu\, \varepsilon_{11}. \tag{9.17}$$

9.1.2. Transversely isotropic case

Now similar steps can be performed for transversely isotropic material

$$\begin{pmatrix} \sigma_{11} \\ \sigma_{22} \\ \sigma_{33} \\ \sigma_{23} \\ \sigma_{13} \\ \sigma_{12} \end{pmatrix} = \begin{pmatrix} c_{11} & c_{12} & c_{12} & 0 & 0 & 0 \\ c_{12} & c_{22} & c_{23} & 0 & 0 & 0 \\ c_{12} & c_{23} & c_{22} & 0 & 0 & 0 \\ 0 & 0 & 0 & c_{44} & 0 & 0 \\ 0 & 0 & 0 & 0 & c_{66} & 0 \\ 0 & 0 & 0 & 0 & 0 & c_{66} \end{pmatrix} \begin{pmatrix} \varepsilon_{11} \\ \varepsilon_{22} \\ \varepsilon_{33} \\ 2\varepsilon_{23} \\ 2\varepsilon_{13} \\ 2\varepsilon_{12} \end{pmatrix}. \tag{9.18}$$

Hydrostatic pressure is given by (9.1) as before. We insert (9.1) into (9.18) to obtain $P = P(\theta)$

$$P = -\frac{1}{3}\left((c_{12} + c_{22} + c_{23})\theta + (c_{12} + c_{11} - c_{22} - c_{23})\varepsilon_1 \right) \tag{9.19}$$

The components of the stiffness matrix can be, of course, expressed using the five independent technical constants E_1, E_T, v_{1T}, v_T, G_{1T}.

We also can use alternative form of Hooke's law for transversely isotropic material [86] when the anisotropy axis is characterised by vector $\boldsymbol{a} = (1,0,0)^{\mathrm{T}}$

$$\sigma_{ij} = \lambda\theta\delta_{ij} + 2\mu_T\varepsilon_{ij} + \alpha\left(\varepsilon_{11}\delta_{ij} + \theta a_i a_j\right) + \beta\varepsilon_{11}a_i a_j + 2(\mu_1 - \mu_T)\left(a_i\varepsilon_{j1} + a_j\varepsilon_{i1}\right), \tag{9.20}$$

where λ, α, β, μ_1, μ_T are five independent material constants.

Then the link between P and θ is obtained as before:

$$P = -\frac{1}{3}\left((3\lambda + \alpha + 2\mu_T)\theta + (4(\mu_1 - \mu_T) + 3\alpha + \beta)\varepsilon_1 \right), \tag{9.21}$$

$$\theta = -\frac{3}{3\lambda + \alpha + 2\mu_T} P - \frac{4(\mu_1 - \mu_T) + 3\alpha + \beta}{3\lambda + \alpha + 2\mu_T}\varepsilon_1. \tag{9.22}$$

We impose incompressibility constraint $\varepsilon_1 + \varepsilon_2 + \varepsilon_3 = 0$ again and observe the mathematical consequence concerning material constants.

We use constitutive equations (Hooke's law) expressed with technical constants

$$
\begin{pmatrix} \varepsilon_{11} \\ \varepsilon_{22} \\ \varepsilon_{33} \\ 2\varepsilon_{23} \\ 2\varepsilon_{13} \\ 2\varepsilon_{12} \end{pmatrix} = \begin{pmatrix} 1/E_1 & -v_{T1}/E_T & -v_{T1}/E_T & 0 & 0 & 0 \\ -v_{1T}/E_L & 1/E_T & -v_{TT}/E_T & 0 & 0 & 0 \\ -v_{1T}/E_L & -v_{TT}/E_T & 1/E_T & 0 & 0 & 0 \\ 0 & 0 & 0 & 2(1+v_{TT})/E_T & 0 & 0 \\ 0 & 0 & 0 & 0 & 1/G_{1T} & 0 \\ 0 & 0 & 0 & 0 & 0 & 1/G_{1T} \end{pmatrix} \begin{pmatrix} \sigma_{11} \\ \sigma_{22} \\ \sigma_{33} \\ \sigma_{23} \\ \sigma_{13} \\ \sigma_{12} \end{pmatrix}, \quad (9.23)
$$

$$
\varepsilon_1 + \varepsilon_2 + \varepsilon_3 = \sigma_1 \frac{1-2v_{1T}}{E_1} + (\sigma_2 + \sigma_3)\frac{1-v_{TT}-v_{T1}}{E_T} = 0 \quad (9.24)
$$

and obtain

$$
\begin{cases} v_{1T} = 0.5 \\ v_{T1} + v_{TT} = 1 \end{cases} \quad (9.25)
$$

In this way, only three material constants are left independent.

And for Lame form (9.20) the equation (9.22) turns to zero for incompressibility case, which corresponds to $\lambda -> \infty$. When we substitute θ from (9.22) to (9.20) we obtain constitutive equations in the new form for incompressible material – with inclusion of hydrostatic pressure. It should be noted, that they do not contain the constant α anymore. It means that the three independent constants are left now - β, μ_1, μ_T. The equations can be seen in the following section (see (9.35)).

9.2. Problem setting

Let us consider a plane strain boundary problem: a simply supported thick transversely isotropic plate, infinite in the x_3 direction, loaded by sinusoidal pressure on the top surface. In this case, the displacements are functions of only two coordinates

$$
\begin{aligned}
u_1 &= u_1(x_1, x_2), \\
u_2 &= u_2(x_1, x_2), \\
u_3 &= 0.
\end{aligned} \quad (9.26)
$$

The material in question is transversely isotropic with high tensile stiffness in x_1 direction. It simulates a fibre-reinforced composite with one family of straight fibres.

First the main equations of the general case of polar elasticity are considered. Equilibrium equations involve components of the couple stress tensor m_i and components of the stress tensor σ_i; $\in_{ijk}$ represents the Levi-Civita symbol.

$$\frac{\partial \sigma_{ji}}{\partial x_j} = 0,$$
$$j,i=1,2 \qquad (9.27)$$
$$\frac{\partial m_{ji}}{\partial x_j} + \in_{ijk} \sigma_{jk} = 0$$

For the present case of plane strain and given that m_{13} is the only couple stress present (corresponding to the bending stiffness of fibres aligned along x_1) the equilibrium equations become:

$$=> \begin{cases} \dfrac{\partial \sigma_{11}}{\partial x_1} + \dfrac{\partial \sigma_{(12)}}{\partial x_2} + \dfrac{\partial \sigma_{[21]}}{\partial x_2} = 0, \\[2mm] \dfrac{\partial \sigma_{22}}{\partial x_2} + \dfrac{\partial \sigma_{(12)}}{\partial x_2} + \dfrac{\partial \sigma_{[12]}}{\partial x_1} = 0, \\[2mm] \sigma_{[21]} = \dfrac{1}{2}\dfrac{\partial m_{13}}{\partial x_1}, \\[2mm] \sigma_{[12]} = -\dfrac{1}{2}\dfrac{\partial m_{13}}{\partial x_1}. \end{cases} \qquad (9.28)$$

This system can be written in the alternative form

$$\begin{cases} \dfrac{\partial \sigma_{11}}{\partial x_1} + \dfrac{\partial \sigma_{(12)}}{\partial x_2} + \dfrac{1}{2}\dfrac{\partial^2 m_{13}}{\partial x_1 \partial x_2} = 0, \\[2mm] \dfrac{\partial \sigma_{22}}{\partial x_2} + \dfrac{\partial \sigma_{(12)}}{\partial x_2} - \dfrac{1}{2}\dfrac{\partial^2 m_{13}}{\partial x_1^2} = 0. \end{cases} \qquad (9.29)$$

Strain-displacement equations relate strains to displacements

$$\varepsilon_{ij} = \frac{1}{2}\left(\frac{\partial u_i}{\partial x_j} + \frac{\partial u_j}{\partial x_i}\right) \qquad (9.30)$$

and the "curvature-strains" component

$$k_{21} = \frac{\partial^2 u_2}{\partial x_1^2}.$$ (9.31)

Boundary conditions include sinusoidal pressure on the top surface of the plate and zero vertical displacement at the ends of the plate, similar to **Fig. 8.1**. More detailed description is given for each material case below.

In the below paragraphs **9.3**, **9.4**, **9.5** the related equations (including the couple stress formulation) for each case are presented. In the paragraph **9.6** numerical illustrations for the cases within classical elasticity $(d_{31}=0)$ are presented..

In the paragraph **9.7** the numerical results for couple stress formulation are presented.

9.3. Incompressibility constraint case

Here the focus is on the incompressible material and corresponding elastic solutions.
Constitutive relations in the following general form [86] for symmetric stress components can be used:

$$\sigma_{(ij)} = \lambda\theta\delta_{ij} + 2\mu_T\varepsilon_{ij} + \alpha(\varepsilon_{11}\delta_{ij} + \theta a_i a_j) + \beta\varepsilon_{11}a_i a_j + 2(\mu_1 - \mu_T)(a_i\varepsilon_{j1} + a_j\varepsilon_{i1}),$$ (9.32)

where $\theta = \varepsilon_1 + \varepsilon_2 + \varepsilon_3$.
Here μ_T and μ_I represent shear moduli in transversal and longitudinal planes, respectively; λ, α and β are material constants to be examined further on.

With regard to material incompressibility we use hydrostatic pressure $P = -\frac{1}{3}(\sigma_1 + \sigma_2 + \sigma_3)$ as introduced in the above section.
Then using (9.32) the following relation between P and θ is obtained:

$$\theta = -\frac{3}{3\lambda + \alpha + 2\mu_T}P - \frac{4(\mu_1 - \mu_T) + 3\alpha + \beta}{3\lambda + \alpha + 2\mu_T}\varepsilon_1$$ (9.33)

With the use of $\lambda->\infty$ (which corresponds to incompressibility), equations (9.33) yield

$$\sigma_{11} = -P + \left(4\mu_{IT} - 2\mu_T + \frac{2}{3}\beta - \frac{4(\mu_{IT} - \mu_T)}{3}\right)\varepsilon_1,$$

$$\sigma_{22} = -P - \left(\frac{1}{3}\beta + \frac{4(\mu_{IT} - \mu_T)}{3}\right)\varepsilon_1 + 2\mu_T\varepsilon_2,$$ (9.34)

$$\sigma_{(12)} = 2\mu_{IT}\varepsilon_{12}.$$

The second part of the constitutive equations is unchanged:

$$m_{13} = d_{31} \frac{\partial^2 u_2}{\partial x_1^{\,2}} \qquad (9.35)$$

Three independent material constants μ_{1T}, μ_T. β are required for the description of a transversely isotropic incompressible material, and four constants (with d_{31}) if the fibre bending stiffness is included in formulation.

With the substitution of equations (9.34, 9.35) into the system (9.29) the resulting governing equations together with the incompressibility constraint $\theta = 0$ take form:

$$\begin{cases} -\dfrac{\partial P}{\partial x_1} + \left(\dfrac{8}{3}\mu_{1T} - \dfrac{2}{3}\mu_T + \dfrac{2}{3}\beta \right)\dfrac{\partial^2 u_1}{\partial x_1^2} + \mu_1 \left(\dfrac{\partial^2 u_2}{\partial x_1 \partial x_2} + \dfrac{\partial^2 u_1}{\partial x_2^2} \right) + \dfrac{1}{2}d_{31}\dfrac{\partial^4 u_2}{\partial x_1^3 \partial x_2} = 0, \\[3mm] -\dfrac{\partial P}{\partial x_2} + \left(-\dfrac{1}{3}\mu_{1T} + \dfrac{4}{3}\mu_T - \dfrac{1}{3}\beta \right)\dfrac{\partial^2 u_1}{\partial x_1 \partial x_2} + 2\mu_T\dfrac{\partial^2 u_2}{\partial x_2^2} - \dfrac{1}{2}d_{31}\dfrac{\partial^4 u_2}{\partial x_1^4} = 0, \\[3mm] \dfrac{\partial u_2}{\partial x_2} + \dfrac{\partial u_1}{\partial x_1} = 0. \end{cases} \qquad (9.36)$$

the solution is sought in the form

$$u_1 = f_1(x_2)\cos\left(\frac{\pi x_1}{L} \right),$$

$$u_2 = f_2(x_2)\sin\left(\frac{\pi x_1}{L} \right), \qquad (9.37)$$

$$P = p(x_2)\sin\left(\frac{\pi x_1}{L} \right).$$

This corresponds to the boundary conditions applied at the plate ends:

$$\begin{cases} \sigma_1(0, x_2) = 0, \\ u_2(0, x_2) = 0, \\ m_{13}(0, x_2) = 0, \\ \sigma_1(L, x_2) = 0, \\ u_2(L, x_2) = 0, \\ m_{13}(L, x_2) = 0. \end{cases} \qquad (9.38)$$

The upper and lower boundary conditions for the present problem, i.e. along the upper and lower surfaces, are set as follows:

$$\begin{cases} \sigma_{21}(x_1, h/2) = 0, \\ \sigma_2(x_1, h/2) = -q_0 \sin(\pi x_1 / L), \\ \sigma_2(x_1, -h/2) = 0, \\ \sigma_{21}(x_1, -h/2) = 0. \end{cases} \qquad (9.39)$$

Or, in alternative form,

$$\begin{cases} \sigma_{(12)}(x_1, h/2) + \dfrac{1}{2}\dfrac{\partial m_{13}(x_1, h/2)}{\partial x_1} = 0, \\ \sigma_2(x_1, h/2) = -q_0 \sin(\pi x_1 / L), \\ \sigma_2(x_1, -h/2) = 0, \\ \sigma_{(12)}(x_1, -h/2) + \dfrac{1}{2}\dfrac{\partial m_{13}(x_1, -h/2)}{\partial x_1} = 0. \end{cases} \qquad (9.40)$$

For a plate under a specified load (the boundary problem (9.36, 9.39)), the solution is sought in the form of (9.37) as mentioned above where

$$f_1(x_2) = \bar{c}_i e^{\mu_i x_2},$$

$$f_2(x_2) = c_i e^{\mu_i x_2}, \qquad (9.41)$$

$$p(x_2) = \tilde{c}_i e^{\mu_i x_2}$$

The governing equations (9.36) yield fourth order differential equation

$$a\frac{\partial^4 f_2}{\partial x_2^4} + b\frac{\partial^2 f_2}{\partial x_2^2} + cf_2 = 0, \qquad (9.42)$$

where a, b, c are constants.

It should be noted that parameters a, b, c in (9.42) are functions of material constants μ_{1T}, μ_T, β, d_{31}.

Four unknown constants μ_i are found from (9.42). Then we use upper and lower boundary conditions (9.40) to determine $c_i, \bar{c}_i, \tilde{c}_i$.

The resulting stresses are as follows:

$$\sigma_1 = \left(-p(x_2) - \frac{\pi}{L}\left(\frac{8}{3}\mu_1 - \frac{2}{3}\mu_T + \frac{2}{3}\beta\right)f_1(x_2)\right)\sin\left(\frac{\pi x_1}{L}\right),$$

$$\sigma_2 = \left(-p(x_2) - \left(\frac{4}{3}(\mu_1 - \mu_T) + \frac{1}{3}\beta\right)\frac{\pi}{L}f_1(x_2) + 2\mu_T f_2'(x_2)\right)\sin\left(\frac{\pi x_1}{L}\right),$$

$$\sigma_{12} = \left(\mu_{1T}\left(f_1'(x_2) + \frac{\pi}{L}f_2(x_2)\right) - \frac{1}{2}\left(\frac{\pi}{L}\right)^3 d_{31}f_2(x_2)\right)\cos\left(\frac{\pi x_1}{L}\right),$$

$$\sigma_{21} = \left(\mu_{1T}\left(f_1'(x_2) + \frac{\pi}{L}f_2(x_2)\right) + \frac{1}{2}\left(\frac{\pi}{L}\right)^3 d_{31}f_2(x_2)\right)\cos\left(\frac{\pi x_1}{L}\right),$$

(9.43)

$$m_{13} = \left(\frac{\pi}{L}\right)^2 d_{31}f_2(x_2)\sin\left(\frac{\pi x_1}{L}\right)$$

(9.44)

We can see that d_{31} is explicitly present in couple stress expression (9.44) and both shear stress expressions in (9.43). Nevertheless, the influence of d_{31} is present in all stresses implicitly, via the constants μ_i (see (9.41)).

If d_{31} is set to zero (fibre bending stiffness is neglected), the problem (9.37, 9.40) reduces to the corresponding conventional elasticity problem for an incompressible material. To the best knowledge of the author, such a case has not been considered in literature before. Therefore we compare the present (extensible) incompressible formulation (EIF) (with hydrostatic pressure as additional unknown and kinematic constraint employed) with a "general" (extensible and compressible) material formulation (GF) below. In general, GF includes five independent material constants for a transversely isotropic material in generalised Hooke's law. The respective solutions can be found in [84] (classical elasticity) and in [1] (polar elasticity). We approach EIF with GF by setting respective material constants closer to the values corresponding to incompressibility. In terms of generalised Hooke's law for transversely isotropic material, perfect incompressibility is achieved by setting Poisson's ratios as follows:

$$\begin{cases} \nu_{1T} = 0.5 \\ \nu_{T1} + \nu_T = 1 \end{cases}$$

(9.45a, b)

In computations, such constitutive description is not applicable since these values would yield division by zero in stiffness matrix and the compliance matrix becomes ill-conditioned [87]. Therefore the constitutive approach (9.34, 9.35, 9.36) is of use for incompressible material.

Conditions (9.45) given for engineering constants correspond to $\lambda - > \infty$ if we return to Lame notation. Hereinafter the parameters that are manipulated in all the computations are engineering constants, since they are more illustrative in terms of their physical meaning.

The relations linking components of the material stiffness matrix to the Lame constants are given in the paragraph **9.7**.

To approximate GF to EIF we adopt the following scheme. We set the respective Poisson ratios close to the conditions (9.45) $v_{1T} = 0.5$ $v_{T1} + v_T = 1$ with the following deviation δ which tends to zero:

$$\begin{cases} v_{1T} = 0.5 - \delta \\ v_{T1} + v_{TT} = 1 - \delta \end{cases} \tag{9.46}$$

The **Fig. 9.1** shows comparison of the normal stress at the end of the plate between EIF model and the general GF formulation models which are tending to EIF $(\delta \to 0)$. The differences are on the order of 10^{-4} or 10^{-5} MPa, thus not visible in the graph. Therefore the table 9.1 presents their numerical values illustrating the convergence of the results obtained with the general formulation (GF) to the results obtained with incompressible formulation (EIF) if the deviation δ approaches zero.
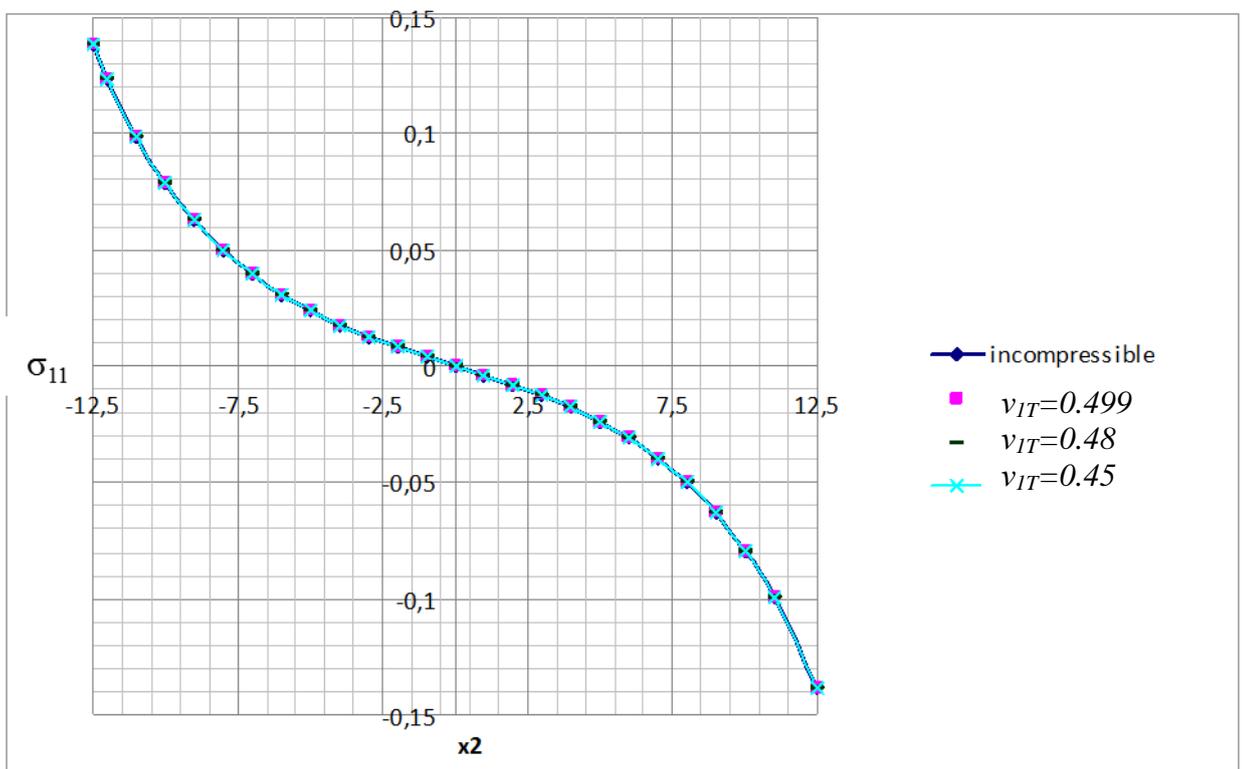

Fig. 9.1. Normal stress in the middle cross-section calculated for different constitutive models

Table 9.1. Error values illustrating convergence

δ	0.05	0.04	0.03	0.02	0.01
Error $\sigma_2{}^{EIF} - \sigma_2{}^{GF}$ at $x_2 = -12.5$	0,000102491	8,319E-05	6,33E-05	4,28E-05	2,163E-05

More comprehensive computational results can be found in Section 9.5.

9.4. Inextensibility constraint case

In this section the material in question is set to be inextensible in x_1 direction (this represents inextensible fibres). The constitutive description involves Lagrange multiplier T which is related to unknown tension in x_1 direction. Applying the corresponding constitutive equations (9.20) for the present plane strain problem we obtain:

$$
\begin{aligned}
\sigma_{11} &= \lambda \varepsilon_2 + T \\
\sigma_{22} &= (\lambda + 2\mu_T)\varepsilon_2 \\
\sigma_{(12)} &= 2\mu_{IT}\varepsilon_{12}
\end{aligned}
\tag{9.47}
$$

The resulting governing equations together with the inextensibility constraint $\varepsilon_1 = 0$ take form:

$$
\begin{cases}
\lambda \dfrac{\partial^2 u_2}{\partial x_1 \partial x_1} + \dfrac{\partial T}{\partial x_1} + \mu_1\left(\dfrac{\partial^2 u_2}{\partial x_1 \partial x_2} + \dfrac{\partial^2 u_1}{\partial x_2^2}\right) + \dfrac{1}{2}d_{31}\dfrac{\partial^4 u_2}{\partial x_1^3 \partial x_2} = 0, \\[2mm]
\mu_{1T}\left(\dfrac{\partial^2 u_1}{\partial x_1 \partial x_2} + \dfrac{\partial^2 u_2}{\partial x_2^2}\right) + (2\mu_T + \lambda)\dfrac{\partial^2 u_2}{\partial x_2^2} - \dfrac{1}{2}d_{31}\dfrac{\partial^4 u_2}{\partial x_1^4} = 0, \\[2mm]
\dfrac{\partial u_1}{\partial x_1} = 0
\end{cases}
\tag{9.48}
$$

Similarly to (9.37) the solution is chosen as follows:

$$
\begin{aligned}
u_1 &= f_1(x_2)\cos\left(\dfrac{\pi x_1}{L}\right), \\
u_2 &= f_2(x_2)\sin\left(\dfrac{\pi x_1}{L}\right), \\
T &= t(x_2)\sin\left(\dfrac{\pi x_1}{L}\right)
\end{aligned}
\tag{9.49}
$$

which corresponds to the boundary conditions applied at the plate ends (9.38).

The the upper and lower boundary conditions are given by:

$$\begin{cases} \sigma_2(x_1, h/2) = -q_0 \sin(\pi x_1 / L), \\ \sigma_2(x_1, -h/2) = 0, \end{cases} \tag{9.50}$$

The shear stress on the the upper and lower surfaces can not be set as boundary conditions in this case.

For a plate under a specified load (the boundary problem (9.48, 9.49, 9.50)), the solution is

$$\begin{aligned} f_1(x_2) &= 0, \\ f_2(x_2) &= c_i e^{\mu_i x_2}, \\ t(x_2) &= \zeta_i e^{\mu_i x_2} \end{aligned} \tag{9.51}$$

The governing equations (9.48) yield

$$\hat{a} \frac{\partial^2 f_2}{\partial x_2^2} + \hat{c} f_2 = 0 \tag{9.52}$$

It should be noted that parameters $\hat{a}$, $\hat{c}$ in (9.52) are functions of the material constants μ_{1T}, μ_T, λ, d_{31}. Two unknown constants μ_i are found from (9.52). Then we use lateral boundary conditions (9.50) to determine c_i, ζ_i.

The shear stress can no longer be prescribed zero on the top and bottom surfaces since it would imply zero displacement field for classical elasticity case (see last relation in (9.53) below). The resulting normal stresses and symmetric shear stress can be expressed as follows:

$$\begin{aligned} \sigma_1 &= \left(t(x_2) - \lambda f_2'(x_2) \right) \sin\left(\frac{\pi x_1}{L} \right), \\ \sigma_2 &= (\lambda + 2\mu_T) f_2'(x_2) \sin\left(\frac{\pi x_1}{L} \right), \\ \sigma_{(12)} &= \mu_{1T} \frac{\pi}{L} f_2(x_2) \cos\left(\frac{\pi x_1}{L} \right). \end{aligned} \tag{9.53}$$

The couple stress is

$$m_{13} = \left(\frac{\pi}{L} \right)^2 d_{31} f_2(x_2) \sin\left(\frac{\pi x_1}{L} \right). \tag{9.54}$$

The general shear stresses can be written as

$$\sigma_{12} = \left(\mu_{1T} \frac{\pi}{L} - \frac{1}{2} d_{31} \left(\frac{\pi}{L} \right)^3 \right) f_2(x_2) \cos\left(\frac{\pi x_1}{L} \right),$$

$$\sigma_{21} = \left(\mu_{1T} \frac{\pi}{L} + \frac{1}{2} d_{31} \left(\frac{\pi}{L} \right)^3 \right) f_2(x_2) \cos\left(\frac{\pi x_1}{L} \right).$$

(9.55)

We can see that d_{31} is explicitly present only in couple stress expression (9.54) and shear stress expressions (9.55). Nevertheless, d_{31} influences all the stresses implicitly, via the constants μ_i (because d_{31} is present in equation (9.52), from which μ_i are calculated).

Such formulation will be referred as EIF (extensible incompressible formulation). Related computational results can be found in Section **9.6** and **9.7**.

9.5. Inextensibility and incompressibility: double kinematic constraint

In this section, the material is assumed to be both incompressible and inextensible, it means also reinforced by inextensible fibres in x_1 direction. Such material with two kinematic constraints was constitutively characterised by Spencer [11].

The corresponding relations in case of plane strain are:

$$\sigma_{11} = -P + T,$$
$$\sigma_{22} = -P,$$
$$\sigma_{(12)} = 2\mu_{1T}\varepsilon_{12} = \mu_{1T} \frac{\partial u_2}{\partial x_1}.$$

(9.56)

Equilibrium equations with constraints give the following system:

$$\begin{cases} -\dfrac{\partial P}{\partial x_1} + \dfrac{\partial T}{\partial x_1} + \mu_{1T}\left(\dfrac{\partial^2 u_2}{\partial x_1 \partial x_2} + \dfrac{\partial^2 u_1}{\partial x_2^2} \right) + \dfrac{1}{2} d_{31} \dfrac{\partial^4 u_2}{\partial x_1^3 \partial x_2} = 0, \\[2mm] \mu_{1T}\left(\dfrac{\partial^2 u_1}{\partial x_1 \partial x_2} + \dfrac{\partial^2 u_2}{\partial x_1^2} \right) - \dfrac{\partial P}{\partial x_2} - \dfrac{1}{2} d_{31} \dfrac{\partial^4 u_2}{\partial x_1^4} = 0, \\[2mm] \dfrac{\partial u_1}{\partial x_1} = 0, \\[2mm] \dfrac{\partial u_1}{\partial x_1} + \dfrac{\partial u_2}{\partial x_2} = 0 \end{cases}$$

(9.57)

Analogously to the previous sections the solution is sought in the form

$$u_1 = f_1(x_2)\cos\left(\frac{\pi x_1}{L}\right),$$

$$u_2 = f_2(x_2)\sin\left(\frac{\pi x_1}{L}\right),$$

$$P = p(x_2)\sin\left(\frac{\pi x_1}{L}\right),$$

$$T = t(x_2)\sin\left(\frac{\pi x_1}{L}\right),$$

(9.58)

which corresponds to the boundary conditions applied at the plate ends (9.38). The system (9.57) is then reduced to:

$$\begin{cases} p - t = 0, \\ \left(-\left(\frac{\pi}{L}\right)^2 \mu_{1T} - \frac{1}{2}d_{31}\left(\frac{\pi}{L}\right)^4\right)f_2 - \frac{\partial p}{\partial x_2} = 0, \\ \dfrac{\partial f_2}{\partial x_2} = 0 \\ f_1 = 0 \end{cases}$$

(9.59)

The solution is then found as follows:

$$f_2 = c_1,$$

$$p = \left(-\left(\frac{\pi}{L}\right)^2 \mu_{1T} - \frac{1}{2}d_{31}\left(\frac{\pi}{L}\right)^4\right)c_1 x_2 + c_2$$

(9.60)

$$t = p$$

$$f_1 = 0$$

The upper and lower boundary conditions are given by (9.50). Two unknown constants c_1, c_2 are determined from the upper and lower boundary conditions.

With the given kinematic constraints the only present strain is the shear strain ε_{12}. The resulting normal stresses and symmetric shear stress can be expressed as follows:

$$\sigma_{11} = 0$$

$$\sigma_{22} = \left(\left(\left(\frac{\pi}{L}\right)^2 \mu_{1T} + \frac{1}{2}d_{31}\left(\frac{\pi}{L}\right)^4\right)c_1 x_2 - c_2\right)\sin\left(\frac{\pi x_1}{L}\right)$$

(9.61)

$$\sigma_{(12)} = \mu_{1T}\frac{\pi}{L}c_1 \cos\left(\frac{\pi x_1}{L}\right)$$

The couple stress is

$$m_{13} = \left(\frac{\pi}{L}\right)^2 d_{31} c_1 \sin\left(\frac{\pi x_1}{L}\right) \qquad (9.62)$$

The total shear stresses can be written as

$$\sigma_{12} = \left(\mu_{1T}\frac{\pi}{L} - \frac{1}{2}d_{31}\left(\frac{\pi}{L}\right)^3\right)c_1 \cos\left(\frac{\pi x_1}{L}\right),$$

$$\sigma_{21} = \left(\mu_{1T}\frac{\pi}{L} + \frac{1}{2}d_{31}\left(\frac{\pi}{L}\right)^3\right)c_1 \cos\left(\frac{\pi x_1}{L}\right). \qquad (9.63)$$

The specifics of this solution in comparison to the previous ones are as follows. Firstly, the normal stress is zero throughout the plate (9.61). Secondly, the influence of d_{31} is present in the normal stress σ_2 both explicitly and implicitly, via the constants c_1, c_2 (see (9.60)). Thirdly, couple stress is constant throughout each cross-section (see (9.62)).

The formulation is here and further abbreviated as IIF (inextensible, incompressible formulation).

9.6. Comparison of results

9.6.1. IIF model vs GF model

The comparison below is done between two models (both within classical elasticity – d_{31}=0) : IIF (inextensible incompressible formulation) and GF (general formulation) accordingly.

IIF requires two upper and lower boundary conditions identical to (9.50) while GF requires four of them [1]. The equivalency of the problems is achieved by setting resulting surface shear stress from IIF solution as boundary conditions for GF.

As it can be seen from the **Fig. 9.2**, if the GF parameters (Poisson's ratios and longitudinal Young's modulus) approach those corresponding to the IIF model (see (9.64)), the normal stress σ_1 tends to zero.

$$\begin{cases} E_1 \uparrow \\ \nu_{1T} \to 0.5 \\ \nu_{T1} = \nu_{1T}\dfrac{E_T}{E_1} \to 0 \\ \nu_{TT} = (1 - \nu_{T1}) \to 1 \end{cases}, \qquad (9.64)$$

Fig. 9.2. Normal stress in the middle cross-section calculated for different constitutive models

The **Fig. 9.3** shows comparison of the shear stresses at the end of the plate between IIF model

and GF models which are approaching the IIF model.
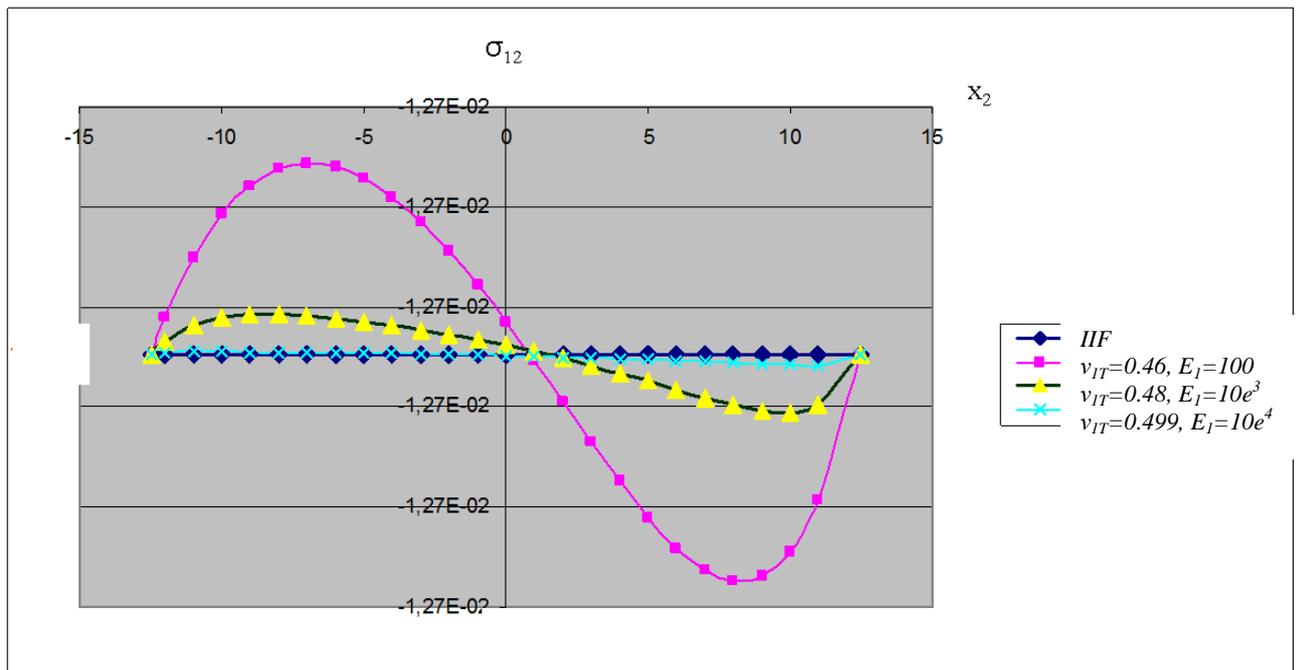
Fig. 9.3. Shear stress in the middle cross-section calculated for different constitutive models

113

9.6.2. IIF model vs ICF model

Another way how to verify the presented models is to compare the IIF model and the inextensible compressible (ICF) model. Relations that are valid for the ICF model:

$$\begin{cases} E_1 \to \infty \\ v_{T1} = v_{1T} \dfrac{E_T}{E_1} = 0 \end{cases} \tag{9.65}$$

Both ICF and IIF require two the upper and lower boundary conditions (9.50).
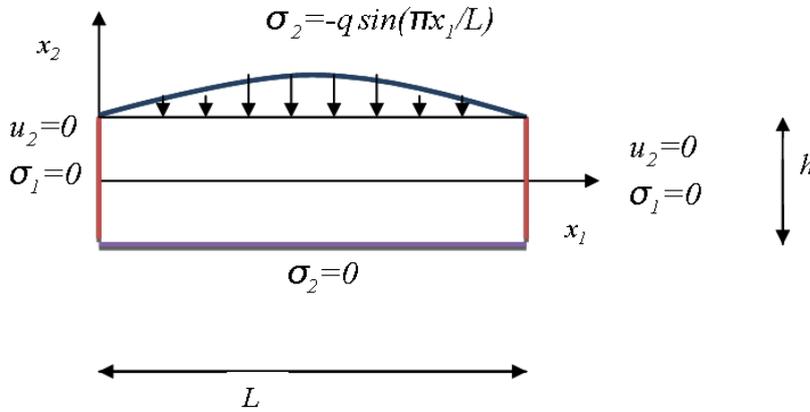
Fig. 9.4. Given boundary conditions for ICF and IIF

In terms of engineering constants the incompressibility of material is characterised by the following:

$$\begin{cases} v_{1T} = 0.5 \\ v_{T1} + v_{TT} = 1 \end{cases} \tag{9.66}$$

Since the IIF model also has restriction $v_{T1}=0$ due to inextensibility, (9.66) acquires the form

$$\begin{cases} v_{1T} = 0.5 \\ v_{TT} = 1 \end{cases} \tag{9.67}$$

In order to converge ICF to IIF, we use second of the relations (9.67) and approach it by varying the parameter v_{TT}: $v_{TT} \to 1$

We don't vary the parameter v_{1T} since it is not explicitly present in the formulation.
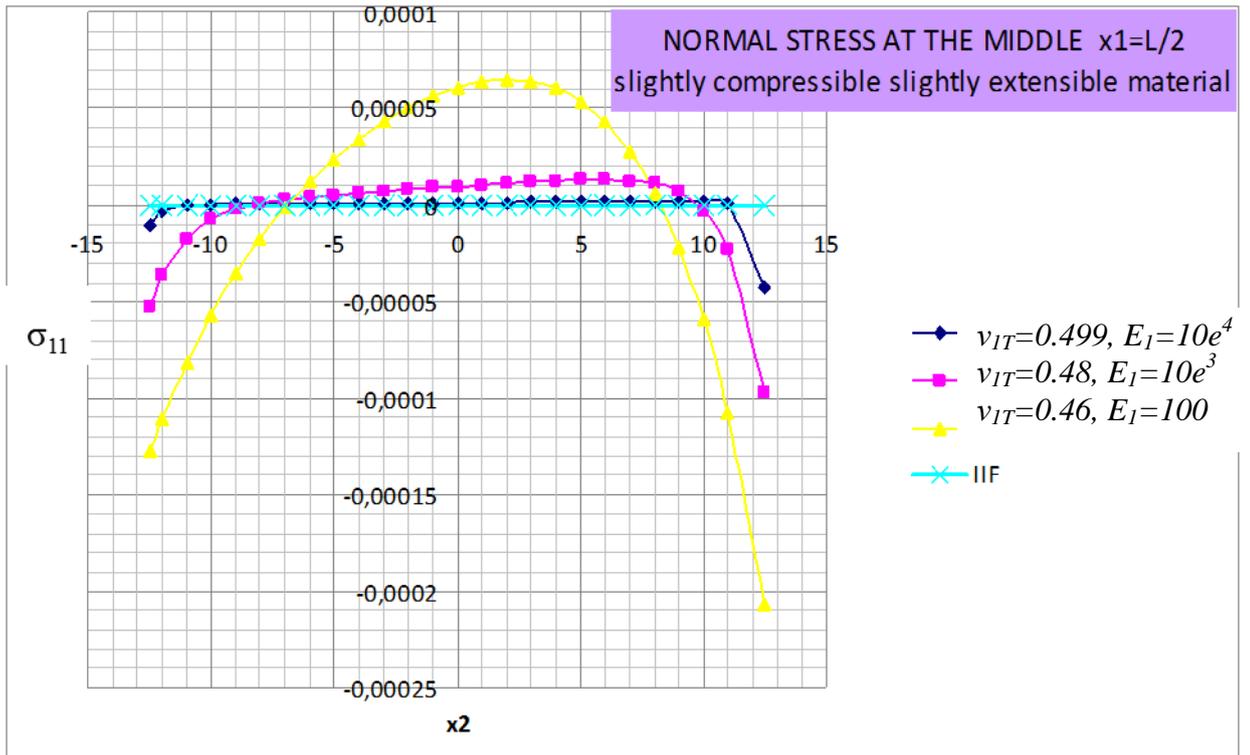
114

By manipulating v_{TT} we converge ICF model to the IIF model.
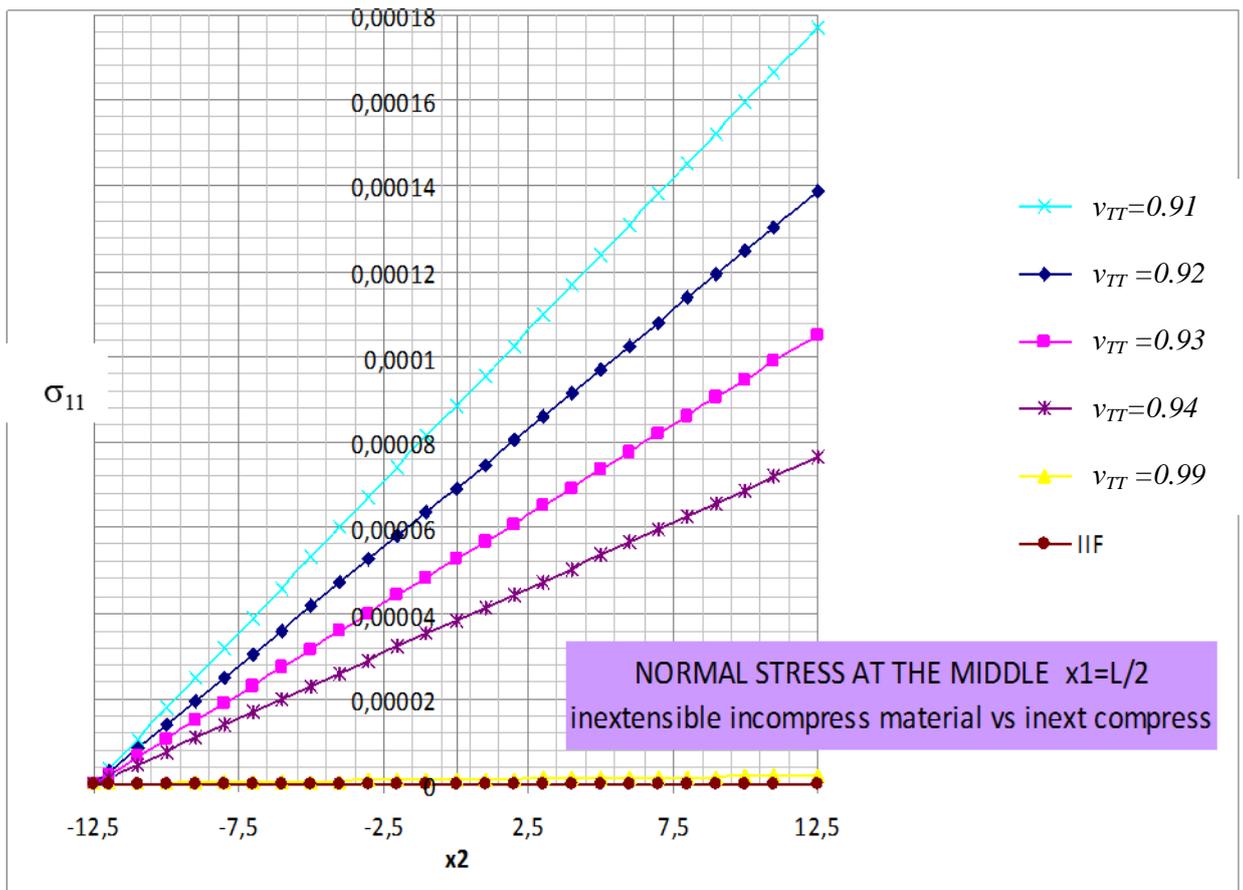
Fig. 9.5. Normal stress in the middle cross-section calculated for different constitutive models
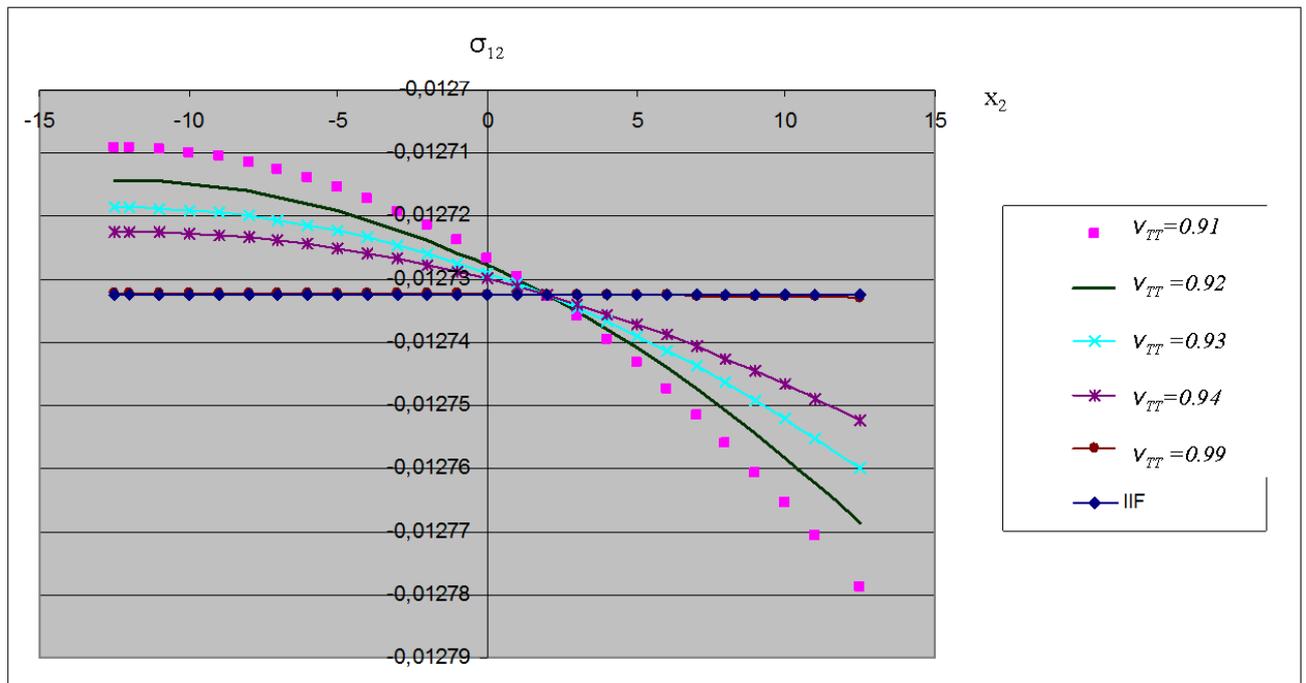
Fig. 9.6. Shear stress at the end of the plate calculated for different constitutive models

Analogously, EIF (extensible incompressible formulation) and IIF (inextensible incompressible formulation) models can be compared. IIF requires two lateral boundary conditions (9.40) while EIF requires four [1]. The equivalency of the problem setting can be achieved by applying resulting surface shear stress from IIF solution as boundary conditions for EIF.

In terms of engineering constants the inextensibility of material in x_1 direction is characterised by the following:

$$\begin{cases} E_1 -> \infty \\ \nu_{T1} -> 0 \end{cases}$$ (9.68)

Then, by manipulating modulus E1 (and, consequently, Poisson ratio $\nu_{T1} = \dfrac{E_T}{E_1}\nu_{1T}$), EIF model can be converged to the IIF model.

9.7. *Effect of additional bending stiffness for inextensible incompressible material*

The results obtained for the models in different formulations with converging their effective properties are still considered, but now with the additional non-zero parameter d_{31} included. In this section the focus is on the resulting couple stress distribution in the middle cross-section of the plate. The d_{31} parameter is set the same in all computations. Different combinations of kinematic constraints and their effect on the couple stress distribution m_{13} are examined below.

The graph in (**Fig. 9.7**) illustrates convergence of the results obtained with general formulation (GF) to the result obtained with (extensible) incompressible formulation (EIF). For both d_{31}=10 N. We converge GF model to EIF by approaching Poisson ratio $\nu_{1T} \to 0.5$.
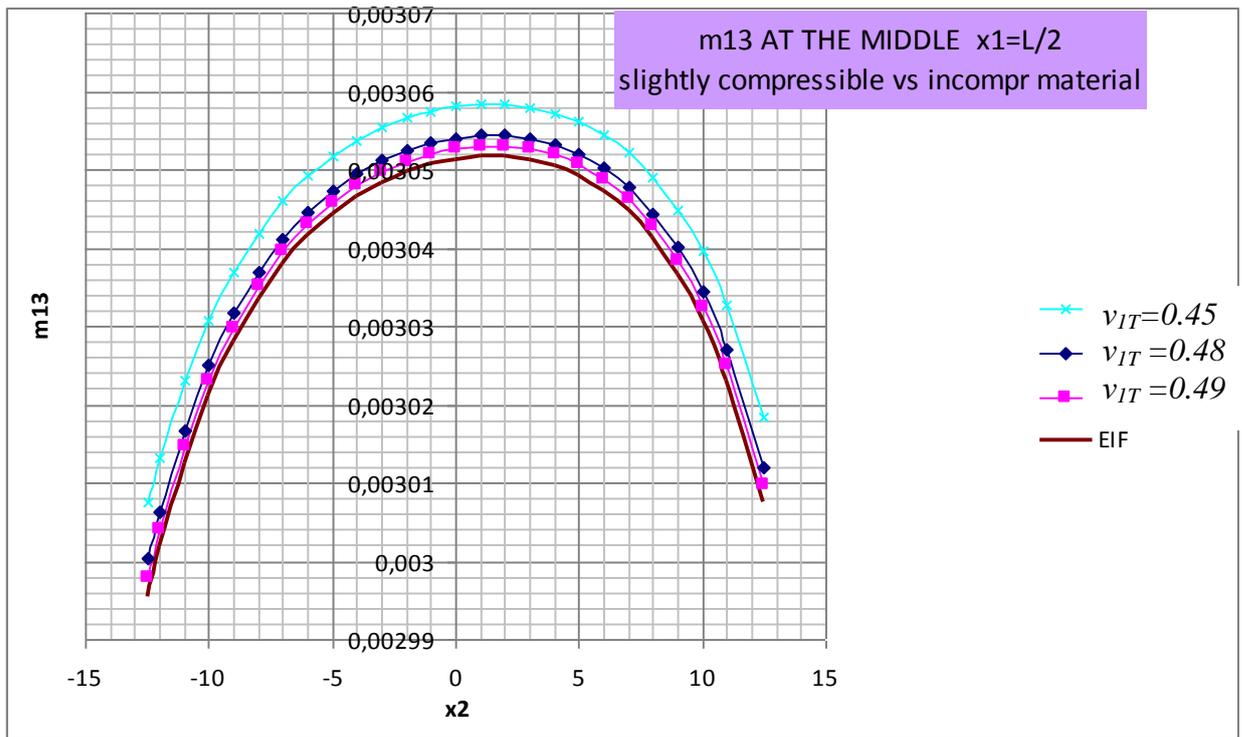
Fig. 9.7. Couple stress at the end of the plate calculated for different constitutive models

The comparison in **Fig. 9.8** is between two models (for both d_{31}=10 N) which we refer to as IIF (inextensible incompressible formulation) and EIF (extensible incompressible formulation) accordingly. The material properties were set such that EIF approaches inextensibility (E_1 is increasing).

IIF requires two upper and lower boundary conditions identical to (9.50) while EIF requires four of them. The equivalency of the problems is achieved by setting the resulting surface shear stress from the IIF solution as boundary conditions for the EIF.

As it can be seen from the figure below, with increasing longitudinal Young's modulus in EIF $E_1 \uparrow$, the couple stress m_{13} tends to constant value throughout the cross-section, as it is for IIF.
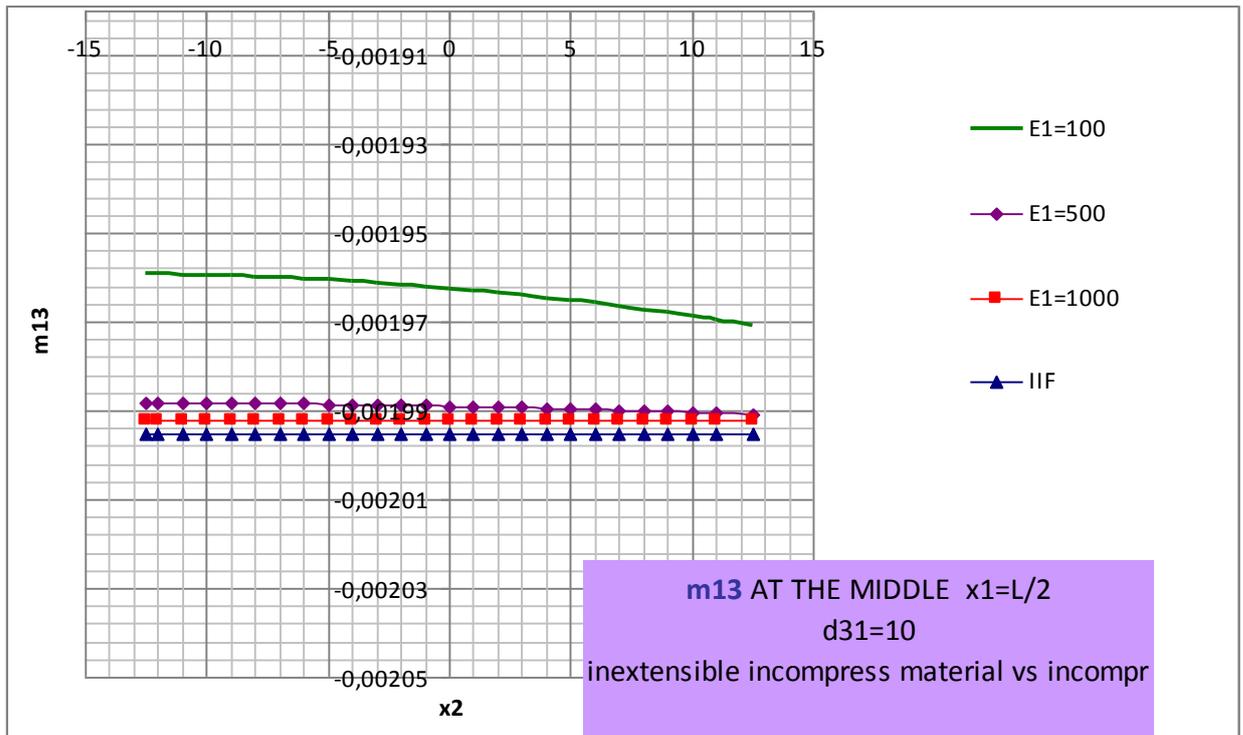
Fig. 9.8. Couple stress in the middle of the plate calculated for different constitutive models

Comparison in the **Fig. 9.9** is between IIF model and inextensible (ICF) model. Relations that are valid for the inextensible (ICF) model:

$$\begin{cases} E_1 \to \infty \\ \nu_{T1} = \nu_{1T} \dfrac{E_T}{E_1} = 0 \end{cases} \tag{9.69}$$

In order to converge ICF to IIF, we take incompressibility relation (9.45b) and approach it by varying the parameter ν_T:

$$\nu_{TT} \to (1 - \nu_{T1}), \text{ so } \nu_{TT} \to 1$$
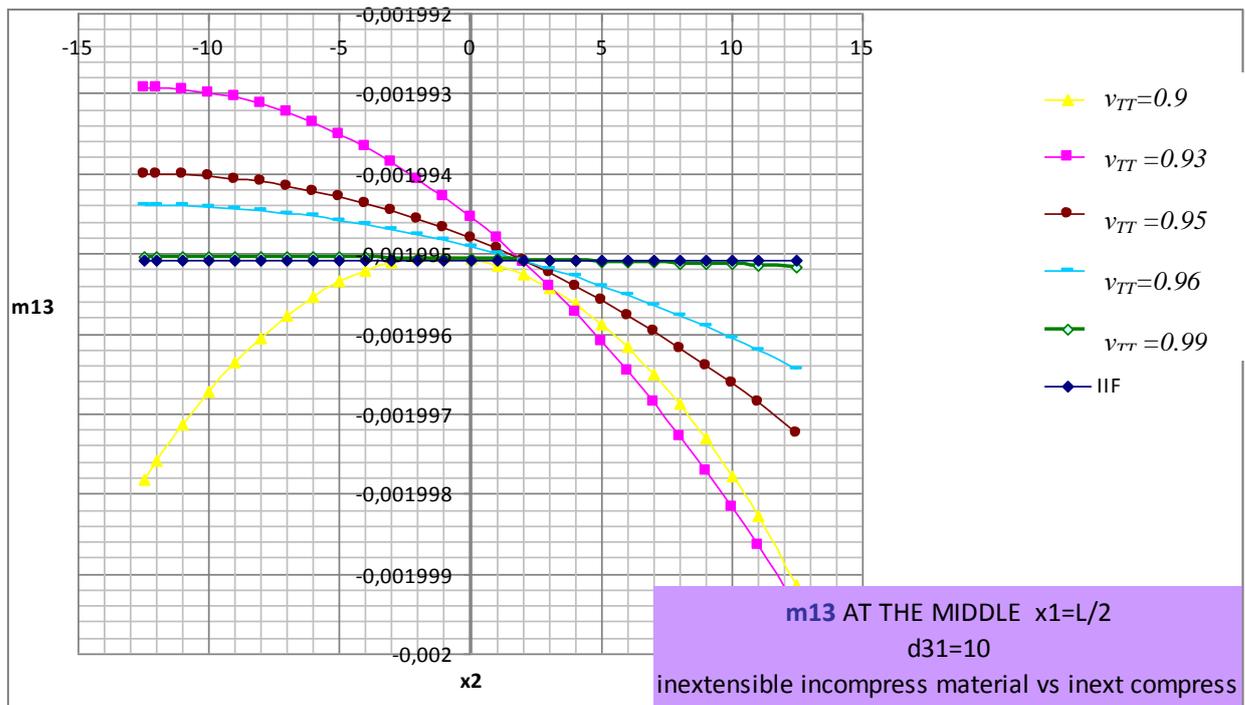
Fig. 9.9. Couple stress in the middle of the plate calculated for different constitutive models

9.8.   Graphs examination

Inextensible (ICF) model response converges to IIF by manipulating Poisson's ratio v_T. Extensible incompressible (EIF) model response converges to IIF by increasing of Young/s modulus E_1.

Classical elasticity graphs:

- Normal stress distribution in the middle cross-section (**Fig. 9.1**) is strongly non-linear for materials close to EIF (incompressible) model, independently of material compressibility;
- For materials close to IIF (incompressible and inextensible case) (**Fig. 9.2)** normal stress throughout the whole middle cross section tends to zero;
- For materials close to IIF, shear stress (**Fig. 9.3**, **9.6**) in the middle cross-section of the plate tends to constant throughout the cross-section;
- inextensible model (ICF) has linear normal stress distribution (**Fig. 9.5)** and only positive values throughout the middle cross section

Polar elasticity graphs:

- EIF model (incompressible material with extensible, though stiff fibres) shows couple stress distribution close to constant in the cross-section. **Fig. 9.7** shows gradual convergence of the GF (general formulation) model results to the EIF ones.

- **Figs. 9.8, 9.9** show gradual convergence of the EIF and ICF results to IIF result (which is constant couple-stress distribution). The impact of compressibility seems to be significantly higher than that of extensibility.

9.9.   Elucidation on the equivalence of constants in different formulations.

The behaviour of linear elastic material can be described in three alternative ways: using stiffness matrix components, using Lame description, or using engineering constants. For the sake of adequate switching between constitutive descriptions, relations linking different constants for the transversely isotropic elastic material are presented below. These relations have been used in the current computations.

General formulation for linear elastic, transversely isotropic material with the anisotropy vector $(1,0,0)^T$ is, as previously stated:

$$\sigma_{(ij)} = \lambda\theta\delta_{ij} + 2\mu_T\varepsilon_{ij} + \alpha\left(\varepsilon_{11}\delta_{ij} + \theta a_i a_j\right) + \beta\varepsilon_{11}a_i a_j + 2\left(\mu_1 - \mu_T\right)\left(a_i\varepsilon_{j1} + a_j\varepsilon_{i1}\right) \quad (9.70)$$

Generalised Hooke's law has the form:

$$
\begin{pmatrix} \sigma_{11} \\ \sigma_{22} \\ \sigma_{33} \\ \sigma_{23} \\ \sigma_{13} \\ \sigma_{12} \end{pmatrix} =
\begin{pmatrix}
c_{11} & c_{12} & c_{12} & 0 & 0 & 0 \\
 & c_{22} & c_{23} & 0 & 0 & 0 \\
 & & c_{22} & 0 & 0 & 0 \\
 & & & c_{44} & 0 & 0 \\
 & symm & & & c_{66} & 0 \\
 & & & & & c_{66}
\end{pmatrix}
\begin{pmatrix} \varepsilon_{11} \\ \varepsilon_{22} \\ \varepsilon_{33} \\ 2\varepsilon_{23} \\ 2\varepsilon_{13} \\ 2\varepsilon_{12} \end{pmatrix}, \quad (9.71)
$$

where $c_{44}=(c_{22}-c_{12})/2$.

The following general relations were derived using the work [88]:

$$
\begin{aligned}
\lambda &= c_{23} \\
\alpha &= c_{12} - c_{23} \\
\beta &= c_{22} + c_{11} - 2c_{12} - 4c_{66} \\
\mu_T &= c_{44} \\
\mu_1 &= c_{66}
\end{aligned}
\quad (9.72)
$$

The relations in question are presented below for each case of kinematic constraint.

9.9.1. Extensible incompressible material
With use of (9.45a, b) and (9.72)) the following is valid for EIF material:

120

α is not present in constitutive equations;

$$\lambda-> \infty,$$

$$\beta = \frac{E_T}{(2-v_{T1})v_{T1}} - 4G_{IT},$$

$$\mu_T = G_T,$$

$$\mu_I = G_{IT}. \qquad (9.73)$$

As expected, 3 material parameters are left independent.

9.9.2. Inextensible compressible material

For ICF material: α and β are not present in constitutive equations, and

$$\lambda = \frac{v_{TT}E_T}{1-v_{TT}^2},$$

$$\mu_T = G_T,$$

$$\mu_1 = G_{1T}. \qquad (9.74)$$

3 of the parameters are left independent.

9.9.3. Incompressible inextensible material

For incompressible inextensible material (IIF):

α and β are not present in constitutive equations, and

$$\lambda-> \infty,$$

$$\mu_T = G_T,$$

$$\mu_I = G_{IT}. \qquad (9.75)$$

2 of the parameters are left independent.

9.10. Concluding remarks regarding results applicability

As mentioned earlier, the general solution of the problem presented in this section was fully mathematically derived in [1] by Farhat and Soldatos. The kinematic constraints, applied in the current work, serve to 1) produce simplified solutions for common characteristics of the material; 2) underscore the influence of the fibre bending stiffness under conditions of the normal stress close to zero.

The ultimate goal of this section is to set conditions for linking the mathematical constitutive dependencies to the actual properties of the material. On the basis of this section, the following scheme is suggested in order to validate the phenomenological model.

Actual composite material (corresponding to the model described above) consists of close to incompressible matrix and close to inextensible fibres. Such material is, for example, rubber and steel cord composite. Such block of material can be used for the mechanical tests correlating with the problem (**Fig. 8.1**.).

Since the experimental measurement of the resulting couple stress distribution m_{13} in the specimen (or the bending moment in each fibre cross-section) does not seem feasible, the less straightforward approach might be used:

- the specimen is set under the given load (**Fig. 8.1**.) and the resulting displacements u_2 are measured;

- resulting values of u_2 are approximated as analytical function in the form of solution (9.37), (9.41) (if the incompressibility assumption only is chosen and paragraph 9.3 is used). The simplest solution form is given in paragraph 9.5 (full incompressibility and full inextensibility of fibres is assumed), where displacement u_1 is zero and u_2 is constant throughout any cross-section;

- consequently, analytical function f_2 is known;

- then equation (9.42) can be used. Parameters *a, b, c* in (9.42) are functions of the material constants – classical elastic constants and d_{31}. Again, the simplest setting is given by 9.5 (IIF formulation) where only two independent classical constants are present – two shear moduli. If the classical moduli are known, the only unknown in (9.42) is d_{31}.

10. Conclusions and future work suggestions

10.1. Summary

Fibre-reinforced hyperelastic materials are conventionally described using phenomenological constitutive models. Phenomenological models are usually constructed by adding additional invariants to existing isotropic strain energy functions. These additional invariants penalise deformation in the fibre direction [69].

Following this logic, the model investigated in this work is augmented with the term that penalises change in curvature in the fibre direction. The model is based on the large strain anisotropic formulation involving couple stresses [2], also referred to as "polar elasticity for fibre reinforced solids" [11], [46], [6]. In continuation of the research conducted by Lasota [3], the present study aims to establish and verify new higher order homogeneous model with the effective material properties that should correctly mimic the response of the given fibrous composite. As it has been shown here and in [2], the need of such formulation arises when the fibre size is comparable to some of the characteristic sizes of the structure.

The current work is an attempt of a systematic study of the so called "polar elasticity for fibre-reinforced solids", its mechanical interpretation and specifics of numerical implementation and represents a natural continuation of Lasota's dissertation [3]. Polar elasticity for fibre reinforced solids operates couple stresses that occur in accordance with bending, "twist", or "splay" mode of fibre deformation (the fibre in question is fictitious, and is modelled by introducing direction vector field) that represent a general case of material behaviour. The full mathematical description of such model was introduced by Spencer and Soldatos and later enhanced by Soldatos. The contribution of fibres to the material stiffness is characterized by the tensile stiffness parameter and the additional parameters related to another fibre deformation mode.

The work starts with an experimental mechanical study with the steel fibre-reinforced rubber specimens. The fibres are comparatively thick and located in the middle plane of the specimen. The study shows the validity of the anisotropic unimaterial constitutive model in case of tension tests but its inability to simulate the bending behaviour of the composite correctly. This result supports the earlier suggestion that main reason of discrepancy lies in the inability of the model to account for the bending stiffness contribution and size effect of fibres. Unless the fibres are infinitesimally thin and uniformly distributed throughout the specimen height, the classical anisotropic unimaterial model does not offer a reliable representation. In other words,

such unimaterial model cannot be deemed fully equivalent to the bimaterial one, even though they have similar behaviour under tension.

As a next step, the general logic of the effective constants derivation is considered for a small strains case of fibre composites. The "rule of mixtures" approach of mechanics of composite materials is recapitulated, and a similar simplifying scheme is employed to include the additional parameter corresponding to the bending stiffness contributed by fibres.

The role of the additional effective constant in the model is investigated further on. The constitutive equations published in Spencer and Soldatos [2] are used to formulate a specific form of strain energy density function on the basis of constraint Cosserat theory (in which couple stresses are introduced and displacements or displacement rates are the only independent unknowns). This approach leads to second derivatives of displacement rates occurring in the finite element formulations. A specific form of strain energy density is proposed with an additional term correcting the effective bending stiffness of the continuum. The model used recently by Lasota [3] is examined and modified in order to make it more mechanically representative. The different invariant is chosen due to some mathematical and physical benefits. New invariant in the energy formulation yields physical relations that link the deformed fibre curvature and the relevant couple stress, especially illustrative in the small strain case. Thus the bending mode of fibre deformation is specifically taken into account, while the invariant used previously by Lasota [3] equals to zero in pure bending deformation. For the modified constitutive model the issue of determination of the additional constant k_3 (associated with the fibre bending stiffness) is considered. Within the small strains framework, the formula is offered linking k_3 to the geometric and material properties of the initial heterogeneous structure (fibrous composite plate).

The finite element code by Lasota [3] is modified to incorporate the additional invariant. Code equations are reformulated in the matrix form instead of index form which reduces the computational time substantially. The corresponding calculation is carried out for the composite plate under bending in the case of small strains. Two examples are considered: composite plate with fibres aligned along the longitudinal axis, and composite plate with fibres aligned under the angle of 30 degrees to the longitudinal axis. It is shown that the discrepancy between the classical homogeneous model and a heterogeneous model can be largely diminished by the presented approach.

A complementary study is also carried out for a thick fibre-reinforced plate under displacement boundary conditions. Polar elasticity equations are employed in linear formulation. The solution of the plane strain boundary problem of polar elasticity for the static and dynamic flexure of a thick laminated plate has been recently derived by Farhat and Soldatos [1]. The

authors take the contribution of the couple stresses into account with the help of one extra modulus of elasticity. In the present study, after having reproduced the solution in [1] for the case of static flexure of a single-layer plate, I extended the solution to different boundary conditions with three extra modules of elasticity applied in the model. In this chapter some new numerical results are presented which complement those in [1].

In Section 7 a new pure bending elasticity solution is derived for the transversely isotropic polar material. It is compared with solutions based on the conventional theory in order to demonstrate how the size effect can be taken into consideration in the homogeneous polar model. With the increasing nominal number of fibres their bending stiffness decreases and the polar elasticity model converges to the conventional elasticity model. In this example, the additional elastic constant has a role of a correcting parameter. It corrects the error in bending stiffness resulting from averaging the Young's modulus.

In Section 8 verification of the new constitutive model and finite element code [8] is carried out using new exact solution for the anisotropic couple stress continuum with the incompressibility constraint. Considerations and techniques employed in Section 6 are used to achieve exact solution of the linear boundary problem. Plane strain boundary problem is solved both analytically and numerically. The finite element calculations and analytical solution show perfect agreement. The large strain problem is also examined. In the large strain range no solution enabling us a comparison was found in literature, so the presented example illustrates only qualitatively the capability of the code to mimic the bending stiffness of the fibres.

In Section 9, a known linear elasticity problem is considered in two new ways. Firstly, constraints of incompressibility and inextensibility in fibre direction are added; secondly, the intrinsic anisotropic bending stiffness (based on polar elasticity) is included in the model. Inextensibility and incompressibility constraints cause the presence of respective Lagrange multipliers in the formulation. The resulting stress fields are compared to those obtained using the slightly compressible and slightly extensible formulation. The observed characteristics of stress distribution are compared and it is shown that those obtained with compressible and extensible formulations tend to the incompressible and inextensible ones with decreasing compressibility and extensibility. The scheme of determination of the additional constant d_{31} is suggested.

10.2. Future work proposal

Limitations of the present work and suggestions for the future research are outlined below.

Additional parameter k_3 in the model (Section 5) represents additional bending stiffness of the homogenised material with respect to the reinforced direction. In the proposed example, k_3 is

calculated for the specific geometry of the specimen under the small strain assumption. It can be stated that the term with k_3 reflects the influence of the geometrical fibre arrangement (while the classic model takes into account the fibre volume fraction only, regardless of their arrangement and size). Then the term containing k_3 is added into the classical homogenous model for the strain energy density. Thus k_3 serves as the corrective parameter. The constant k_3 can be approximately computed for the small strain case. Having computed k_3 for the case of fibres aligned along x_1, we can then use this value for problems with the different fibre angle (but the same fibre arrangement) by changing the vector A. Thus, the enhanced bending characteristics of the specimen are accounted for by the vector A (present in invariant I_6) and the constant k_3 in the constitutive model (5.40). Current stage of the study suggests future steps in 2 main directions: 1) examining the mathematical ways how to derive the constant k_3 for the elastic fibres/ hyperelastic matrix case; 2) carry out additional mechanical tests in bending, complementing those in Section 3, with the focus on the specimens with the fibre declination; establish, if possible, the correlation between the new tests and the FEM simulations for the polar model; validate, if the use of constant k_3 obtained by the formula (5.55) from Section 5 and used in FEM simulations yields agreement with the tests for the small/large strain cases.

In Section 7 the exact analytical (polar elasticity) solution is presented for a transversely isotropic thick plate under pure bending (and compared with the alternative solutions). To deepen the mathematical understanding of the couple stresses presence in the current model, other analytical problems can be examined, and if possible, adjusted for the polar elasticity model. For instance, the bending problem of a plate under a concentrated force. It does present analytical difficulty though, due to the use of the stress function (while the pure bending problem is solved in displacements).

The analytical verification of the FEM code by Lasota is carried out for the small strains case in the Section 8, using the two-dimensional linear problem of polar theory. Also, a small numerical study is performed to illustrate the capacity of the code regarding the non-linear problems and the influence of parameter k_3. Essentially, the verification of the large strain computations by this code is still an open question. The attempt of the analytical verification can be made using some large-strain analytical solution for the two-dimensional problem with kinematic constraints. Such problems (bending of a fibre-reinforced rectangular block and area-preserving azimuthal-shear deformation of a fibre-reinforced tube) were extended to polar theory by Soldatos [46].

In Section 9 two-dimensional linear elastic problems with the kinematic constraints are considered with and without fibre bending stiffness. The most simple and illustrative case is the

IIF (inextensible incompressible formulation). The solution yields zero normal stress throughout the whole plate and constant couple stress throughout each cross-section. Fibres are curved, but not compressed or elongated. The bending moment acting on the plate cross-section has zero classical part and non-zero ($h \cdot m_{13}$ in this case) couple stress part (see also (5.30), (5.31)). The constant value of couple stress in each cross-section is dictated by the constant d_{13} (bending stiffness parameter for the linear elastic case) (9.62), plate length L, and applied pressure amplitude q_0 (9.50). This solution can be used in future to study the size effect of fibres. It can be compared with the analogous solution for the heterogenous (bimaterial) fibre reinforced plate (modelled by FEM, modelled analytically, or obtained, if feasible, from the actual test with the specimen). Partly analytical/partly experimental scheme of determination of the additional constant d_{31} (suggested in 9.10) can be verified.

References

[1]   England AH (1999) Finite elastic deformations of a tyre modelled as an ideal fibre-reinforced shell. *J Elasticity* 54: 43-71

[2]   Spencer AJM, Soldatos KP (2007) Finite deformations of fibre-reinforced elastic solid with fibre bending stiffness. *Int J Nonlinear Mech* 42:355-368

[3]   Lasota T (2013) *Computational modelling of mechanical behaviour of "elastomer – steel fibre" composite.* Dissertation, Brno University of Technology

[4]   Lasota T, Burša J, Fedorova S (2012) Constitutive equations and finite element formulation for anisotropic hyperelastic composites based on constrained Cosserat continuum. *ECCOMAS 2012 – European Congress on Computational Methods in Applied Sciences and Engineering*, e-Book full papers: 3379-3389

[5]   Fedorova S, Lasota T, Burša J, Skácel P (2012) Experimental verification of a constitutive model of fibre composite with hyperelastic matrix. *Proceedings of Conference EAN 2012*, Tabor, CZ

[6]   Soldatos KP (2013) Foundation of polar linear elasticity for fibre-reinforced materials. *J Elasticity* 114(2):155-178

[7]   Farhat AF, Soldatos KP (2015) Cylindrical bending and vibration of polar material laminates. *Mech Adv Mater Struct* 22:885-896

[8]   Fedorova S, Lasota T, Burša J (2016) Computational modelling of fibre composites with thick fibres as homogeneous structures with use of couple stress theory. In: Marcal PV, Yamagata N (Eds.), Design and Analysis of Reinforced Fiber Composites, *Proceedings of Symposium at WCCM XI - ECCM V - ECFD VI, Barcelona 2014* :25-48. ISBN 978-3-319-20006-4

[9]   Lasota T, Burša J (2011) Simulation of mechanical tests of composite material using anisotropic hyperelastic constitutive models. *Eng Mech* 18(1): 23-32

[10] Burša J, Zemánek M (2008) Evaluation of biaxial tension tests of soft tissues. *Stud Health Technol Inform* 133:45–55

[11] Spencer AJM (1972) *Deformations of Fibre-reinforced Materials*. Oxford University Press, London

[12] Demiray H (1972) A note on the elasticity of soft biological tissues. *J Biomech* 5:309-311

[13] Rachev A, Hayashi K (1999) Theoretical study of the effects of vascular smooth muscle contraction on strain and stress distributions in arteries. *Ann Biomed Engr* 27:459-468

[14] Zulliger MA, Rachev A, Stergiopulos N (2004) A constitutive formulation of arterial mechanics including vascular smooth muscle tone. *Am J Physiol Heart Circ Physiol* 287:H1335-H1343

[15] Klosner JM, Segal A (1969) Mechanical characterization of a natural rubber. *PIBAL Report* 6942 Polytechnic Inst. Brooklyn, NY

[16] Weiss JA, Maker BN, Govindjee S (1996) Finite element implementation of incompressible, transversely isotropic hyperelasticity. *Comput Meth Appl Mech Engrg* 135:107-128

[17] Ruter M, Stein E (1999) Analysis, finite element computation and error estimation in transversal isotopic nearly incompressible finite elasticity. *Comput Meth Appl Mech Engrg* 190:519-541

[18] Bonet J, Burton AJ (1998) A simple orthotropic, transversely isotropic hyperelastic constitutive equation for large strain computations. *Comput Meth Appl Mech Engrg* 162:151-164

[19] Reese S, Raible T, Wriggers P (2001) Finite element modelling of orthotropic material behaviour in pneumatic membranes. *Int J Solids Struct* 38:9525–9544

[20] Horgan CO, Saccomandi G (2005) A new constitutive theory for fiber-reinforced incompressible nonlinearly elastic solids. *J Mech Phys Solids* 53:1985–2015

[21] Nam TH, Marvalova B (2004) Deformation analysis of inflated cylindrical membrane of composite with rubber matrix reinforced by cords. *XXI International Congress of theoretical and applied mechanics ICTAM*

[22] Forest S, Sab K (1998) Cosserat overall modelling of heterogeneous materials. *Mechanics Research Communications* 25(4):449-454

[23] de Borst R (1993) A generalisation of J2 –flow theory for polar continua. *Comput Method in Appl M* 103:347-362

[24] Sansour C, Skatulla S, Zbib H (2010) A formulation for the micromorphic continuum at finite inelastic strains. *Int J Solids Struct* 47:1546–1554

[25] Isbuga V, Regueiro RA (2011) Three-dimensional finite element analysis of finite deformation micromorphic linear isotropic elasticity. *Int J Eng Sci* 49:1326–1336

[26] Tsiatas GC (2009) A new Kirchhoff plate model based on a modified couple stress theory. *Int J Solids Struct* 46:2757–2764

[27] Park SK, Gao X-L (2006) Bernoulli–Euler beam model based on a modified couple stress theory. *J Micromech Microeng* 16:2355–2359

[28] Lam DCC, Yang F, Chong ACM, Wang J, Tong P (2003) Experiments and theory in strain gradient elasticity. *J Mech Phys Solids* 51:1477–1508

[29] Bauer S, Schäfer M, Grammenoudis P, Tsakmakis Ch (2010) Three-dimensional finite elements for large deformation micropolar elasticity. *Comput Method Appl M* 199:2643–2654

[30] Chen W, Si J (2013) A model of composite laminated beam based on the global–local theory and new modified couple-stress theory. *Compos Struct* 103:99–107

[31] Fleck NA, Shu JY (1995) Microbuckle initiation in fibre composites: a finite element study. *J Mech Phys Solids* 43(12):1887–1918

[32] Nowacki W (1966) Couple stresses in theory of thermoelasticity, *Proc. of the IUTAM symposia*, Vienna

[33] Lasota T, Burša J (2009) Size effect in computational simulations of experiments with composite materials. In *26th Symposium on Advances in Experimental Mechanics*. Montanuniversität Leoben, Austria 133-134. ISBN: 978-3-902544-02- 5

[34] Forest S, Sievert R (2006) Nonlinear microstrain theories. *Int J Solids Struct* 43:7224–7245

[35] Cosserat E, Cosserat F (1909) Théorie des corps déformables. A. Hermann et Fils, Paris

[36] Eringen AC (1962) Nonlinear Theory of Continuous Media. McGraw-Hill, New York

[37] Altenbach J, Altenbach H, Eremeyev VA (2010) On generalized Cosserat-type theories of plates and shells: a short review and bibliography. *Arch Appl Mech* 80:73–92

[38] Eringen AC (1999) Microcontinuum field theories I: Foundations and solids. Springer, New-York

[39] Eringen AC, Suhubi ES (1964) Nonlinear theory of simple micro-elastic solids. *Int J Eng Sci* 2(2):189–203

[40] Eringen AC (1966) Linear theory of micropolar elasticity. *J Math Mech* 15:909–923

[41] Eringen AC (1968) Theory of micropolar elasticity. In: Liebowitz H (Ed.) *Fracture, Volume II, Mathematical Fundamentals*. Academic Press, New York

[42] Koiter WT (1964) Couple stresses in the theory of elasticity I and II. *Proc Kon Ned Akad Wetensch* 67:17–44

[43] Mindlin RD (1963) Influence of couple-stresses on stress concentrations. *Exp Mech* 3:1–7

[44] Mindlin RD, Tiersten HF (1963) Effects of couple-stresses in linear elasticity. *Arch Ration Mech Anal* 11: 415–448

[45] Toupin RA (1964) Theories of elasticity with couple-stress. *Arch Ration Mech Anal* 17(2):85–112

[46] Soldatos KP (2009) Azimuthal shear deformation of an ideal fibre-reinforced tube according to a second-gradient hyper-elasticity theory. In: Ambrosio J et al. (Eds.), *Proceedings of the Seventh EUROMECH Solid Mechanics Conference, Lisbon*

[47] Soldatos KP (2010) Second-gradient plane deformations of ideal fibre-reinforced materials: implications of hyper-elasticity theory. *J Eng Math* 68(1):99-127

[48] Soldatos KP (2012) On loss of ellipticity in second-gradient hyper-elasticity of fibre-reinforced materials. *Int J Nonlinear Mech* 47:117-127

[49] Nakamura S, Benedict R, Lakes R (1984) Finite element method for orthotropic micropolar elasticity. *Int J Engrg Sci* 22:319–330

[50] Providas E, Kattis MA (2002) Finite element method in plane Cosserat elasticity. *Comput Struct* 80:2059–2069.

[51] Li L, Xie S (2004) Finite element method for linear micropolar elasticity and numerical study of some scale effects phenomena in MEMS. *Int J Mech Sci* 46:1571–1587

[52] Beveridge AJ, Wheel MA, Nash DH (2013) A higher order control volume based finite element method to predict the deformation of heterogeneous materials. *Computers and Structures* 129:54–62

[53] de Borst R (1993) A generalisation of J_2 –flow theory for polar continua. *Comput Method in Appl M* 103:347-362

[54] Sharbati E, Naghdabadi R (2006) Computational aspects of the Cosserat finite element analysis of localization phenomena. *Comput Mater Sci* 38(2): 303–315

[55] Sansour C, Skatulla S, Zbib H (2010) A formulation for the micromorphic continuum at finite inelastic strains. *Int J Solids Struct* 47:1546–1554

[56] Huang F, Yan B, Yan J, Yang D (2000) Bending analysis of micropolar elastic beam using a 3-D finite element method. *Int J Eng Sci* 38(3):275–286

[57] Bauer S, Schäfer M, Grammenoudis P, Tsakmakis Ch (2010) Three-dimensional finite elements for large deformation micropolar elasticity. *Comput Method Appl M* 199:2643–2654

[58] Bauer S, Dettmer W, Perić D, Schäfer M (2012) Micropolar hyperelasticity: constitutive model, consistent linearization and simulation of 3D scale effects. *Comput Mech* 50:383–396

[59] Isbuga V, Regueiro RA (2011) Three-dimensional finite element analysis of finite deformation micromorphic linear isotropic elasticity. *Int J Eng Sci* 49(12):1326–1336

[60] Garg N, Han C-S (2013) A penalty finite element approach for couple stress elasticity. *Comput Mech* 52(3):709-720

[61] Kahrobaiyan MH, Asghari M, Ahmadian MT (2014) A Timoshenko beam element based on the modified couple stress theory. *Int J Mech Sci* 79: 75-83

[62] Zhang B, He Y, Liu D, Gan Z, Shen L (2014) A non-classical Mindlin plate finite element based on a modified couple stress theory. *Finite Elem Anal Des* 79:22-39

[63] Ristinmaa M, Vecchi M (1996) Use of couple-stress theory in elasto-plasticity. *Comput Method Appl M* 136: 205-224

[64] Mooney M (1940) A Theory of Large Elastic Deformation. *J Appl Phys* 6:582-592

[65] Rivlin RS, Saunders DW (1951) Large elastic deformations of isotropic materials VII. Experiments on the deformation of rubber. *Philos Trans R Soc London A* 243:25-288 ISSN:1364-503X

[66] Legorju-jago K, Bathias C (2002) Fatigue Initiation and Propagation in Natural and Synthetic Rubbers. *Int J Fatigue* 24:85-92, 0142-1123

[67] Rivlin RS, Thomas AG (1953) Rupture of rubber. Part 1. Characteristic energy for tearing. *J Polym Sci A Polym Chem* 10:291-318 ISSN:0887-624X

[68] Lanir Y (1983) Constitutive equations for fibrous connective tissues. *J Biomech* 16:1–12

[69] Spencer AJM (1984) Constitutive theory for strongly anisotropic solids. In: Spencer AJM (Ed.) *Continuum Theory of the Mechanics of Fibre-Reinforced Composites, CISM Courses and Lectures.* International Centre for Mechanical Sciences, Springer-Verlag, Wien

[70] Holzapfel GA, Gasser TC, Ogden RW (2000) A new constitutive framework for arterial wall mechanics and a comparative study of material models. *J Elasticity* 61:1-47

[71] Mullins L (1947) Effect of stretching on the properties of rubber. *J RUBBER RES* 16: 275-289 ISSN:1511-1768

[72] Li Y, Barbič J (2014) Stable Orthotropic Materials. In: Koltun V, Sifakis E (Eds) *SCA '14 Proceedings of the ACM SIGGRAPH/Eurographics Symposium on Computer Animation* 41-46

[73] Fleck NA, Liu D, Shu JY (2000) Microbuckle initiation from a hole and from the free edge of a fibre composite. *Int J Solids Struct* 37:2757-2775

[74] Zheng QS (1994) Theory of representations for tensor functions. *Appl Mech Rev* 47:554

[75] Toupin RA (1962) Elastic materials with couple-stress. *Arch Ration Mech Anal* 11:385-414

[76] Holzapfel GA (2000) Nonlinear solid mechanics. A Continuum Approach for Engineering. John Wiley & Sons, Chichester

[77] Timmel M, Kolling S, Kaliske M (2007) Phenomenological and Micromechanical Modeling of Anisotropic Effects in Hyperelastic Materials. *LS-DYNA FORUM 6*, Frankenthal

[78] Huebner KH, Dewhirst DL, Smith DE, Byrom TG (2001) The Finite Element Method for Engineers, 4th Edition. Wiley-Interscience, New-York

[79] Nori M, Nemat-Nasser S (1999) On two micromechanics theories for determining micro-macrorelations in heterogeneous solids. *Mech Mater* 31:667–682

[80] Gross D, Seelig T (2011) Fracture Mechanics. With an Introduction to Micromechanics. Springer-Verlag Berlin Heidelberg

[81] Shutian Liu, Wenzheng Su (2009) Effective couple-stress continuum model of cellular solids and size effects analysis. *Int J Solids Struct* 46:2787–2799

[82] Srinivas S, Joga Rao CV, Rao AK (1970) An exact analysis for vibration of simply-supported homogeneous and laminated thick rectangular plates. *J Sound Vib* 12:187–189.

[83] Aimmanee S, Batra RC (2007) Analytical solution for vibration of an incompressible isotropic linear elastic rectangular plate, and frequencies missed in previous solutions. *J Sound Vib* 302:613–620

[84] Pagano NJ (1969) Exact solutions for composite laminates in cylindrical bending. *J Compos Mater* 3:398-411

[85] Dagher MA, Soldatos KP (2011) On small azimuthal shear deformation of fibre-reinforced cylindrical tubes. *J Mech Mater Struct* 6(1-4):141-168

[86] Spencer AJM (1982) The formulation of constitutive equation for anisotropic solids. In: Boehler JP (Ed.) *Mechanical behavior of anisotropic solids*. Martinus Nijhoff Publishers, The Hague

[87] Itskov M, Aksel N (2002) Elastic constants and their admissible values for incompressible and slightly compressible anisotropic materials. *Acta Mech* 157:81-96

[88] Lubarda VA, Chen MC (2008) On the elastic moduli and compliances of transversely isotropic and orthotropic materials. *J Mech Mater Struct* 3(1):153-171

Appendix

Analytical solution to flexure of a thick plate under sinusoidal pressure load (from Farhat and Soldatos [1]).

Let us consider a planar boundary problem: a thick transversely isotropic plate, infinite in the x_3 direction, subjected to boundary conditions corresponding to the plane strain as specified in (**Fig. 8.1**). In this case, the displacements are functions of only two coordinates

$$
\begin{aligned}
u_1 &= u_1(x_1, x_2), \\
u_2 &= u_2(x_1, x_2), \\
u_3 &= 0.
\end{aligned}
\tag{A.1}
$$

The following equations in terms of displacements u_1, u_2, obtained by Spencer and Soldatos [2] for the case of the plane strain problem of a plate with fibres initially aligned along the x_1 direction, will be further employed:

$$
\begin{aligned}
c_{11}\frac{\partial^2 u_1}{\partial x_1^2} + (c_{12} + c_{66})\frac{\partial^2 u_2}{\partial x_1 \partial x_2} + c_{66}\frac{\partial^2 u_1}{\partial x_2^2} + c_3\frac{\partial^4 u_2}{\partial x_1^3 \partial x_2} &= 0, \\
c_{66}\frac{\partial^2 u_2}{\partial x_1^2} + (c_{12} + c_{66})\frac{\partial^2 u_1}{\partial x_1 \partial x_2} + c_{22}\frac{\partial^2 u_2}{\partial x_2^2} - c_3\frac{\partial^4 u_2}{\partial x_1^4} &= 0.
\end{aligned}
\tag{A.2}
$$

The relations for the symmetric part of the stresses are given in the form of the generalized Hooke's law for transversely isotropic materials:

$$
\begin{pmatrix} \sigma_{11} \\ \sigma_{22} \\ \sigma_{33} \\ \sigma_{(12)} \end{pmatrix} = \begin{pmatrix} c_{11} & c_{12} & 0 \\ c_{12} & c_{22} & 0 \\ c_{12} & c_{23} & 0 \\ 0 & 0 & c_{66} \end{pmatrix} \begin{pmatrix} \varepsilon_{11} \\ \varepsilon_{22} \\ 2\varepsilon_{12} \end{pmatrix}
\tag{A.3}
$$

where ε_{11}, ε_{22}, ε_{12} are the only non-zero strain tensor components conventionally derived as

$$
\varepsilon_{ij} = \frac{1}{2}\left(\frac{\partial u_i}{\partial x_j} + \frac{\partial u_j}{\partial x_i} \right)
\tag{A.4}
$$

The theory employed in the present paper assumes that the spin vector (rotation vector in a static setting) $\boldsymbol{\omega}$ is not independent but related to the displacement vector $\boldsymbol{u}$ in the following way:

$$
\omega_i = \frac{1}{2}\epsilon_{ijk}\frac{\partial u_k}{\partial x_j}.
\tag{A.5}
$$

The components of the symmetric and antisymmetric parts of the stress tensor are denoted as $\sigma_{(ij)}$ and $\sigma_{[ij]}$ respectively so that

$$\sigma_{ij} = \sigma_{(ij)} + \sigma_{[ij]}. \tag{A.6}$$

The linearised relation for the non-zero couple stress are given as follows [2]:

$$m_{13} = 2c_3 \frac{\partial^2 u_2}{\partial x_1^2}, \tag{A.7}$$

It should be noted that the above linear constitutive law (A.3), (A.7) can be set equivalent to the hyperelastic law (5.21) in Section 5 under small strain by a respective translation of the constants. In particular, the following relation connects constants c_3 and k_3: $c_3 = 4/3k_3$.

With the 6 boundary conditions applied at the plate ends:

$$\begin{cases} \sigma_1(0, x_2) = 0, \\ u_2(0, x_2) = 0, \\ m_{13}(0, x_2) = 0, \\ \sigma_1(L, x_2) = 0, \\ u_2(L, x_2) = 0, \\ m_{13}(L, x_2) = 0, \end{cases} \tag{A.8}$$

the solution is sought in the form [1]

$$\begin{aligned} u_1 &= f_1(x_2)\cos\left(\frac{\pi x_1}{L}\right), \\ u_2 &= f_2(x_2)\sin\left(\frac{\pi x_1}{L}\right), \end{aligned} \tag{A.9}$$

where

$$f_1(x_2) = a_i e^{\mu_i x_2}, \quad f_2(x_2) = \bar{a}_i e^{\mu_i x_2}. \tag{A.10}$$

The four remaining lateral boundary conditions are as follows:

$$\begin{cases} \sigma_2(x_1, h/2) = -q_0 \sin\left(\frac{\pi x_1}{L}\right), \\ \sigma_{21}(x_1, h/2) = 0, \\ \sigma_2(x_1, -h/2) = 0, \\ \sigma_{21}(x_1, -h/2) = 0. \end{cases} \tag{A.11}$$